Zinc recovery from steelmaking wastes

Recycling in HIsarna

M. Strijker

Technische Universiteit Delft

TU Delft

Zinc recovery from steelmaking wastes

Recycling in HIsarna

by

M. Strijker

to obtain the degree of Master of Science in Material Science and Engineering

at the Delft University of Technology,

December 1, 2020

Frontpage image downloaded from recycling today [1]

TU Delft

Acknowledgements

I would like to thank everyone that helped me during the process of my thesis. A special thanks to my supervisor Dr. Timothy Kerry for his involvement in this project, the help during the experiments and his provided feedback and to Dr. Yongxiang Yang for his support and feedback.

Another big thanks to Sander van Asperen to whom I could reach for any question about the laboratory, Ruud Hendrix for his XRF analysis, XRD analysis, interpretation and discussion and Kees Kwakkernaak for his support on using the SEM. A thanks to all for making time to discuss about the best possibilities for analysing the samples and other things in life.

M. Strijker
Delft, December 2020

Abstract

During the production of steel, a dust waste stream is created that contains a significant amount of zinc which makes it difficult to treat and to recycle. Various furnaces have been developed that can deal with those dusts like rotary hearth furnaces and the DK process but none are fully optimal yet. HIsarna, a furnace in development by Tata steel, is able to treat those zinc bearing dust by separating zinc from iron whilst being an ironmaking furnace. Basic oxygen furnace (BOF) dust, blast furnace (BF) dust and historical oxychalk sludge (HOKS) have been the dusts under investigation for recycling in HIsarna. BF dust is a source of zinc and carbon whilst both BOF dust and HOKS contain a large share of iron. Micrograniulates have been made from BOF dust and HOKS with different additions of BF dust which provides carbon that can be used for reduction reactions. With the help of thermo gravimetric analysis (TGA) and a horizontal furnace for isothermal experiments at 1000°C and 1300°C, the best two micrograniulates (one HOKS/BF dust, one BOF dust/BF dust) were chosen that could completely reduce all zinc and iron oxides in a nitrogen atmosphere. Because HIsarna has a reducing atmosphere, this thesis focuses on answering the question how the self reduction behaviour of zinc in the micrograniulates compares to the reduction behaviour in an atmosphere of 50% CO and 50% CO_2. It appears that during isothermal experiments at 1000°C, the zinc separates more efficiently in nitrogen than in the 50/50 atmosphere. However this was not seen at 1300°C. At this temperature, the zinc concentration in the BOF dust micrograniulates decreased in similar ways in both atmospheres while the zinc in the HOKS micrograniulates reduced much faster in this reducing atmosphere. Besides isothermal experiments, a vertical tga furnace was used for a non-isothermal experiment up to 1500°C at a large enough scale to analyse the samples after treatment. However, not much difference in zinc reduction ability was found between the different atmospheres. The dust from those experiments was collected and showed to contain zinc and lead present in elemental form, oxides and carbonates as well as potassium chloride. The results show to be promising for the recycling of dusts in HIsarna.

Contents

List of Figures

List of Tables

1

Introduction

Since the industrial revolution, both the world wide consumption patterns and our living standards have greatly increased. This could never start without coal and iron. Coal was needed as fuel for the steam engines while iron was used for the production of industrial and consumer goods. The discovery of coke, which burns at a higher temperature than coal, was one of the main drivers in the development of the iron industry and those developments have never stopped since. Nowadays, the drawbacks of the industrialisation are more and more noticeable. Raw material stocks are depleting, waste management is increasingly complex and (air-) pollution has become a problem. These problems are the reason that one of the 17 sustainable development goals of the United Nations focuses on ensuring sustainable consumption and production patterns [16]. Secondary raw materials have become important. These are waste materials that can be used instead of virgin materials. End of life products can be processed in such a way that its components can be used to make other products and waste streams created during production can be partly converted into valuable by-products. The steel production, for example, converts only 63.6% of the raw materials into steel products. The remaining is mainly converted into valuable by-products and only 3.7% has to go to landfill [17]. Whilst this is a small fraction of the total production (which is 1800 million tonnes per year), this translates into an enormous quantity of material and therefore cannot be neglected.

During steel production, the main waste streams are slags, dusts/sludges and off-gasses. Slag is a substance that floats on top of the liquid metal and contains many impurities in the form of oxides. The amount of slag produced is between 170 and 400 kg per tonne of crude steel depending on the production method and most of it has a valuable use as an aggregate in the cement or road construction [17]. About 3% of the charge into a furnace is collected as dust [18]. Dusts and sludges are collected together with the off-gasses in the off-gas system in which they will be separated. The cleaned off-gas is exhausted while dusts or sludges are left behind. Whether dust or sludge is formed depends on the type of off-gas treatment: dust forms a sludge when water is used to collect the particles in the off-gas system. Dust is created either by particles that move upward together with the gas flow or by the evaporation of metals. The usage of this dust as by-product or any other type of recycling is made difficult by the amount of heavy and toxic metals like zinc, lead, cadmium and chromium.

With the recycling of steel, a large amount of zinc enters the furnaces because galvanised steel scrap is used as feed material. Steel is one of the most widely used materials and has been produced for almost 4 millennia. However, its lifetime is limited because steel can be corroded. A solution would be to galvanise: a thin layer of zinc covers the outer layer of steel. The zinc is sacrificed to protect steel from oxidation and therefore increases its lifespan. It can be seen in figure 1.1 that the usage of zinc has increased a lot over the last 40 years, especially for the galvanization of steel but this seems to stabilize. When galvanised steel is recycled, the challenge is created to separate the zinc from the steel and recycle both into new valuable materials.

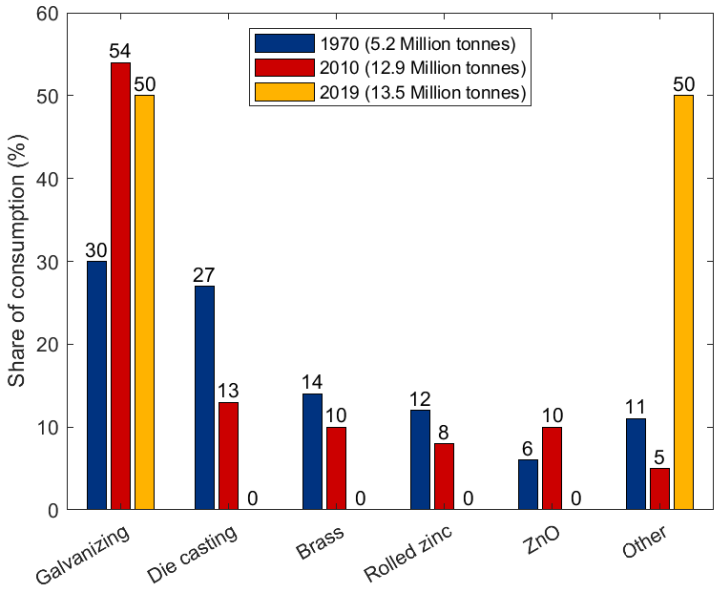

Figure 1.1: The estimated global refined zinc consumption by end use [2], [3]

At this moment, 45% of all zinc reaching their end-of-life is recycled globally [19]. Zinc sheet even has an end-of-life recylcing rate of over 95% as it can mainly be remelted while the recycling of zinc used for galvanised steel was only 14% of the total amount of secondary recycled zinc in 2005 [20]. The need for proper secondary zinc resources is increasing due to reduced ore grades, environmental concerns and a possible shortage of mines [21].

Besides resource saving, the greenhouse gas emissions of metals production cannot be neglected either. In 2017, about 1.83 tonnes of CO_2 were produced per tonne of steel which means that the steel industry produces 7-9% of the total greenhouse gas emissions. Recycling one tonne of steel saves 1.5 tonne of CO_2, 1.4 tonne of iron ore, 740 kg of coal and 120 kg of limestone[17].

Different waste streams are produced by the steel industry but the dusts are most difficult to recycle due to their high heavy metals content. The production of steel and current technologies to recycle their processing dusts are described in chapter 2. A new ironmaking process is introduced as well: HIsarna. This is a very promising new furnace both for ironmaking and for the recycling of steel dusts. A pilot plant has been operating at the Tata steel site in IJmuiden, the Netherlands, where it showed to have little need for raw materials processing, a high flexibility in raw material and it was found that zinc can be properly concentrated and collected in the process dust. The development of HIsarna was stimulated by the European ULCOS program - ultra low carbon dioxide steelmaking - because it has the potential to reduce carbon dioxide emissions of steelmaking by at least 20%. Besides that, the off-gas contains less NO_x and SO_x and it has a reduced need for metallurgical coals. Lower quality and more volatile thermal coals can be used because part of the created gasses are still needed in the top part. Besides that, it has the ability to capture up to 80% of the CO_2 emissions for geological storage because of an N_2 poor off-gas.

Currently, it is stimulated by the RECLAMET project which focuses on the RECLAmation of valuable METals from process residues through HIsarna ironmaking. HIsarna has a big potential to recycle zinc out of iron and zinc rich waste streams and has therefore the ability to make both zinc and steel circular, which is graphically shown in figure 1.2. In ideal circumstances, the zinc and iron bearing dusts from steel production can be recycled in HIsarna next to zinc coated scrap and iron bearing residues from the zinc industry. Those waste streams have a relatively high zinc content which can be concentrated in the HIsarna dust. Subsequently, those dusts can be processed by the zinc smelter. In the mean time, HIsarna produces crude iron which can be further processed to steel and used for the steel production.

However, more research is needed to optimise this process. This thesis will focus on finding the optimal composition of a combination of different iron and steelmaking dusts to make sure that all compounds are used in the best way and to analyse the effect of different atmospheres onto this reduction behaviour. The research questions can be found in chapter 3, the experimental methods used are described in chapter 4. The results as well as the discussion about these results can be found in chapter 5 after which the conclusions and recommendations are presented in chapter 6.

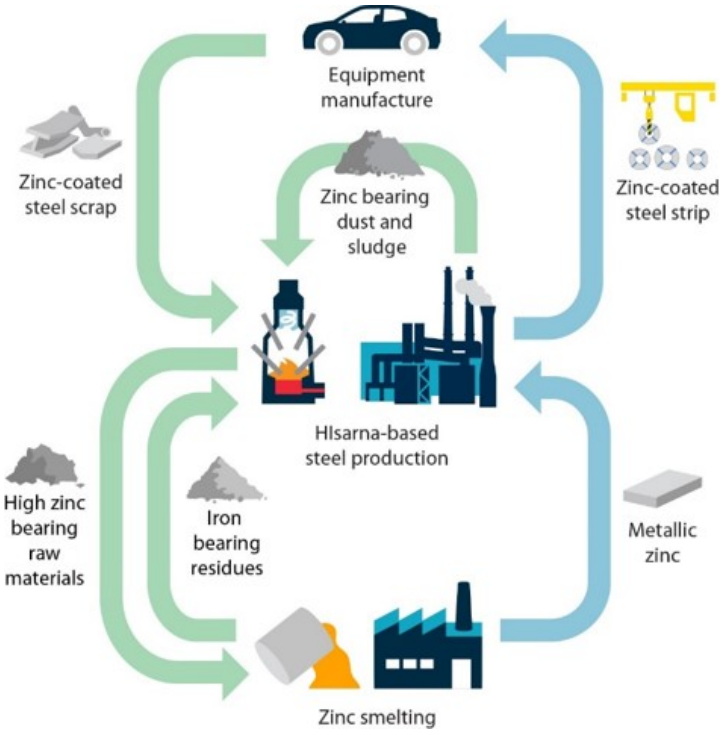

Figure 1.2: The optimal way to recycle both iron and zinc with HIsarna

2

The generation and recycling of zinc rich waste dusts

One of the most difficult waste streams from the steel industry to recycle are those that contain a lot of heavy metals. They cannot be used as construction materials as the heavy metals can leach out and pollute the environment and our drinking water. The same issue needs to be taken into account at a landfill site. This chapter describes the most common routes for the production of steel and zinc as well as the existing recycling methods that are used to separate a zinc rich stream from an iron rich stream.

2.1. Steel production

The production of steel is done pyrometallurgically, which means that the ore materials (mainly in the form of oxides and sulfides) are reduced to metals at high temperatures. Reaction 2.1 describes the basic reaction taking place. A metal oxide (MO_2) can be reduced with another component (R) to form a metal. The conditions must be controlled tightly to ensure that the formation of RO_2 is more energetically favourable. This is dependent on the temperature, the oxygen pressure and the kinetics of the reaction[22].

$$MO_2 + R \rightleftharpoons M + RO_2 \tag{2.1}$$

Often, carbon is used to reduce metal oxides. Most of this reaction goes indirectly through the Boudouard reaction (eq. 2.2) because gasses can spread much more easily than solid carbon. The metal is reduced according to reaction 2.3.

$$C(s) + CO_2(g) \rightleftharpoons 2CO(g) \tag{2.2}$$

$$MO(s) + CO(g) \rightleftharpoons M + CO_2(g) \tag{2.3}$$

The next sections explain different routes for steel making. The blast furnace (BF), the basic oxygen furnace (BOF) and the electric arc furnace (EAF) are the most used furnaces for the steel production, see figure 2.1. The BF-BOF route produces 75% of all steel while the EAF produces almost all remaining 25% [23].

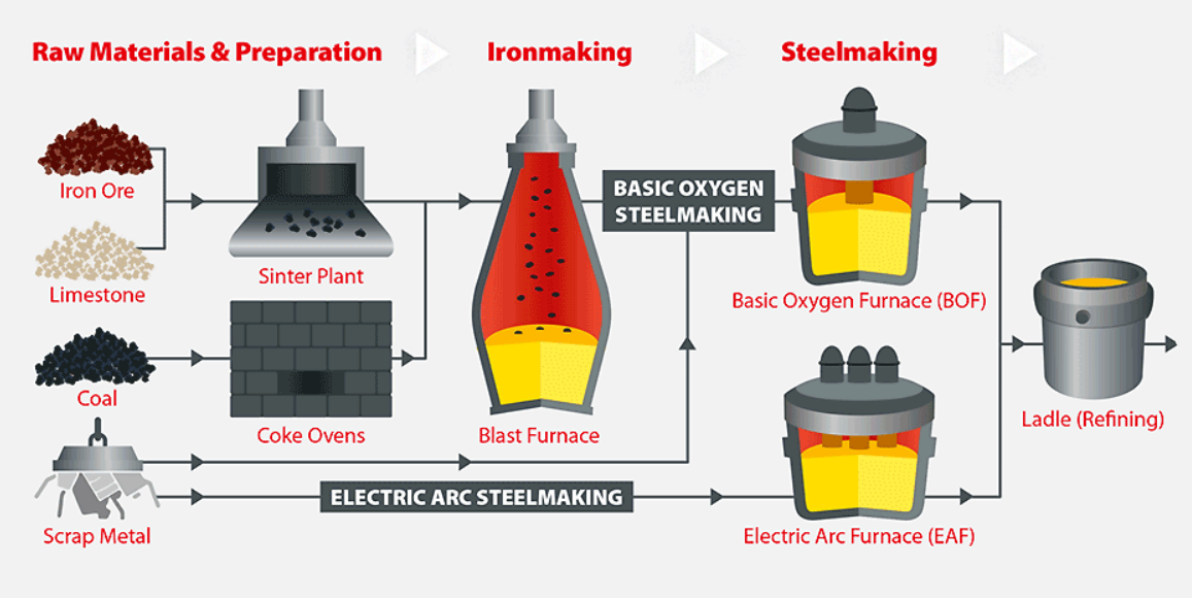

Figure 2.1: The production of steel through the BF-BOF route and the EAF route [4]

2.1.1. The BF-BOF route

The first step in the BF-BOF route is the sintering of iron ore. During sintering, iron ore fines and limestone are agglomerated to obtain big enough particles. The porous product has an increased permeability and makes reduction with coke easier [24]. The BF uses coke as reducing agent which is made by heating coal in the absence of oxygen. Coke has a high carbon content and during its production, impurities like sulphur and oxygen have volatilised. Both sinter and coke are fed into the BF in alternating layers. In the BF, the iron oxides are reduced into metallic iron under a temperature that reaches more than 2000°C. Besides that, a slag consisting of limestone and impurities and a dust are produced as side products. The slag is a layer with many oxides and a lower density than the molten metal. Consequently, it floats on top of the molten metal and can be removed easily. The fluxing agents (e.g. limestone) are added to stimulate this slag forming.

In the BOF, pure oxygen is blown into a bath of molten pig iron received from the blast furnace (with contains ±4% carbon) together with up to 25% of iron scrap, some lime and other fluxing agents. The main goal is to oxidise the carbon and eliminate some other impurities (like P, Si, Mn, Ti, V) into the slag. The charge is mainly heated by exothermic reactions of the oxidation of silicon, carbon, phosphor and manganese. The energy released by the oxidation greatly increases the temperature so often scrap is added to decrease the temperature [22, 25]. Resultantly, 85% of the energy used in the BF/BOF route is used for ore preparation and operating the blast furnace and only a small amount of energy is needed for operating the BOF [26].

2.1.2. EAF route

The EAF is mainly charged with iron scrap together with some lime/limestone, iron ore and coke. The charge is melted with an electrical current. This process does not oxidise as many impurities as the BOF with the result that it often has a higher carbon and nitrogen content. Just like the BOF furnace, many impurities can be removed through the slag (about 100kg/ton crude steel). However, some impurities brought by the scrap are very difficult to remove and reduce the quality of the steel [22, 25].

Galvanised steel is part of the feed material and this increases the zinc content in the charge. After the reduction of the zinc oxides, the zinc evaporates (>907°C) and enters the off-gas system in which it is collected as zinc oxide dust together with iron oxides and calcium oxides [27]. A ton of steel generates 15-20 kg dust which has a zinc concentration of 18-35% [28].

2.1.3. Alternative ironmaking routes

Next to those two most common routes, new ironmaking processes are in development which are able to use lower quality ores and reduce the CO_2 emission. Two processes exist that can be used: direct reduction and direct smelting after which their product can be used in the EAF or BOF.

Direct reduced iron (DRI) is iron ore reduced below its melting temperature (around 1300°C). Compared to BF metal, DRI is based on the removal of oxygen and the addition of carbon. Other elements remain in the metal while this would partly end up in the slag during production in the BF. The advantages of direct reduction processes is that they have lower capital requirements, fewer emissions and a wider choice of fuels compared to the BF [29].

Direct smelting has the advantage that no coke making is necessary. The first step of this technology is similar as producing DRI after which it is directly melted and further reduced in a smelting reduction vessel. The smelting vessel gasifies coal which produces heat and a CO-rich gas that either reduces iron or is burnt for extra heat. The direct smelter eliminates coke production and lowers the energy consumption while the quality of the hot metal is similar to BF hot metal. To reach this quality, lower quality ores can be used which is important because high quality ores are increasingly expensive. However, using lower quality ores has the trade-off that more coal is needed which again is at the cost of an increased CO_2 emission [12]. A disadvantage of these processes is the need for large quantities of pure oxygen.

An important direct smelting technology for this thesis is HIsarna, which is a bath smelting process in development. Similar to other direct smelting processes, neither sinter nor coking plant is needed which reduces the energy consumption by 20%. This is possible because the prereduction is done in the top part of the furnace. Besides that, there is a lower need for high quality ore materials. HIsarna is able to reject more impurities like phosphorous and titanium into the slag because of better mixing and relatively oxidising conditions compared to the BF. In this way, lower quality ores can be used compromising on a higher loss of iron into the slag (4-5% FeO compared to less than 1% in BF slag [12]).

2.2. Zinc production

55% of the zinc mines are found in China, Australia and Peru in which zinc is often present as sphalerite (ZnS) [30]. The total amount of zinc in the zinc ore is only 5-15% so it needs to be concentrated. After concentrating up to ±55% it can be processed by zinc smelters. Firstly, the sulphur in the concentrate is removed by roasting which creates zinc oxide and sulphur dioxide. The latter will subsequently be transformed to sulphuric acid through a reaction with water and oxygen. Other impurities like iron, lead and silver can be removed by either hydrometallurgical or pyrometallurgical processes. Those processes can also be used to recycle the zinc from the steel dusts after they have been separated in a zinc rich stream with a high enough zinc concentration (typically 54% [31]).

2.2.1. Hydrometallurgical zinc production

Most (80%) of the zinc refining processes is done hydrometallurgically which is schematically described in figure 2.2. For this process, the sulphuric acid produced after roasting is used to dissolve zinc oxide. Iron will precipitate in this solution and lead and silver will remain undissolved so both can be removed by filtering. To increase the purity, a cementation step is necessary. Cementation is a process that uses an addition of zinc metal dust. Impurities that are more electropositive than zinc (like copper, nickel, cobalt and cadmium) can precipitate. The precipitates can be removed and most of it can be sold as by-product. At last, the zinc can be recovered with an electrolytic process [32–34].

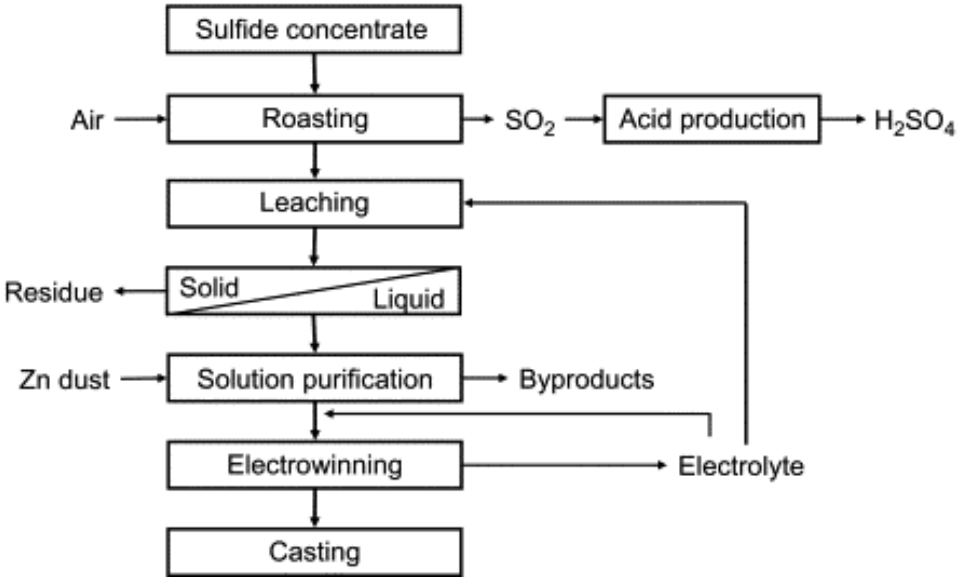

Figure 2.2: A flow chart of hydrometallurgical zinc making [5]

2.2.2. Pyrometallurgical zinc production

The pyrometallurgical primary production of zinc is based on its low boiling point (907°C) and takes place in a zinc blast or imperial smelting furnace. Its schematic process can be found in figure 2.3. During an imperial smelting process, sinter is often made from lead and zinc sulphide concentrates. They are oxidised after which the resulting oxides are reduced by carbon monoxide. Because of its low boiling point, the zinc gas can be collected in the off-gas. In the mean time, lead is often recovered at the bottom of the blast furnace[6].

The temperature of the off-gas will be maintained above 1000°C to ensure that the zinc gas does not reoxidise. In the lead splash condenser, the zinc gas is dissolved in a shower of lead particles. During cooling, the zinc and lead will create separate layers. The zinc can be recovered and the lead will be returned to the splash condenser. The resulting zinc with about 1.2% lead can be used for, for example, galvanizing processes[35].

A distillation refining step could be necessary to improve the purity to high grade zinc. In this step, zinc is distilled out of the mixture and leaves behind metals with a higher boiling point like iron and lead. As a second step, impurities with a lower boiling point than zinc, like cadmium, can be distilled out [35].

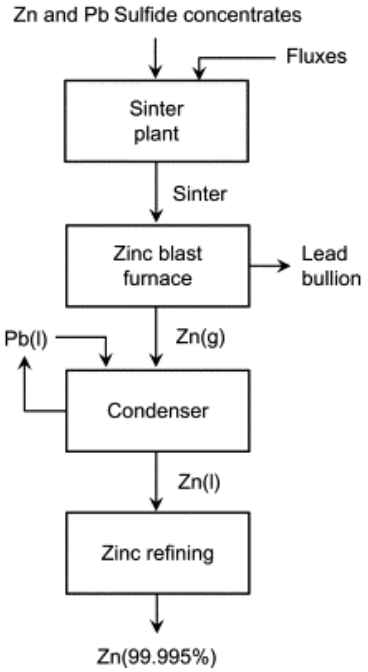

Figure 2.3: A flow chart of pyrometallurgical zinc making [6]

2.3. Zinc recycling methods for steelmaking dusts

Recycling of steelmaking dusts is only a limited possibility in the BF-BOF route. BF and BOF dust are often recycled through sintering but this can reduce the quality of the sinter in too large quantities. Besides, it causes an increased coke consumption and increasing dust emissions in the case of recycling fines [36].

Due to increasing scrap recycling rates in the BOF, the amount of zinc in the BOF increases. Most zinc ends up in dusts or sludges with the result that the zinc concentration in the dust increases. When this is recycled through sintering, it can give some complications by influencing the sinter quality, strenght or productivity [37]. During sintering, about 15% of the zinc will volatilize [38] which is a good thing for the BF because this furnace cannot handle a high zinc input. The zinc can build up in the BF which deteriorates the lining and reduces its lifespan. Therefore, the maximum levels allowed in the BF are usually around 0.1-0.5 kg zinc per ton of hot metal [5]. However, this volatilisation is a loss of zinc. Sometimes, BOF dust is also recycled in the BOF itself which can increase the zinc concentration in the BOF dust up to 20% [39]. Another option is that the sludge is separated in a fine and coarse fraction as most lead and zinc are concentrated in the fine fraction. In this case, it is possible to only recycle the coarse fraction through sintering [40] but the small fraction is still difficult to handle.

The electric arc furnace is mainly used for recycling scrap material with the result that a lot of zinc enters these furnaces. Most of this zinc is collected as EAF dust and the zinc concentration is sometimes increased through repeatedly recycling within the EAF. The amount of zinc is dependent on the amount of galvanized scrap added to the furnace. The high zinc content makes that this dust is a valuable material to recycle for zinc recovery. This chapter describes the most important processes that can deal with the recycling of steel dusts. The Waelz process is very important for the recycling of EAF dust and is described below. Because the recycling of lower zinc containing dusts is more challenging, the other processes will mainly focus on those materials.

2.3.1. The Waelz process

The most well known process is the Waelz process that recycles around 80% of the steel dust created in an electric arc furnace [7, 8, 41]. When the zinc concentration reaches a minimum value of 18%, it can be recycled with the Waelz process [40]. The main part of the Waelz process is a slightly inclined rotary heart furnace (2-3% inclined, ±55 meters long, rotary speed of ±1.2 rpm) to which the zinc containing dust, flux and coke are added in dry, compact-moist or pelletized form. The charge material is firstly pelletized to guarantee a homogeneous input material after which it is fed at the top of the Waelz kiln while hot air and gas are added at the bottom, see fig. 2.4.

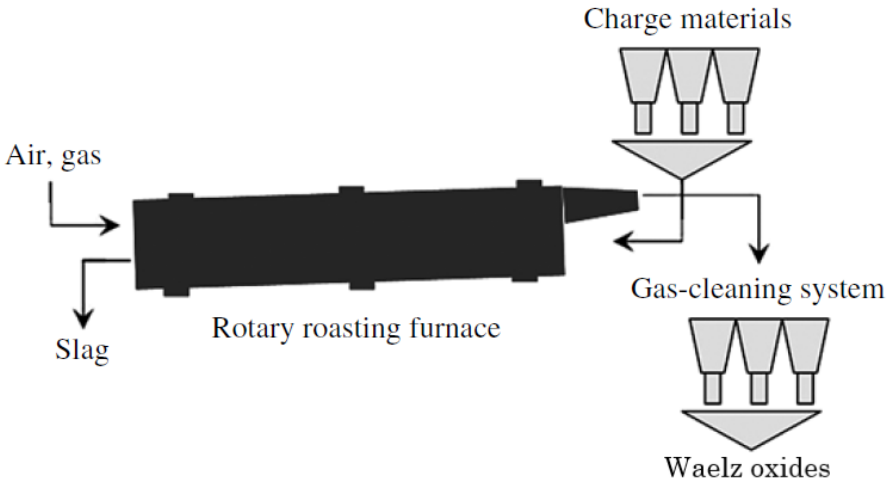

Figure 2.4: The Waelz kiln [7]

In the kiln, the charge material is dried and heated by the kiln gas. The reduced zinc, other heavy metals, chlorine and alkalis vaporize selectively and are collected in the gas cleaning system in which the zinc is reoxidised and separated from the gas. This Waelz oxide still has a high level of impurities (<68% zinc) but can be used by the zinc smelters after washing. A washing stage is required to leach alkalis and halides out of the Waelz zinc oxide. Alkalis and halides are harmful to the hydrometallurgical zinc production so many zinc smelters require a chloride and fluoride concentration of no more than 0.1%. Processes are in development that can deal with higher percentages but those are not the standard [8, 42].

Unfortunately, there are no methods yet to properly recover the slag even though the iron oxide content can reach 50% [7, 8]. To give an idea about the composition of Waelz oxide dust and slag, the main elements are shown in table 2.5 of which the zinc is mainly present as zinc oxide and zinc ferrite.

	Steel plant flue dust	Slag (acid)	Slag (basic)	Waelz oxide	Waelz oxide (washed)
Zn	18 – 35	0.2 – 1.5	0.5 – 2	55 – 58	60 – 68
Pb	2 – 7	0.5 – 1	0.5 – 2	7 – 10	9 – 11
Cd	0.03 – 0.1	< 0.01	< 0.01	0.1 – 0.2	0.1 – 0.3
F	0.2 – 0.5	0.1 – 0.2	0.1 – 0.2	0.4 – 0.7	0.08 – 0.15
Cl	1 – 4	0.03 – 0.05	0.03 – 0.05	4 – 8	0.05 – 0.1
C	1 – 5	3 – 8	3 – 8	0.5 – 1	1 – 1.5
FeO	20 – 38	30 – 40	30 – 50	3 – 5	4 – 7
$Fe_{(met)}/Fe$		80 – 90	80 – 90		
CaO	6 – 9	8 – 9	15 – 25	0.6 – 0.8	0.7 – 1.2
SiO_2	3 – 5	35 – 37	6 – 12	0.5 – 0.7	0.5 – 1
Na_2O	1.5 – 2	1.2 – 1.6	1.2 – 1.6	2 – 2.5	0.1 – 0.2
K_2O	1 – 1.5	0.7 – 0.9	0.7 – 0.9	1.5 – 2	0.1 – 0.2

Figure 2.5: The composition of the feed material and the products of the Waelz process [8]

Modern Waelz plants use an improvement called the SDHL process in which only 70% of the coke is

added. This is possible because the metallic iron is reoxidised which generates part of the necessary heat [8].

Advantages[43]

- Relatively low energy consumption
- Big scale - well known principle
- Crude zinc oxide output that can be used by the zinc industry

Disadvantages[43]

- iron and other metals are lost in slag waste with the result that there is a high amount of newly generated residues (±700kg/ton charged dust)
- still quite low product quality
- Only able to recycle high zinc containing EAF dust

2.3.2. DK process

Most of the low zinc containing steelmaking dusts are recycled through sintering with an average of 12.7kg/ton of sinter in europe [37]. There is a process that can sinter with 80% of steel waste materials: the DK process which recycles a large share of european dusts in its two small blastfurnaces in Germany. BOF dust and sludge, BF dust and sluge, mill scale, some sand, coke and iron ore are mixed in predetermined ratios before the sintering process takes place which is similar to a normal sintering process. Subsequently, the sinters are fed to a small blast furnace that is operated with a higher top gas temperature compared to other blast furnaces. This is needed because it has a high zinc input of 45kg/ton hot metal as well as a higher alkali and lead concentration [44]. The blast furnace sludge of the DK process contains 65-68% zinc which can be used by the zinc smelters [45]. Although no proven answer can be found, it seems likely that part of the zinc is lost during the sintering process.

Next to a zinc rich dust, pig iron is produced that can be fed into the BOF, a slag that can be used as construction material and only 2% needs to be landfilled. This 2% is the dust generated by the sinter off-gas cleaning systems [45].

Advantages

- Can deal with a large variety of materials [46]
- Zinc output contains a low amount of fluorides and chlorides [45]

Disadvantages

- Continuous tests are needed to provide a suitable sinter quality
- Higher fuel and coke consumption than regular BF [38]
- BF dust, BF sludge and mill scale decrease sinter quality and so are only recyclable in small amounts [44]

2.3.3. Rotary hearth furnace

Rotary hearth furnaces (RHF) have shown to be very flexible in material input and are therefore used to recycle low zinc containing steel wastes. A rotary hearth furnace (RHF) consist of a ring in which the hearth rotates, filled with a thin layer of pellets. The gas flow is countercurrent to the feed material to optimise the thermal and reduction properties.

Multiple types of RHFs are commercialized that are mainly used in China and Japan. The FASTMET process and DRyIron are used for the recycling of dusts. The FASTMET process used to work with metallic oxides from steel mill waste or iron ore fines together with solid carbon as a reductant but

mainly its Japanese plant in Fukuyama is able to process steelmaking dusts with a higher zinc content. To reach a good enough composition, a long enough reduction time inside the furnace is needed. This means that a very large rotary hearth furnace is necessary[9]. Subsequently, the formed (direct reduced) iron can be processed in a BOF or EAF [47]

The zinc is evaporated after reduction by carbon. Enough air is added to the gasses to make sure that the zinc and carbon monoxide are reoxidised. The gasses are cooled down and the dust is captured in a bag filter in the off-gas system. This dust consists mainly of crude zinc oxide, see table 2.1. After washing, the composition can be improved up to 98% of ZnO and PbO.

Flue gas dust [%]		**DRI [%]**	
Zn	56.4	T-Fe	68.0
Pb	4.99	M-FE	57.8
T-Fe	0.32	FeO	13.3
Na	3.13	C	2.00
K	10.79	S	0.52
S	1.69	Mn	1.07
Cl	4.86	CaO	4.35
F	0.15	SiO2	5.95
C	0.01		

Table 2.1: An example of the chemical composition of the FASTMET plant Kakogawa[15]

In fig. 2.6, the process inside the rotary hearth furnace is described. Before feeding, the pellets are dried and the temperature increases slowly to a maximum of 1400 degrees. The total residence time inside the furnace can take up to 30 minutes depending on the feed material [9, 48].

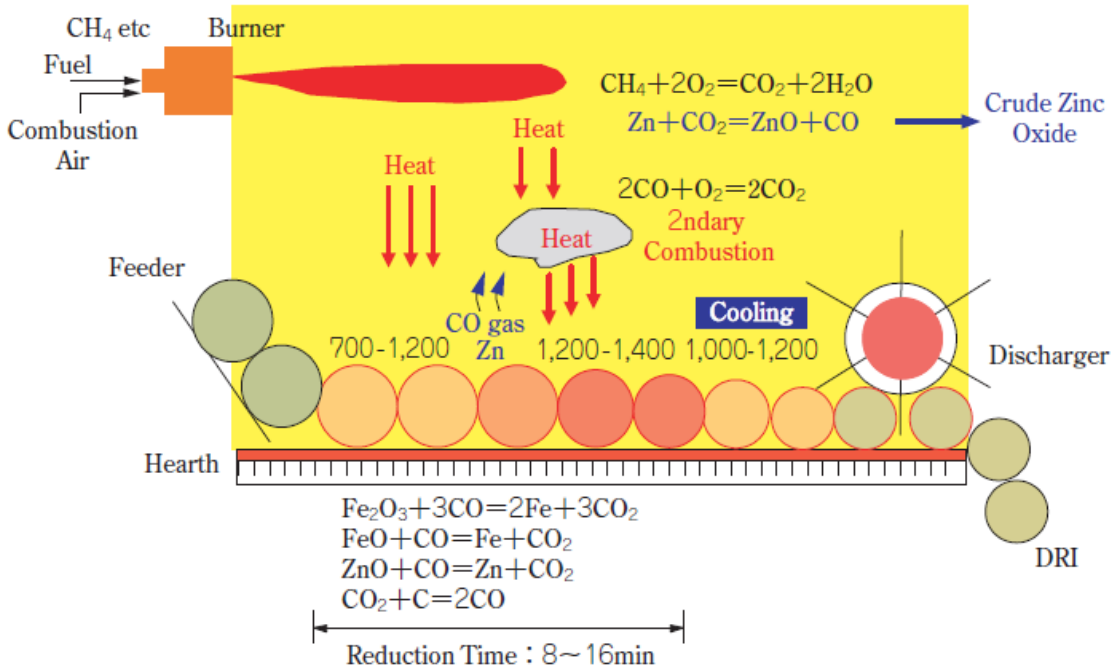

Figure 2.6: A schematic drawing of the FASTMET process [9]

Advantages

- Focuses on steel but can be made to recycle zinc
- Decreased CO_2 emissions because the emitted CO from the feed can be used as fuel for the furnace.
- Lower quality feed required [49]
- Lower energy consumption than blast furnace [50]

Disadvantages

- Difficult to scale up [51]
- Harsh slag conditions reduce refractory lifetime [51]

A big problem for recycling are wet sludges. It is difficult to remove the moisture efficient and sufficient and there is a danger of formation of agglomerates that seldom disintegrate. It is mentioned that those last agglomerates are suitable for reactions in the RHF after proper drying [52]. This is especially mentioned for the DRyIron process that can be made into briquettes together with coke fines and EAF dust [53]

2.3.4. The OxyCup process

The OxyCup furnace is a combination of a cupola furnace and a blast furnace with a facility in Germany and China. The advantage of the cupola is that it has no difficulties with high zinc concentrations and therefore can be used for the recycling of BOF dust, BF dust and sludge, mill scale and scrap. The iron bearing wastes are added as self reducing briquettes together with carbon (12-14%) and a cement binder (10-12%). They are melted in the cupola with an oxygen enriched blast. Due to the presence of coke in the briquettes and the high temperatures (900-1400°C), the iron oxides can be reduced in about 20-30 min. The reaction is noticeable above 1000°C and fast above 1400°C, see fig. 2.7.

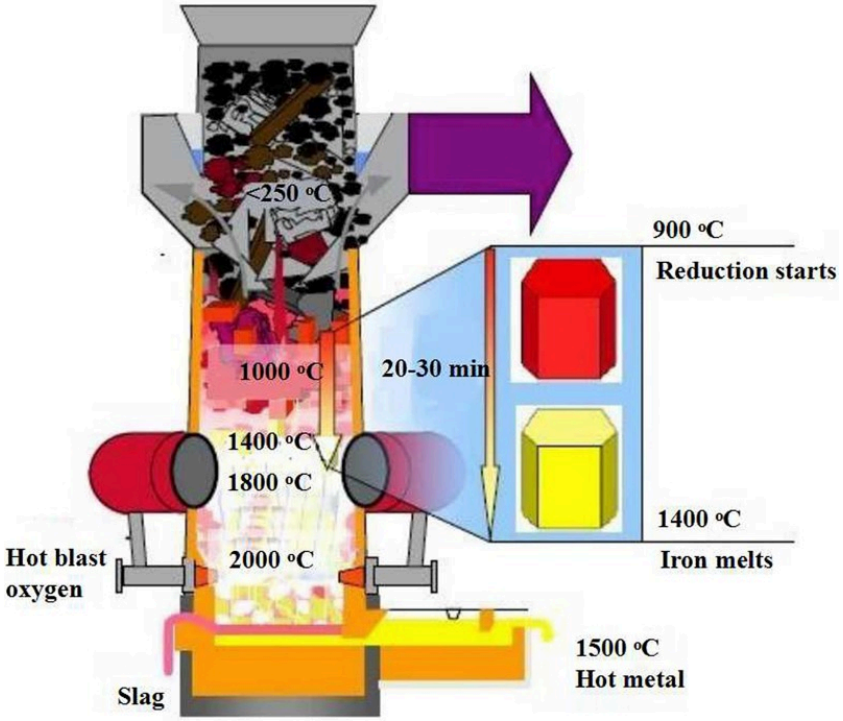

Figure 2.7: The oxycup process [10]

Firstly, the briquettes are heated up to 500°C by waste gasses. A metallic coating around the briquettes

is created which protects it from further reduction and decomposition at higher temperatures. As soon as the carbonate inside the briquette decomposes (which creates CO_2 needed for the Boudouard reaction), the reduction of the oxides inside starts. Above 1450 °C, the whole briquette should be transferred to sponge iron and it is melted afterwards.

The flue dust contains about 30% of zinc particles which is not a lot but could be considered for further processing [54].

Advantages

- Recycles both iron (DRI) and zinc
- Low amount of emissions like SO_x, NO_x and dioxines

Disadvantages

- Low quality of the zinc sludge (±30% Zn)

2.3.5. The PRIMUS process

The PRIMUS process is based on an old process: a multi-hearth furnace. The material is added at the top and drops several floors down alternatively at the centre or at the wall side, see fig. 2.8. This process has been in use with a furnace in Luxembourg and Taiwan.

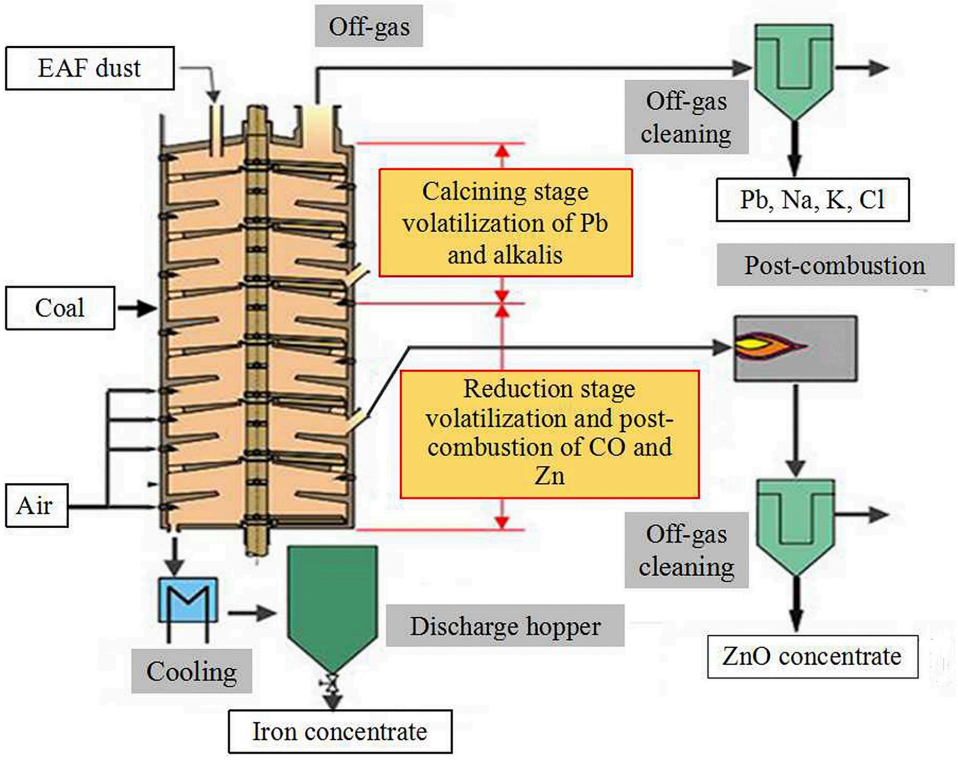

Figure 2.8: A schematic drawing of the PRIMUS process [10]

It should be able to handle EAF dust, BF dust, BOF dust, oily sludges, mill scale and iron ore as long as they are fine charging materials. It is said to be most suited for watery and oily substances because of the continuous motion of the materials. Another advantage of the mixing inside the furnace is that no premixing is required of the ingredients (coal fines and metal oxide materials). The furnace operates at 1100°C and focusses on producing direct reduced iron (DRI) with a metallised content of more that 90% (mill scale takes the longest time upon metallization). The pilot furnace based on EAF dusts is able to remove more that 95% of the zinc. An improvement was made to increase the purity of the

ZnO product by separating the evaporation processes of zinc from the evaporation of lead, alkalis and chlorine. Firstly, the dust is heated under an oxidising atmosphere at 950-1050°C in which lead, the fluorines and the alkalis will evaporate. Coal is added afterwards to reduce zinc which can be collected separately, see fig. 2.8. The single off-gas system contained about 55% of ZnO and the goal for the separation of the zinc dust was a 90% pure zinc oxide dust. It is not mentioned what purity was reached [10, 55].

Advantages[10, 56]

- Recycles both iron (DRI) and zinc
- Energy efficient because of a high degree of post combustion

Disadvantages

- Expensive

2.3.6. HIsarna

HIsarna is a combination of a Cyclone Converter Furnace (CCF) and a Smelt Reduction Vessel (SRV). The top part of the furnace belongs to the CCF, the bottom part to the SRV from HIsmelt. HIsmelt used more energy than the blast furnace [57] so a combination with the CCF is seen as the ideal solution for HIsarna. As visible in figure 2.9, the feed materials and oxygen are injected to the CCF part of the furnace. In this part, the off gas of the SRV is burned which generates heat for melting (±1450°C) and partially reduces the ore from magnetite to wüstite or iron (10-20% reduction estimated). The partially molten ore runs downwards into the SRV and dissolves directly into the slag. Slag and metal are mixed by the coal injection which is injected directly into the molten iron bath and provides enough dissolved carbon to maintain the reduction processes. Because of this mixing, there is a big interfacial area for reducing the pre-reduced iron oxides in the slag layer. This reduction is done by carbon and releases a lot of CO. Thereafter, the CO can be post-combusted in the CCF [58]. Besides iron ores, HIsarna shows a big opportunity to recycle iron wastes and scrap with a high zinc content. The zinc is directly reduced in the CCF part of the furnace and carried upwards together with the off-gas.

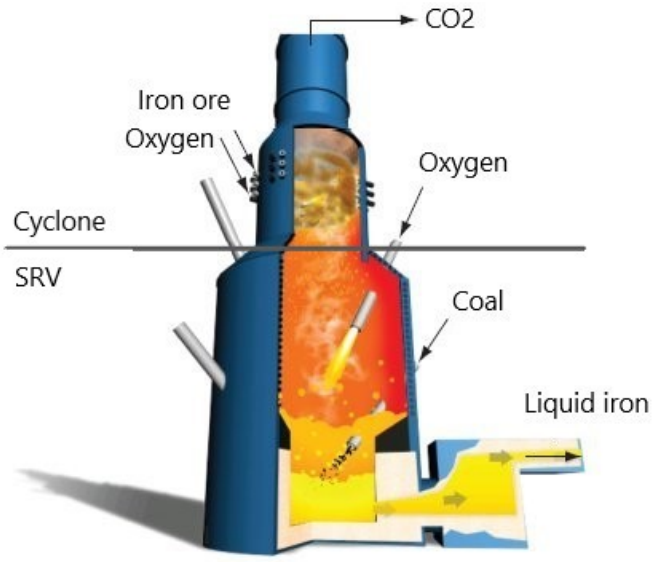

Figure 2.9: The HIsarna furnace [11]

Advantages[58, 59]

- Recovers both zinc and iron
- Low energy consumption
- Reduced air pollution
- Raw materials flexibility

Disadvantages

- Only tested on a pilot scale
- Still uncertain zinc concentration

2.4. Conclusion

This chapter described some different routes to recycle zinc bearing dusts created by the recycling of galvanised scrap in the steel industry. However, it is still not common practice to recycle dusts with a low zinc content. Especially those that have a too low zinc content to be used in the Waelz kiln while it has a too high zinc content to be recycled through common steelmaking practice. The Waelz process is the only process that is applied at a large industrial scale. However, with its drawback of only recycling zinc, it is far from optimal. Other furnaces have been developed to deal with low zinc containing steel dust but they are either expensive, difficult to operate, difficult to scale up or do not provide a zinc stream with a high enough zinc concentration. The big advantage of HIsarna is that it is an ironmaking facility and it will be optimised and made profitable for steel making. On top of that, it has a very good viability for recycling resulting in a reduced need for different furnaces and a recycling system that will be profitable in any case. To make this true, a high zinc quality needs to be guaranteed for which more development is needed. This thesis will discuss the usability of a combination of those dusts as feed material into HIsarna to recover the highest amount of zinc.

3

Research questions

This thesis focuses on the recycling of waste materials from the steel industry in HIsarna with the goal to recover the zinc and iron in a separate stream. One of the possibilities to introduce those wastes materials into the furnace is in the form of microgranulates. Different type of dusts have different properties which can be used to optimise the reduction process. This is further explained in section 4.1. The aim of this thesis is to understand the reduction and vaporisation behaviour of these microgranulates and compare the effect of different atmospheres on this behaviour with a specific focus on the removal of zinc.

How does the self reduction behaviour of zinc present in the microgranulates compare with this behaviour in an atmosphere of 50% CO and 50% CO_2?

This question is answered with the help of subquestions which are described below:

1. *What is the exact composition of the microgranulates and how could that affect the reduction behaviour?*

Research has already been done into the self-reducing behaviour of some metallurgical wastes in the form of dusts by A. Peters [60]. He proposed a combination of different dusts to optimise the reduction processes. To support the delivery into the furnace, these proposed combinations are used for the production of microgranulates instead of using loose dust.

2. *What processes take place at which temperature?*

To get a full understanding of the processes that take place in the microgranulates, it is meaningful to know how the different reactions follow each other up and at what temperature they can happen.

3. *What mechanisms take place during isothermal self reduction processes and what is its timescale?*

In order to optimise the reduction processes, it is important to know what processes use or generate energy or which ones aid the reducing or oxidising reactions. In this way, the optimal circumstances for a quick removal of zinc can be determined.

4. *Can the reduction behaviour be optimised by using different atmospheres?*

Different atmospheres can induce different reactions and alternate the reaction speed of others. Some of those reactions are preferred, others not. This thesis focuses on comparing the reduction behaviour in a nitrogen atmosphere to the behaviour in a 50% CO and 50% CO_2 atmosphere.

5. *What is the composition of the HIsarna dust and is it suitable for the zinc industry?*

The last question is about the quality of the separated zinc rich dust stream. It is essential to know in what form the zinc can be recovered and how many impurities are present. The quality of this zinc rich dust determines whether it is suitable for usage by the zinc industry.

4

Materials and experimental methods

This chapter elaborates on the requirements of the microgranulates, the atmospheres used during the experiments, the experimental setups and characterisation methods. In order the answer the questions outlined in chapter 3, the microgranulates were characterised, used in experiments and characterised again which can be seen in figure 4.1.

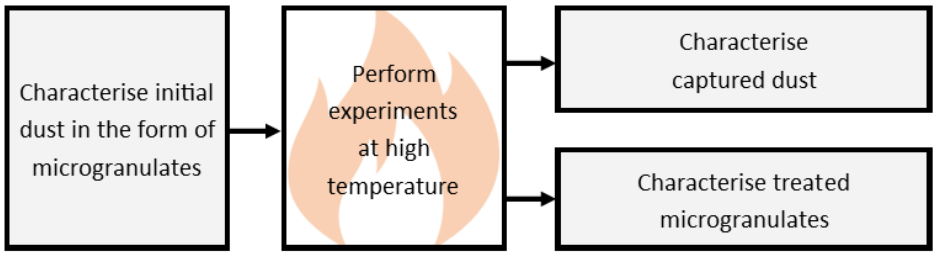

Figure 4.1: A guideline of the performed experiments and characterisations

4.1. Feed material

The dusts created by different furnaces from the steel industry contain a lot of iron, zinc and/or other impurities. Also, the dust from the BF contains a lot of carbon. By combining different dusts from different furnaces, this carbon can be used to reduce iron, zinc and other components and less carbon is needed from other carbon sources. However, adding them together to the furnace as a powder increases carryover to the off-gas system, decreases the separating abilities of the furnace and could complicate the transportation towards the furnace [61]. Besides that, it decreases the ability of the carbon to reduce elements in one of the other particles. Pelletizing the dusts is therefore a solution that was considered helpful.

Bigger particles are usually made with the help of sintering, briquetting or pelletizing. Sintering has the advantage that it does not need a binder. The bond is created by recrystallisation and partial melting (at 1300-1480°C). The disadvantage of this process is that it is not very resistant against wear and the high temperature could vaporize the zinc which is lost if not collected. Briquetting does not need additives either because the bond is created by mechanical deformation. However, it is a relatively expensive process and it needs a lot of energy. The pelletizing process uses a binder to stick the particles together. This method is mainly used for ores that need to be transported over long distances. It is important to notice that the binder needs to be burnt as well but when using a binder based on carbon it could possibly aid the reduction process. In general, a granulate should have sufficient strength to withstand

the external forces applied during transport and other handlings. Besides that, it needs a uniform size, shape, weight and has to fulfill safety regulations[62].

Multiple zinc containing waste materials can be considered as feed for HIsarna. For this thesis, BOF dust, BF dust and historical oxykalksludge (HOKS) are chosen to experiment with because of their high zinc, iron and/or carbon contents. Tatasteel IJmuiden (the Netherlands) has a landfill with 1.2 million tonnes of historical oxykalksludge which was dumped between 1975 and 1985. HOKS is a material consisting mainly of iron oxides and calcium oxides. This landfill is continually monitored and does not do any harm [63] but it would be ideal to recycle it through HIsarna and recover the valuable material. BF and BOF dust are continuously produced varying from 10-15 kg per ton hot metal and 10-20 kg per ton of liquid steel respectively [64]. BF dust is mixed with either HOKS or BOF dust as a carbon and zinc source as both elements have limited presence in HOKS and BOF. In this way, an optimal composition of iron oxides, zinc oxide and carbon can be reached. The microgranulates are produced by CRM, an R&D company with one of its focuses on the recycling of metallic materials. They used 0.25% of an organic binder called Peridur® 300D which is a long chain polyelectrolyte based on cellulose. The combustion products are water vapour and carbon dioxide which both escape together with the off gasses. The composition of the microgranulates and their naming used throughout thesis can be found in table 4.1.

Name	HOKS [%]	BOF dust [%]	BF dust [%]
Pure HOKS	100		
HOKS 80 (large)[1]	80		20
HOKS 80 (small)[1]	80		20
HOKS 76	76		24
Pure BOF		100	
BOF 85		85	15
BOF 76		76	24
Pure BOF (old)[2]		100	

Table 4.1: The microgranulate samples used for the experiments

4.2. Reducing atmospheres in HIsarna

As mentioned before, the top part of HIsarna is based on the cyclone from the cyclone converter furnace (CCF). This cyclone is added on top of the SRV. The SRV contains a molten iron bath in which the final reduction takes place. The off-gasses from the SRV have a temperature of around 1500°C and a relative high reduction potential. The composition of the off-gasses at this point can be found in table 4.2. In the cyclone, oxygen and fine iron ore are injected tangentially causing the rising gas to rotate. The oxygen stimulates post combustion causing a higher temperature but it also creates a more oxidising atmosphere. The highest gas temperature in the cyclone is estimated between 1700 and 1800°C [65]. In the cyclone, iron ore is reduced from hematite to magnetite and partially to wüstite. The iron ore melts and runs down via the wall of the furnace into the slag layer of the converter vessel in which final reduction takes place.

An advantage of the cyclone over other pretreatment steps is the direct connection to the melter. In this way, both chemical and thermal energy of the smelting gas can be used in the cyclone. The higher temperature in the cyclone causes pre-reduction degrees (PRD) of 20-25% even at a high post-

[1] large and small refers to the average size fraction of the microgranulates
[2] These microgranulates were produced a year ago and will be used to determine the effect of aging of the microgranulates

Substance	Mass%	Mols%
CO	27.61	29.89
CO_2	49.47	34.08
H_2	0.319	4.80
H_2O	11.55	19.44
H_2S	0.045	0.0402
N_2	10.70	11.58
NH_3	$6.67*10^{-06}$	$1,19*10^{-05}$
O_2	$1.85*10^{-06}$	$1.76*10^{-06}$
SO_2	0.236	0.111

Table 4.2: The composition of the off-gas of the SRV

combustion ratio (PCR) of the smelter gas, see equation 4.1 and figure 4.2.

$$PCR = \frac{CO_2 + H_2O}{CO + H_2 + CO_2 + H_2O} \tag{4.1}$$

In HIsarna, it is aimed to have zinc vaporised in the CCF part of the furnace to maximise the amount of zinc that can easily escape with the gas flow. Therefore, it is important that the composition of the granulates stimulate reduction in the atmospheres of the cyclone. This atmosphere consists of several gasses that are partly reducing and change along the trajectory the particles travel. CO and H_2 can reduce zinc oxides of the feed material by reaction 4.2 while CO_2 and H_2O can oxidise. Although the reaction with CO is less in favour than the reaction with solid carbon (reaction 4.3), it is easier because gasses move freely.

$$ZnO(s) + CO/H_2(g) \rightleftharpoons Zn(g) + CO_2/H_2O(g) \tag{4.2}$$

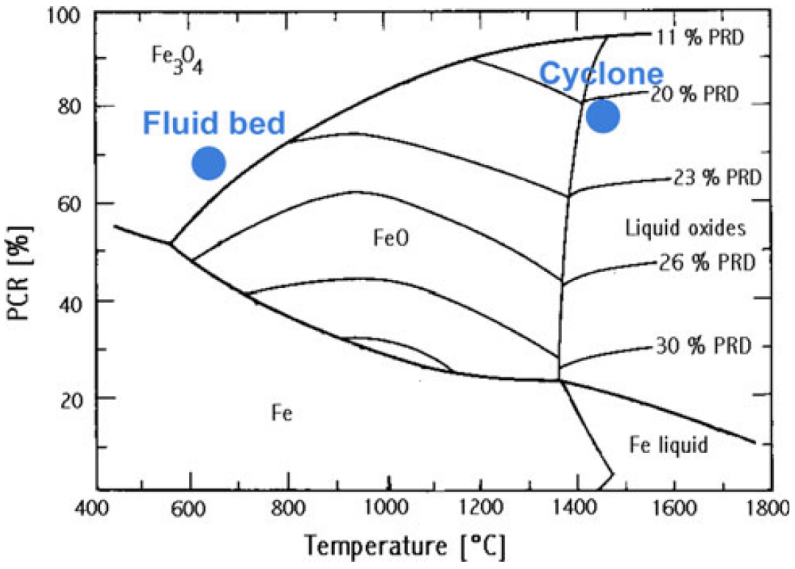

Figure 4.2: A comparision between the pre-reduction of iron ore with a fluid bed and with a cyclone [12]

$$ZnO(s) + C(s) \rightleftharpoons Zn(g) + CO(g) \tag{4.3}$$

The atmosphere in the cyclone consist of different gasses that are partly reducing and partly oxidising. It is important to understand their effect on the reactions that take place in the micrograniulates. The Baur-Gleassner diagram (figure 4.3) can give insight in the equilibrium state of the iron oxides depending on the gas composition and the temperature. The three regions of magnetite, wüstite and iron are visible. Hematite is not visible because it only needs a very small amount of CO to be reduced [13]. The diagram can give an idea about the type of reactions that could happen in HIsarna. The high temperatures in the cyclone should result in wüstite being the equilibrium phase even at a higher concentration of CO_2.

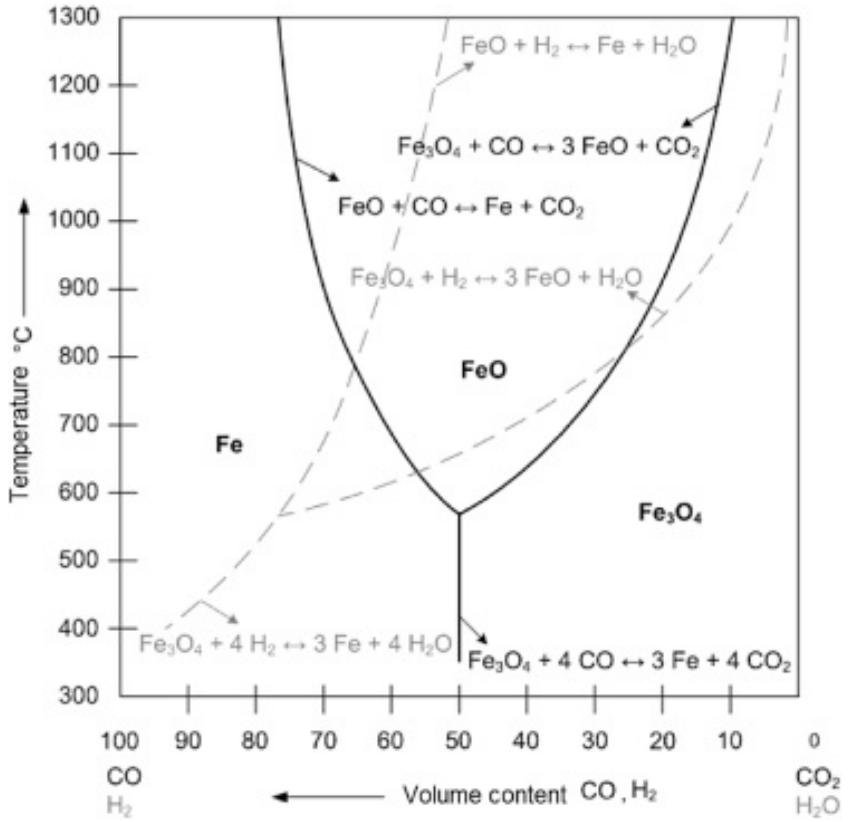

Figure 4.3: The Baur-Gleaessner diagram [13]

In this thesis, it was chosen to analyse the effect of the atmosphere consisting of 50% CO and 50% CO_2 (which has a PCR of 50) which is a very similar concentration to the off-gas from the SRV. In this way, the experiments simulate the behaviour of the micrograniulates at that specific point. According to the Baur-Gleaessner diagram, the equilibrium phase at that point is wüstite for all temperatures above 600°C. However, other elements could change this equilibrium and the extra carbon present in the micrograniulates could result in a higher reduction potential.

The effect of other elements on the reduction behaviour was researched by Lee [66]. He looked at the optimal reduction circumstances of zinc oxide. The reduction of pure dense zinc oxide increased with temperature and P_{CO} in CO/N_2 and CO/CO_2 gas mixtures. Besides that, adding 1 wt% of other oxides had either positive or negative influences on this reduction rate. CaO and MnO enhanced the reduction rate while MgO and FeO had the opposite effect in the temperature range of 900 to 1100°C. It will be shown that those four components are present in different quantities in the micrograniulates, some much more than 1%, so it is expected that they will influence the reduction of zinc oxide.

4.3. Boundaries set by industry

Another important thing to keep into account is that the feed materials into any furnace should not be detrimental for the quality of the final materials as well as the efficiency of the process and the lifespan of the production materials. Therefore, it is important to analyse whether the waste materials can be processed in the furnaces. A problem for any pyrometallurgical (steel)maker are impurities that are more noble than the required material. For iron, metals like copper cannot be removed to the slag because it will oxidise later than iron itself. A small amount of copper is not a big problem but increasing recycling rates can build up the amount of unwanted impurities. Copper, but also elements like sulphur and phosphorous are unwanted in the final steel because it makes the material more brittle.

A problem for the hydrometallurgical zinc industry is the existence of halides. The problem with ZnCl is that it can form the insoluble basic zinc chloride when it comes into contact with water, see reaction 4.4 [67]. Besides that, chloride and fluoride cause problems like corrosion of the aluminium cathode which reduces the productivity [68].

$$\mathrm{ZnCl_2 + ZnO + H_2O \rightarrow 2ZnOHCl} \tag{4.4}$$

Zinc ferrite is another compound that is difficult to leach. It has a very stable spinel structure and requires very harsh, expensive treatment in order to be leached. Therefore, the formation (reaction 4.5) of these compounds in the zinc rich dusts should be detected, analysed and reduced. About half of the zinc in EAF dust is present as zinc ferrite and it is said that large contact areas between the zinc ferrite and hematite as well as an increased temperature stimulates the forming of the zinc ferrites [69]. The standard Gibbs free energy is always in favour of the formation of zinc ferrite but the atmosphere should be oxidizing enough to be in favour of the formation of hematite.

$$\mathrm{ZnO + Fe_2O_3 = ZnFe_2O_4} \qquad \Delta G^{\circ}_{1000} = -28.05\,\mathrm{kJ} \tag{4.5}$$

4.4. Experimental setup

To get a total overview of the behaviour of the microgranulates, experiments are done with a Netzsch STA 409 cell TGA furnace (fig.4.4), a horizontal furnace (fig. 4.5a) and a vertical TGA furnace (fig. 4.7a).

4.4.1. Thermo gravimetric analysis

The TGA is used to determine what separate reactions could take place along an increase in temperature and to estimate the amount of mass loosing compounds present in the microgranulates. To achieve this, all microgranulates have been analysed under an inert atmosphere (nitrogen). The microgranulates were heated from room temperature up to 1400°C with a heating rate of 5°C/min after which it stayed on 1400°C for 20 minutes more to make sure no more mass loss occurred. About 50 mg of the microgranulates was placed in a small alumina crucible with a second empty crucible as a reference. To make sure this sample represents the average material properties, a bigger batch of at least 2 grams was ground and mixed of which a small scoop was used for analysis.

4.4.2. Horizontal furnace

The horizontal furnace is used to determine the isothermal properties of the microgranulates at 1000°C and 1300°C and in different atmospheres: an inert atmosphere (nitrogen) and an atmosphere of 50% CO and 50% CO_2. All microgranulates have been tested at 1000°C under an inert atmosphere. Only

Figure 4.4: The TGA furnace at TU Delft

two microgranulates (HOKS 80 (small) and BOF 76) were heated at 1300°C and in the CO/CO_2 atmosphere.

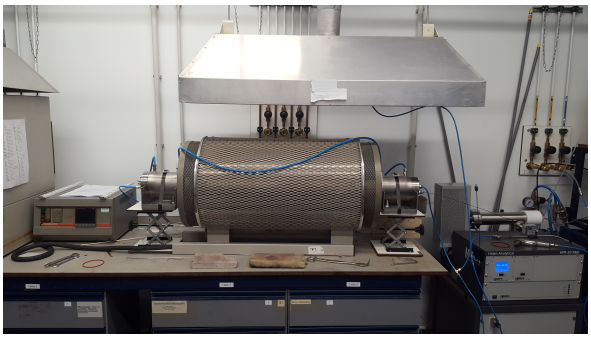

(a)

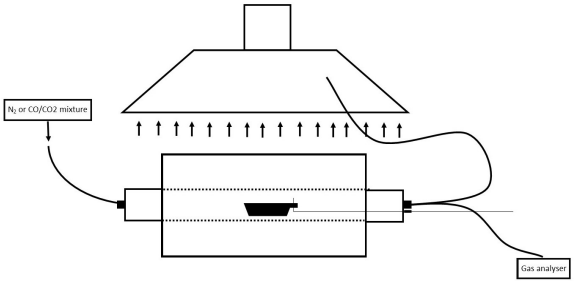

(b)

Figure 4.5: The horizontal furnace

The heating element of the horizontal furnace is in the middle, resulting in a gradient in temperature that is the hottest in the middle part. Although the programming temperatures were 1000°C and 1300°C, the actual temperature appeared to be slightly lower. At a programmed temperature of 1000°C, the hot zone was 960°C $\pm$ 4°C and at a programmed temperature of 1300°C, the hot zone was 1268°C $\pm$ 3°C, both ranging over a distance of 10 cm in the middle of the furnace, see figure 4.6.

An alumina tube was positioned horizontally in which an alumina crucible could be moved towards the centre. This was done with the help of a molybdenum wire attached to a hole in the crucible as can be seen in figure 4.5b. The crucible was filled with 5-6 grams of microgranulates for the 1000°C experiments. 6 samples were taken at 1, 2, 5, 10, 20 and 30 minutes inside the furnace. In this way, a graph could be made from the loss of mass and elemental concentrations after different time spans inside the furnaces.

At 1300°C, some of the microgranulates seemed to melt with the result that smaller crucibles were chosen to not waste the bigger crucibles. Two smaller crucibles, next to each other placed inside a bigger crucible, each containing around 2.5g, supplied the necessary amount for characterisation. At

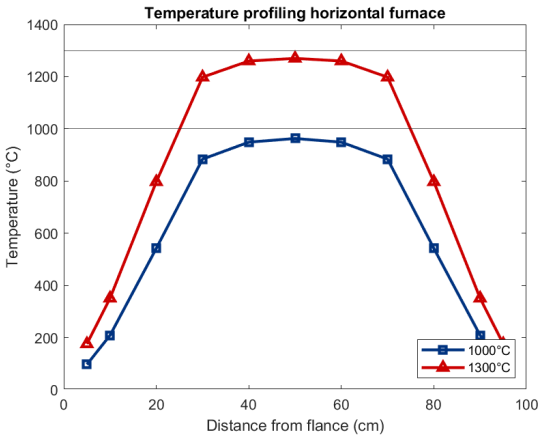

Figure 4.6: The temperature profile of the horizontal furnace at 1000°C and 1300°C of which the temperature in the middle 10 cm show 960°C $\pm$ 4°C and 1268°C $\pm$ 3°C respectively.

1000°C, a slow but continuous movement was made to push the crucible in the middle of the furnace by the wire. This took about 30 seconds. Due to a higher increase in temperature towards 1300°C, the crucible was stopped halfway for 10 seconds to create more time to adjust to the new temperature and therefore decreasing the chance for fracture. For all experiments, a gas flow of 0.5L/min was used.

4.4.3. Vertical TGA furnace

This large scale TGA furnace has the advantage that the experiments can be done in larger quantities and therefore showing a more representative result. Next to this, the experiments can also be performed in different atmospheres. The furnace has a balance on top that measures the weight change during the experiments. An alumina crucible with the sample material hung on an alumina stick that was connected to that balance, see figures 4.7.

(a)

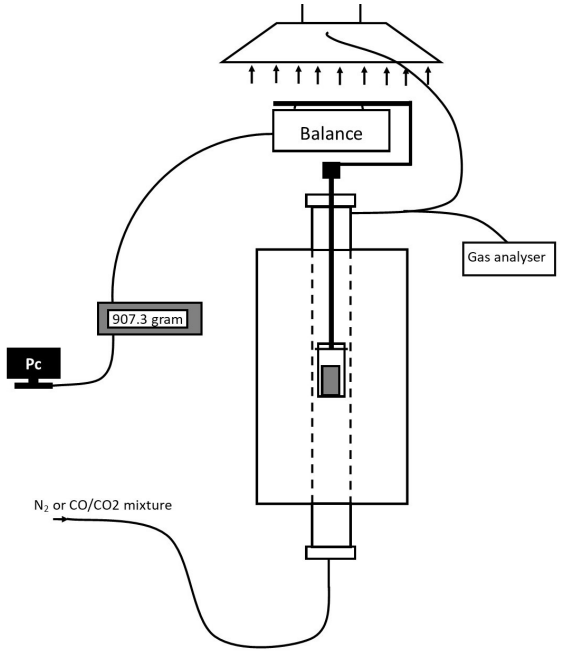

(b)

Figure 4.7: The vertical furnace

A temperature profile in the tube was made at different programmed temperatures to determine the position of the highest temperature, see figure 4.8. The distance was measured from the top of the cooled flanch downwards. At 1000°C, the high temperature range was from 62-75 cm. At 1300°, the range of high temperature changed slightly to 64-79 cm and at 1500°C, the hottest part was from 59 to 77 cm. The hanging crucible is positioned in such a way that the bottom was at a depth of 67 cm and the crucible was filled with a maximum height of 8 cm. This resulted in a temperature of 997 $\pm$6°C, 1302 $\pm$1°C and 1502 $\pm$2°C at a programmed temperature of 1000°C, 1300°C and 1500°C respectively.

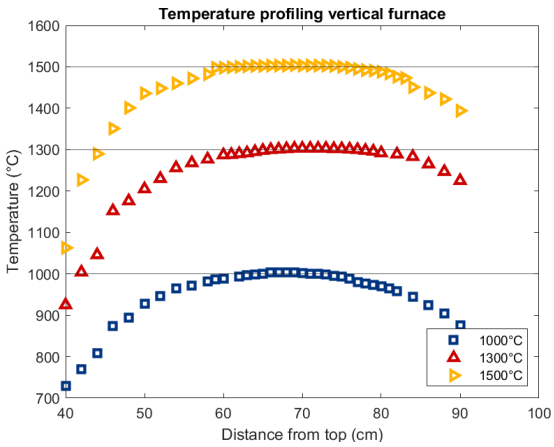

Figure 4.8: The temperature profile of the vertical furnace with a temperature of 997 $\pm$6°C, of 1302 $\pm$1°C and of 1502 $\pm$2°C at a programmed temperature of 1000°C, 1300°C and 1500°C respectively in the zone from 67-75 cm.

A smaller crucible filled with ±70 grams of material was put inside a bigger crucible to make sure the bigger crucible could be used multiple times. A gas flow of a total of 1L per minute was maintained for all tests. The furnace was heated with 10°C/min from room temperature till 700°C after which the heating rate was decreased to 3°C/min until 1500°C. Directly after, the temperature was brought back to room temperature with a rate between 1 and 2°C/min after which the sample could be analysed. During some of the experiments, a water bottle was connected in between the tubing towards the gas analyser to reduce the amount of dust towards the gas analyser and to capture the dust for further analysis. A detailed step-by-step procedure about the usage of the furnace is written below:

1. Check whether all tubing are properly connected, for example towards the fume hood and the off-gas analyser.

2. Weight the amount of sample material in a crucible that fits inside the larger crucible. This to make sure the larger crucible can be used multiple times.

3. Insert the small crucible inside the larger crucible and connect it to the rod. The sample can very carefully be positioned inside the tube of the vertical furnace. To ease the connection process, another tube can be positioned at the lower half of the furnace on which the crucible can rest.

4. The heavy top of the flange can be slid over the rod and should be tightly connected with the bolts. A rubber ring should be present in between.

5. Put the balance and the fume hood in position. Turn the balance on and let it calibrate. After calibration, the rod can be connected to the balance arm in such a way that the crucible is hanging (2-3 cm above the tube it was standing on).

6. Check whether the rod does not touch the sides of the furnace. This can be felt as scraping to the sides of the furnace when carefully turning the rod. Also, the balance should give a stable value when not scraping any sides. This value should be around 770 grams (the mass of the rod and bigger crucible) plus the mass of the smaller crucible and the sample.

7. Turn on the gas analyser, connect the balance to the computer so its readings can be saved and double check the leak tightness of the gas tubing. Connect a CO detector on top of the furnace during the whole experiment when using reducing gasses.

8. Make sure the gasses have reached an equilibrium before starting the experiment.

9. Program the temperature of the furnace. Check the starting time and temperature so the temperature can be connected to the readings of the balance and the off-gas analyser.

10. The moment that the furnace has reached its maximum temperature, no reducing gasses are needed any more so the gas flow can be changed to nitrogen. Also, the readings of the balance and off-gas analyser can be saved and the apparatus can be switched off.

11. After cooling down, the removal of the sample goes following the same steps but in opposite direction. When removing the crucible, be sure to place some paper towel on a table as there will be a lot of dust attached to it. This can be recovered for analysis if desired.

12. Weight the sample to determine its final weight loss. Now, the sample can be removed from the crucible and analysed for further characterisation.

13. Clean the furnace after each use as a lot of dust is collected at the sides.

The first trial tests showed that a methodology should be developed to produce more accurate results. Based on these trials, a couple of things were detected to influence the balance measurements: the crucible should not touch the sides of the alumina tube as this affects the measurement of the balance, the buoyancy effect of the gasses needs to be taken into account as its density changes with increasing temperature and the high temperature may influence the readings of the balance. The effects of those improvements can be seen in figure 4.9. The last measurement shows a much more stable line with a smaller deviation. To eliminate the buoyancy effect, a base line was created that can be subtracted from the final results. This base line is created with the same gas flow (1 L nitrogen per minute) and heating rates but with an empty crucible. This base line can be seen in figure 4.10 and as expected increases with temperature. After 700°C, the weight stabilises but fluctuates. The black line 'Average' is the average of the three tests and used to subtract from the data derived with samples. The black line in figure 4.9 shows the result with the subtraction of that base line.

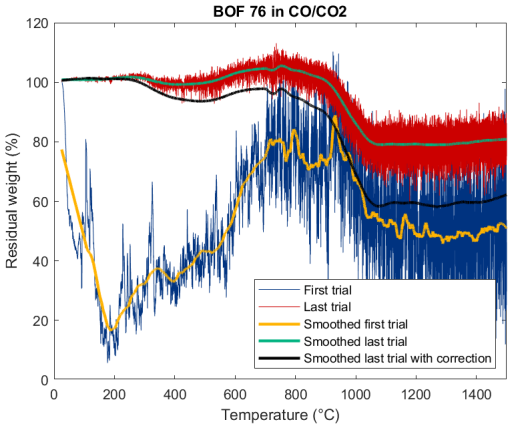

Figure 4.9: The difference between the first trial and an improved last trial in the vertical TGA furnace.

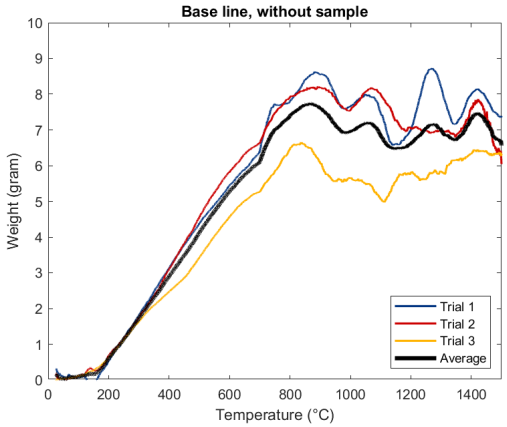

Figure 4.10: Balance base line for the vertical furnace used to correct for the buoyancy effect.

4.5. Characterisation methods

Different analytical methods are used to analyse what has happened at the high temperatures.

- **Weight loss determination**
  The masses of the samples are determined with a scale before and after each experiment to provide insight in the speed of the reduction of volatile components in the case of the horizontal furnace. For both TGA furnaces, the weight is measured during the experiment as well.
- **Morphology and phase determination**
  This was analysed using two types of SEMs. SEM 1 :a Jeol JSM 6500F Scanning Electron Microscopy - Electron Dispersive X-ray Spectroscopy (SEM/EDS) or SEM 2: a smaller JSM IT100. The phases were also determined with a Bruker D8 Advance diffractometer (XRD)
- **Chemical composition**
  This was analysed with a Pananalytical Axios Max WD-XRF spectrometer for most of the elements. The carbon content was measured with a LECO CS 744.
- **Off gas analysis**
  The gasses leaving the furnaces are analysed either using a mass spectrometer, a Hiden Analytical HPR-20 R&D or using a K1550 airTOX gas photometer GPM.

4.6. Error determination

Because the tests in the horizontal furnace are done on a very small scale (<6g), it is important to know how reliable those tests are. Section 5.1 will show that there is quite some difference in composition between the different microgranulate sizes. Keeping this in mind, it is expected that the composition will be the largest uncertain factor as there was only the possibility to run every test once due to time constraints. One sample, namely BOF 76, was ran three times for 5 minutes at 1000°C showing an average reduction of 17.8% with a standard deviation of 1.12%.

Also, the effect of the amount of material was determined with BOF 76 in a nitrogen atmosphere at 1300 °C, see table 4.3. Visible is that more material experiences a slower reduction process while the final weight loss is the same. More tests are needed to determine the effect of speed towards the middle of the furnace as the temperature gradually increases and therefore the potential to start reactions.

BOF 76	6.6 ±0.3 g	2.8 ±0.1g
1 min	11.5	14.5
2 min	18.0	24.8
5 min	34.9	35.3

Table 4.3: The effect of the amount of material on the reduction degree (%)

Three tests have been done with BOF 76 in the vertical furnace to check the reproducibility of those results. The mass of the samples was 78.8$\pm$5.8. They had an average reduction of 35.7% with a standard deviation of 1.88%, measured with the same scale before and after analysis.

The balance readings from two of those tests can be seen in figure 4.11. All results are corrected with the base line and smoothed. At the beginning, the samples show very similar weights. However, there was an extra peak at 730°C in the first trial and the reduction seems to continue longer causing a much higher weight loss. This first peak could be caused by a build up of gasses released during the reactions but more research is needed to eliminate this. To check the viability of the base line subtraction, the maximum weight loss measured by the TGA balance (the difference between an average of the first 50 data points and the last 50 data points) minus the base line is compared to the measurements of a separate scale before and after treatment. Table 4.4 shows this from 5 different samples. Except for BOF 76 N_2 (1), which is the same trial (1) as in figure 4.11, much better results are shown with the base line subtraction.

When looking with more detail to the off-gas analysis of three different BOF 76 samples in nitrogen

Sample	Separate scale (%)	TGA balance (%)	TGA balance with baseline subtracted (%)
BOF 76 N_2 1	37.1	38.7	46.7
BOF 76 N_2 2	36.9	30.3	37.7
BOF 76 N_2 3	36.8	26.7	35.3
HOKS 80 (small) PCR 50	29.6	19.2	27.4
HOKS 80 (small) N_2	30.4	20.4	28.9

Table 4.4: A comparison between the readings from the TGA balance and a separate scale to determine the suitability of the base line subtraction

in figure 4.12, it can be seen that the peaks follow each other quite neatly (The peaks are scaled to each others sizes). The biggest difference is the peak around 800°C which is very small for the sample shown as a full line compared to the other two.

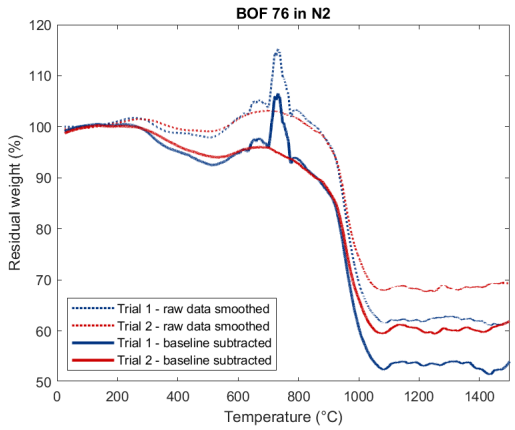

Figure 4.11: Balance results of two samples from BOF 76 corrected with the base line.

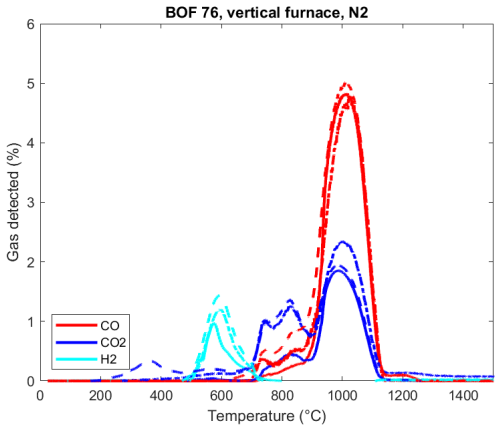

Figure 4.12: Detected gas of three samples from BOF 76 in N_2.

5

Results and discussion

This chapter shows the results obtained by the experiments in the small TGA, the horizontal furnace and the vertical TGA furnace as well as all characterisation done before and after the experiments.

5.1. Initial characterisation of the samples

The microgranulates are made from either HOKS or BOF dust combined with different concentrations of BF dust. HOKS and BOF dust contain a lot of iron while BF contains both zinc and carbon. The average composition of the microgranulates, measured with XRF, can be found in table 5.1.

	Pure HOKS	HOKS 80 (large)	HOKS 80 (small)	HOKS 76	Pure BOF (old)	Pure BOF	BOF 85	BOF 76	BF dust [60]
Fe_2O_3	56.93	54.21	52.87	53.54	82.51	81.68	74.45	70.97	35.36
SiO_2	9.22	8.27	8.87	8.44	1.35	1.67	2.68	3.30	3.25
CaO	25.65	20.88	19.14	19.41	9.63	9.65	7.97	7.08	2.32
ZnO	1.22	2.16	2.57	2.40	0.52	0.54	1.35	1.73	6.22
Al_2O_3	0.93	1.68	1.83	1.82	0.13	0.16	0.70	1.03	1.96
MgO	1.26	1.52	1.41	1.45	1.62	2.00	1.92	1.82	0.70
C	2.19	7.19	8.52	8.59	2.64	2.55	8.07	10.50	39.90
SO_3	0.25	1.15	1.24	1.24	0.10	0.16	0.89	1.25	1.63
MnO	0.92	0.77	0.75	0.76	0.93	0.94	0.83	0.79	
PbO	0.23	0.44	0.47	0.47			0.25	0.35	1.64
Total	88.7	89.7	100.2	90.8	109.5	95.7	91.9	90.6	91.7

Table 5.1: The composition of the microgranulates measured with XRF as oxide. Carbon is measured with LECO

Iron oxide, silica and calcium oxide are the elements present in the highest concentration with calcium oxide and silica being clearly more present in HOKS than BOF dust. Zinc is mostly present in BF dust and in small amounts in HOKS and BOF dust. BF dust is the biggest carbon source with almost 40% carbon. Lead is detected in BF dust but only very little in HOKS and no presence was found in both pure BOF microgranulates. Cadmium is an element that can be present as trace element based on other papers [70], [71] and Peters [60] detected its presence in BF dust once as well. This thesis does not mention any cadmium at all but its presence has been detected in only two of the many samples.

Once in HOKS 80 (small) (3.6%) and a single time in BOF 76 (4.7%). Those values are not negligible and give the expectation that a few, but big cadmium particles are present in the microgranulates.

5.1.1. The effect of size on its composition

To obtain a better idea about the homogeneity of the samples, the differences between the size fractions were analysed. This showed that the composition especially varied in the HOKS samples. The particle size distribution of the HOKS microgranulates is measured by CRM, see figures 5.1 and 5.2. To gain information about the different compositions of some size fractions, they were separated by sieves in three or four size fractions and analysed with XRF, XRD and LECO.

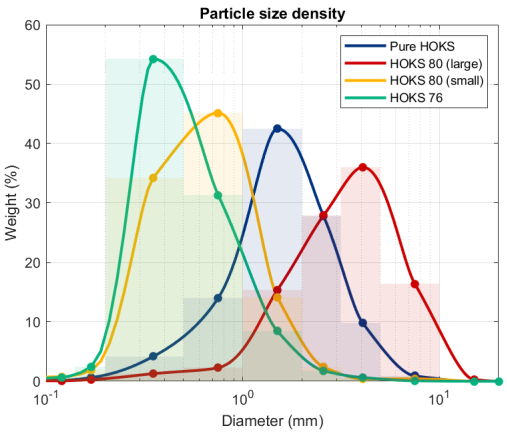

Figure 5.1: The size distribution of the microgranulates measured by CRM

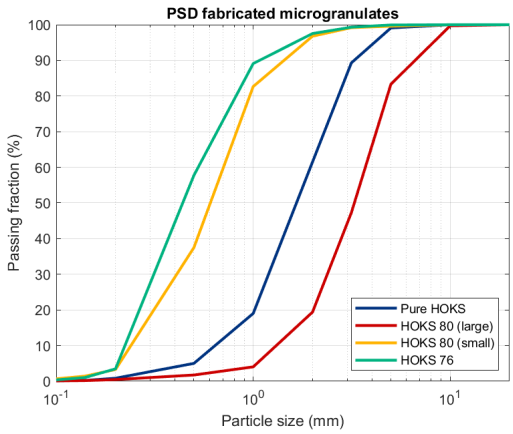

Figure 5.2: The cumulative distribution function of the four HOKS samples. D50 are 1.70 mm, 3.27 mm, 0.60 mm, 0.44 mm for respectively pure HOKS, HOKS 80 (large), HOKS 80 (small) and HOKS 76 [14].

In general, the BOF microgranulates show only a small difference between the size fractions while the HOKS microgranulates show a clear increase of iron concentration with increasing size and a silica content that decreases with increasing size which can be clearly seen in figure 5.3. The SEM image in figure 5.4 shows that many small particles in the HOKS samples consist of almost purely silica.

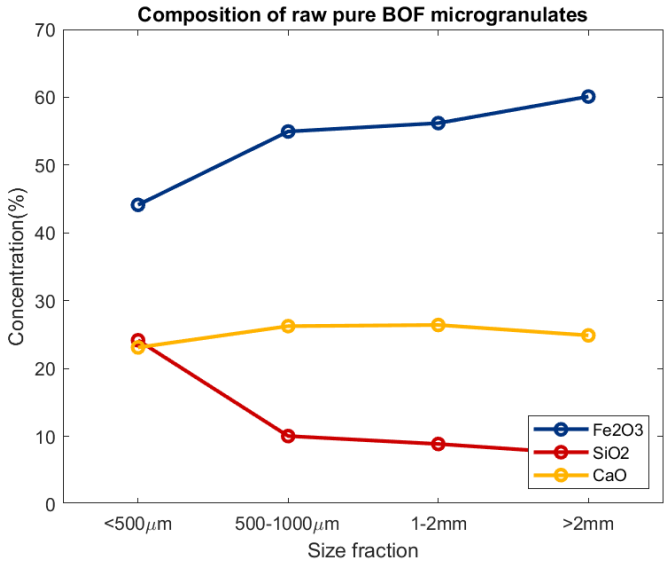

Figure 5.3: The concentration of different elements in different size fractions of pure HOKS measured with XRF as oxides

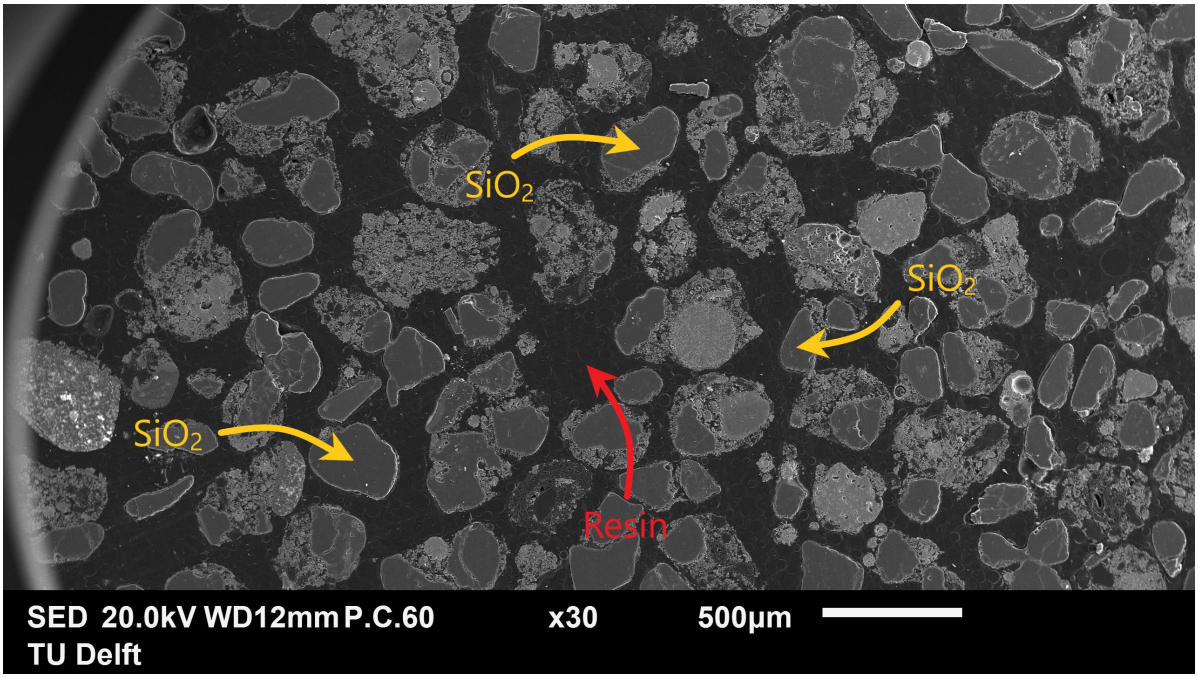

Figure 5.4: A micrograph of many microgranulates of HOKS 80 (small). The background resin is black. The dark phases in the particles present silica and are often particles on its own.

The most important constituents for this thesis are zinc, carbon and iron. Therefore, it is most interesting to see the distribution of those elements over the size fractions which is shown in figures 5.5. It is clearly visible that the iron content increases with size for all samples. The BOF samples show a small but consistent reduction in the amount of zinc and carbon with increasing size. This decrease in zinc and carbon content and increase of iron in coarser fractions is also seen by Cantarino [72] in BOF sludge. The HOKS samples show more variability between the size fractions but it can be said that the bigger HOKS microgranulates (pure HOKS and HOKS 80 (large)) show a slightly more constant concentration compared to the smaller microgranulates.

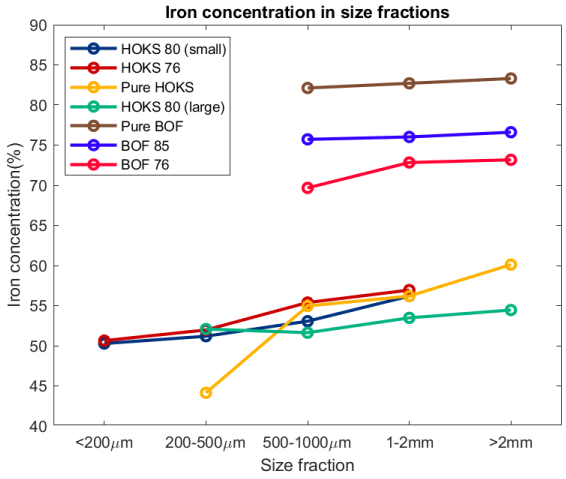

(a) Measured as Fe_2O_3-equivalent with XRF

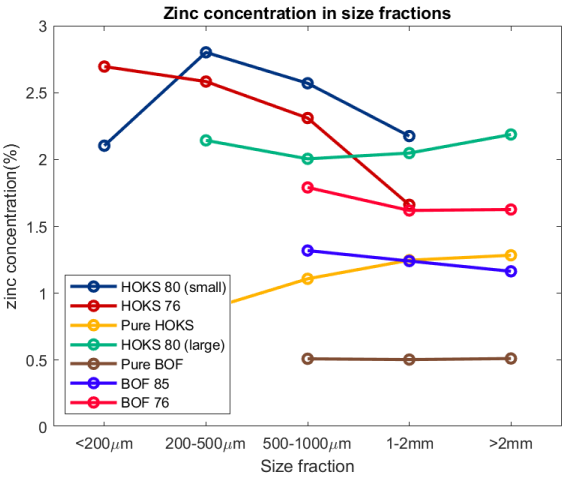

(b) Measured as ZnO with XRF

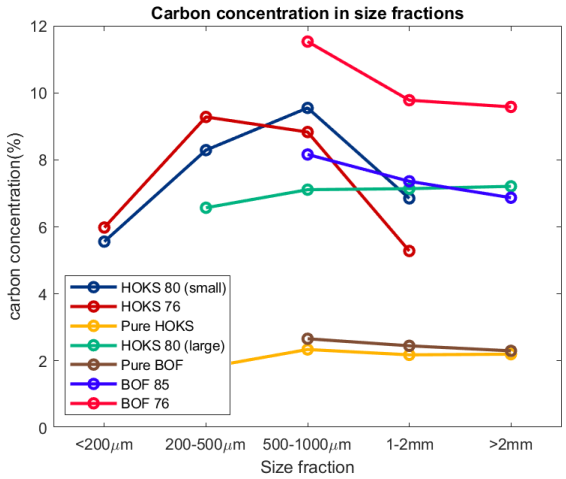

(c) Measured with LECO

Figure 5.5: The concentration of different elements depending on the size fractions

5.1.2. The phases present in the different microgranulates

XRD was used to determine the phases in the microgranulates. In figure 5.6, the diffractograms of the BOF microgranulates can be found. They contain high amounts of iron and wüstite and low amounts of magnetite, hematite and calcite. Besides, the microgranulates with added BF show an increasing amount of carbon due to its high content in the BF dust. No significant difference can be found between BOF old and pure BOF. It could have been expected that some oxidation would take place during the year of storage but the older pure BOF microgranulates even show a higher amount of metallic iron than the amount of wüstite compared to the new BOF sample.

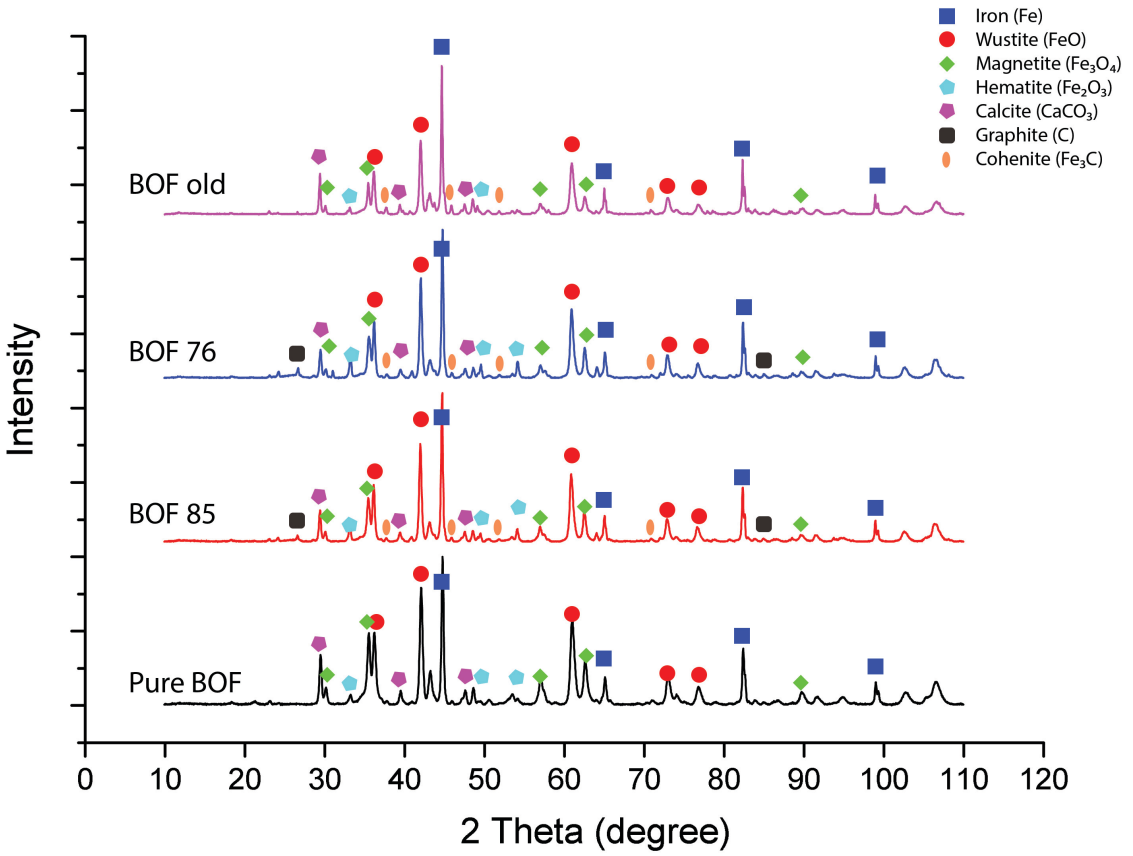

Figure 5.6: XRD diffractograms from the BOF microgranulates

The diffractograms from the HOKS samples can be found in figure 5.7. Those diffractograms show many more different phases than the BOF. The high silica content is directly remarkable as well as the higher oxidation states of the iron (magnetite and hematite). XRF showed a large amount of calcium in the HOKS which is next to calcite also present as portlandite, calcium iron oxide carbonate hydrate and possibly fairchildite. It can be said that the zinc in the samples mixed with BF dust is partly present in the form of zinc oxide, partly in the form of wurtzite (ZnS) [60].

Based on these phases, possible reduction reactions were determined and calculated with HSC chemistry 6. Those equations can be found in table 5.2 as well as the standard Gibbs free energy at 1000°, 1300°C and 1500°C, whether the enthalpy is positive or negative ($\Delta H°$) and at what temperature the reaction starts to happen based on the moment $\Delta G°$ switches sign ($T_{change\Delta G°}$).

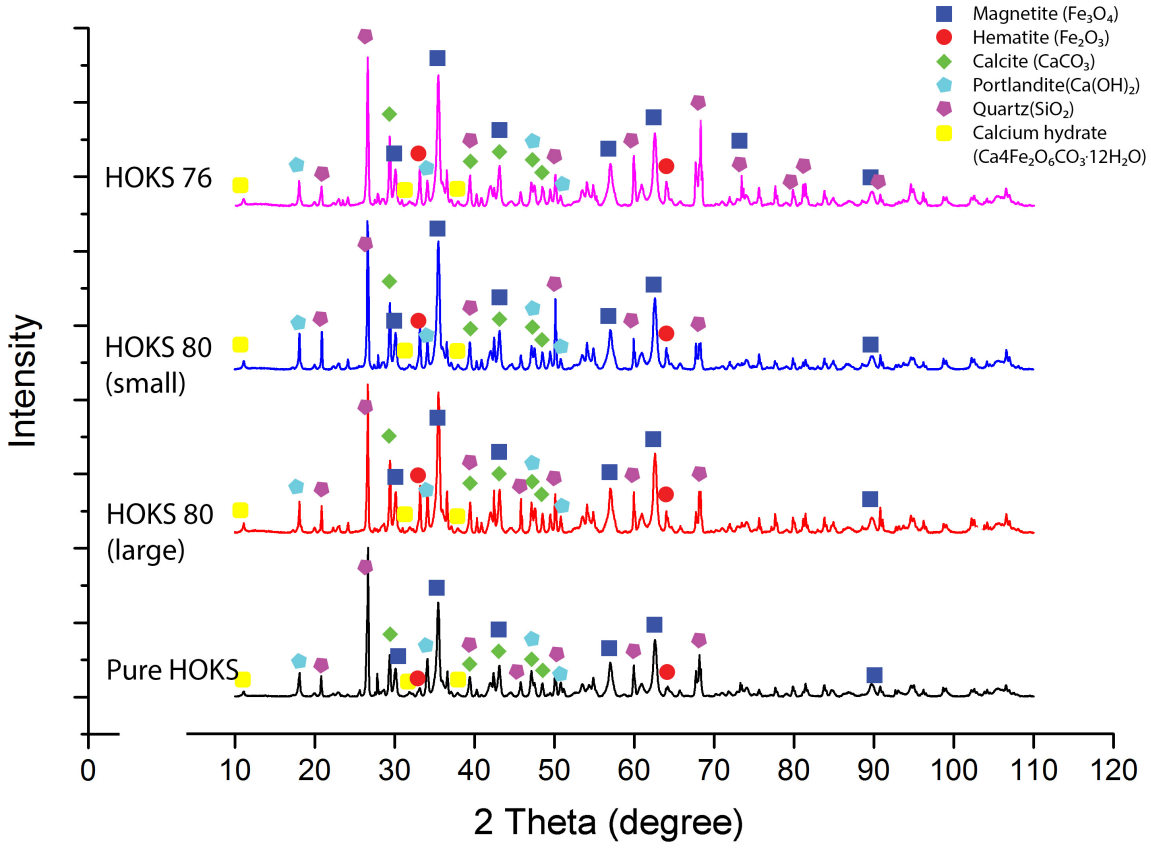

Figure 5.7: XRD diffractograms from the HOKS microgranulates

Formula	$T_{change\Delta G^\circ}$	ΔH°	$\Delta G^\circ_{1000°C}$	$\Delta G^\circ_{1300°C}$	$\Delta G^\circ_{1500°C}$
$CaO + Fe_2O_3 \longrightarrow CaFe_2O_4$	-	<0	-36.96	-43.15	-58.40
$2\,CaO + Fe_2O_3 \longrightarrow Ca_2Fe_2O_5$	-	<0	-36.96	-43.15	-58.40
$3\,Fe_2O_3 + CO(g) \longrightarrow 2\,Fe_3O_4 + CO_2(g)$	-216°C	<0	-113.93	-131.75	-143.21
$ZnS + O_2(g) \longrightarrow Zn(g) + SO_2(g)$	-21°C	>0	-136.88	-174.28	-198.76
$3\,Fe_2O_3 + C \longrightarrow 2\,Fe_3O_4 + CO(g)$	296°C	>0	-166.21	-235.48	-280.87
$Ca(OH)_2 \longrightarrow CaO + H_2O(g)$	518°C	>0	-49.79	-71.59	-84.42
$Fe_3O_4 + CO(g) \longrightarrow 3\,FeO + CO_2(g)$	529°C	>0	-6.70	-11.40	-20.19
$CaCO_3 + ZnS \longrightarrow CaS + ZnO + CO_2(g)$	665°C	>0	-94.99	-188.40	-254.50
$2\,CaCO_3 + Fe_2O_3 \longrightarrow Ca_2Fe_2O_5 + 2\,CO_2(g)$	665°C	>0	-103.07	-191.48	-245.04
$Fe_3O_4 + C \longrightarrow 3\,FeO + CO(g)$	686°C	>0	-58.96	-115.13	-158.15
$C + CO_2(g) \longrightarrow 2\,CO\,(g)$	700°C	>0	-52.27	-103.73	-137.66
$FeO + C \longrightarrow Fe + CO(g)$	720°C	>0	-43.26	-88.80	-116.86
$2\,FeO + Fe_3C \longrightarrow 5\,Fe + CO_2(g)$	738°C	>0	-31.77	-68.70	-89.52
$3\,CaFe_2O_4 + C \longrightarrow 3\,CaO + 2\,Fe_3O_4 + CO(g)$	763°C	>0	-55.31	-106.04	-105.66
$PbO + C \longrightarrow Pb(g) + CO(g)$	765°C	>0	-62.32	-136.47	-184.87
$PbO + CO(g) \longrightarrow Pb(g) + CO_2(g)$	876°C	>0	-10.05	-32.73	-47.21
$CaCO_3 \longrightarrow CaO + CO_2\,(g)$	887°C	>0	-16.17	-59.60	-80.32
$ZnO + C \longrightarrow Zn(g) + CO(g)$	949°C	>0	-15.15	-101.70	-158.62
$CaO + ZnS + C \longrightarrow CaS + Zn(g) + CO(g)$	988°C	>0	-3.60	-90.88	-148.47
$ZnO + Fe \longrightarrow Zn(g) + FeO$	1206°C	>0	28.12	12.91	-41.75
$3\,Ca_2Fe_2O_5 + C \longrightarrow 6\,CaO + 2\,Fe_3O_4 + CO(g)$	1262°C	>0	45.98	-6.63	-27.66
$ZnO + CO(g) \longrightarrow Zn(g) + CO_2(g)$	1318°C	>0	37.12	2.03	-20.96
$Fe + ZnS \longrightarrow FeS + Zn(g)$	1350°C	>0	50.21	7.14	-24.69
$MnO + C \longrightarrow Mn + CO(g)$	1402°C	>0	66.79	17.42	-17.04

Table 5.2: Possible reactions happening in the microgranulates calculated with HSC chemistry 6. ΔG° are in kJ

5.2. Non-isothermal weight change and self-reduction behaviour

All microgranulate are heated in the small TGA. At first the pure HOKS and pure BOF microgranulates are compared in figure 5.8. Similar to the research done by Ahmed [73], it is expected that the weight loss below 400°C (point 1. in figure 5.8) is due to the evaporation of excess water (mainly below 100°C) and the loss of chemical bound water by among others the calcium salt hydrate in HOKS which was detected by XRD.

Around 400°C (point 2.), a clear weight loss occurs in the HOKS sample which was detected as the decomposition of Portlandite (reaction 5.1) which is present in HOKS but not in BOF. Around 600°C (point 3.), all microgranulates have a large decrease in weight which is due to the decomposition of Calcite (reaction 5.2).

$$\mathrm{Ca(OH)_2} \longrightarrow \mathrm{CaO + H_2O\,(g)} \tag{5.1}$$

$$\mathrm{CaCO_3} \longrightarrow \mathrm{CaO + CO_2(g)} \tag{5.2}$$

At the end of the temperature range, a last weight loss is seen, especially for pure BOF (old) just below 1200°C. At this temperature, iron starts to melt which could result in either the release of captured gas or carbon having access to parts of the material that could still be reduced.

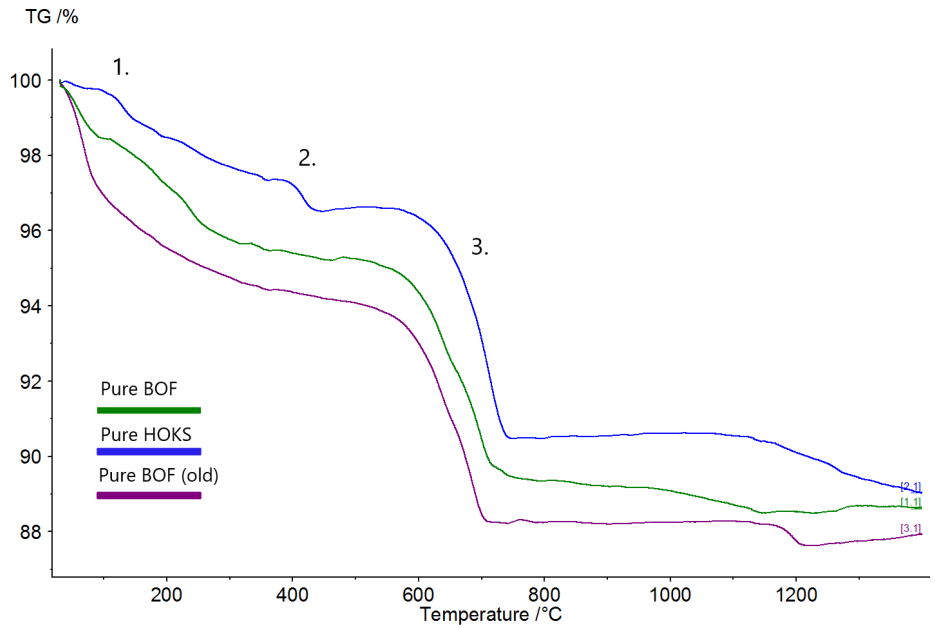

Figure 5.8: TGA results of the pure microgranulates

The results of the four HOKS samples and the four BOF samples can be seen in figure 5.9 and 5.10 respectively. The mixed microgranulates show the same behaviour as the pure microgranulates below 800°C. However, from this temperature on, a strong deviation with the non-blast furnace dust containing microgranulates becomes visible (point 4). This deviation is due to the carbon in the BF dust which is able to reduce more oxides and leaves the sample as CO or CO_2. A couple of substances have the ability to be reduced in this temperature range of 870-1020°C for the BOF samples and up to a temperature of 1150°C for the HOKS samples. For the BOF-BF microgranulates, this slope is mainly caused by the reduction of magnetite and wüstite. However, the reduction takes much longer for the HOKS microgranulates as the speed decreases around 1000°C. The next section will show that the high calcium oxide content of HOKS causes the formation of different calcium ferrites. It is expected that the reduction of those calcium ferrites happen to be slower than the reduction of the pure iron

oxides, for example through reactions 5.3 and 5.4 that have an onset temperature of 763°C and 950°C respectively. However, more work is needed for a full explanation.

$$3\,CaFe_2O_4 + C \longrightarrow 3\,CaO + 2\,Fe_3O_4 + CO\,(g) \tag{5.3}$$

$$3\,CaFe_2O_4 + CO\,(g) \longrightarrow 3\,CaO + 2\,Fe_3O_4 + CO_2(g) \tag{5.4}$$

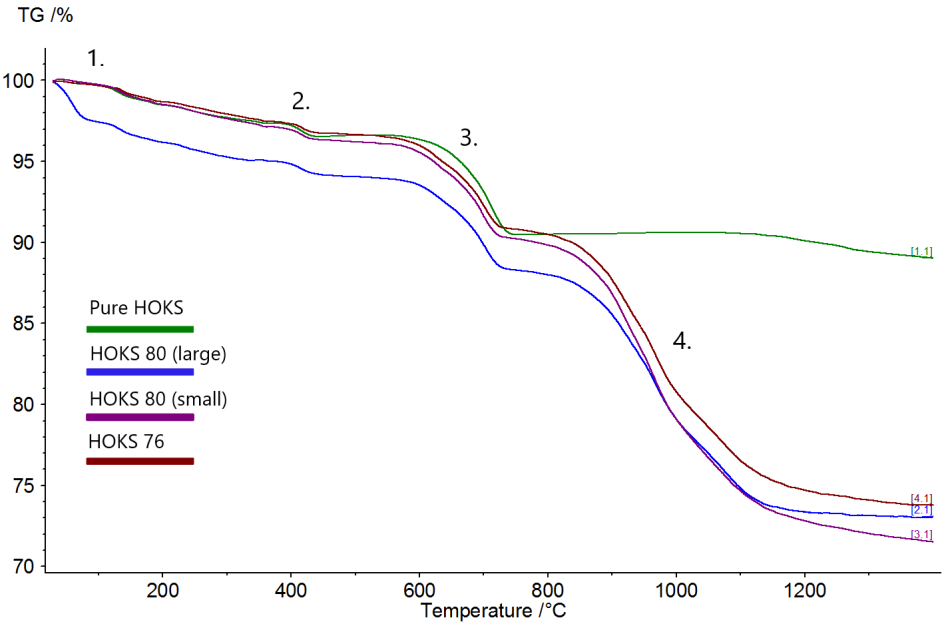

Figure 5.9: TGA results of the four HOKS samples

A quick comparison is made between the different samples of one base material (HOKS or BOF). Both HOKS 80 (small) and HOKS 76 are very similar while the curve of HOKS 80 (large) separates early from the others due to a high water content. The rest of the curves show weightlosses at the same positions with slight deviations in amount due to the slightly different compositions. In the case of the BOF samples, it is visible that a higher BF content in the substance causes a lower loss due to calcite decomposition (point 3.). Indeed, less calcium is detected in BF with XRF. Also, a higher weight loss caused by the reductions of the iron oxides (point 4.) is clearly present which is possible because of the higher carbon content.

To determine the effects of size, the microgranulates were put as a whole in the TGA. A sample with 2 big granules of 3 to 4 mm diameter and another sample with many small 1 to 2 mm microgranulates were heated. The results can be seen in figure 5.11. It is clear that most of the water is contained by the small microgranulates in the case of HOKS 80 (large). The difference between using particles or powder is visible in the last descent of the reduction (4.). The fist part is steeper using microgranulates while the second part is less steep. The better mixing and smaller particle size cause slightly more gradual reactions.

To provide an overview, the weight losses caused by the different compounds can be found in table 5.3. These are based on the extrapolated onset and offset temperature of the different weight losses.

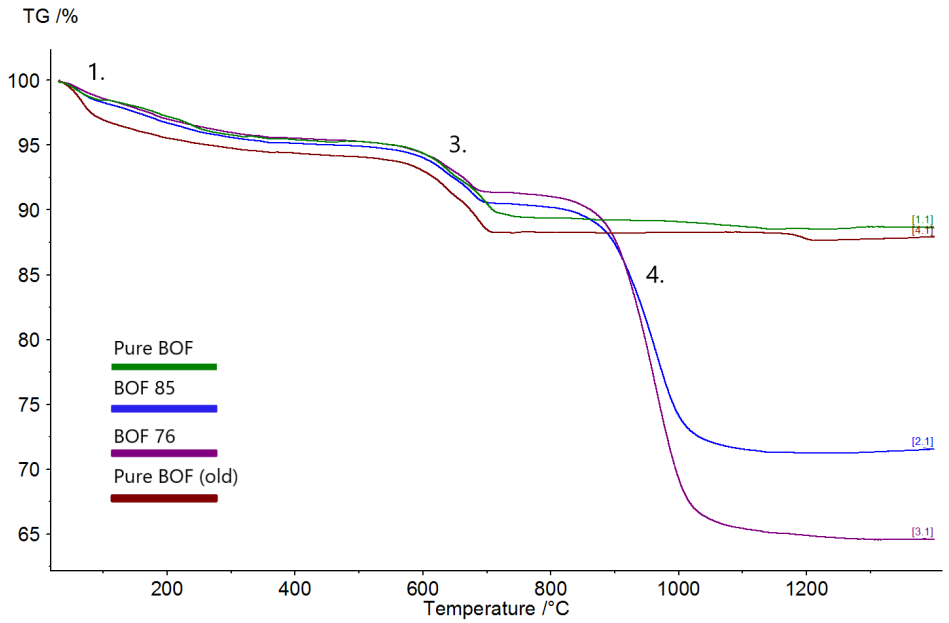

Figure 5.10: TGA results of the BOF microgranulates

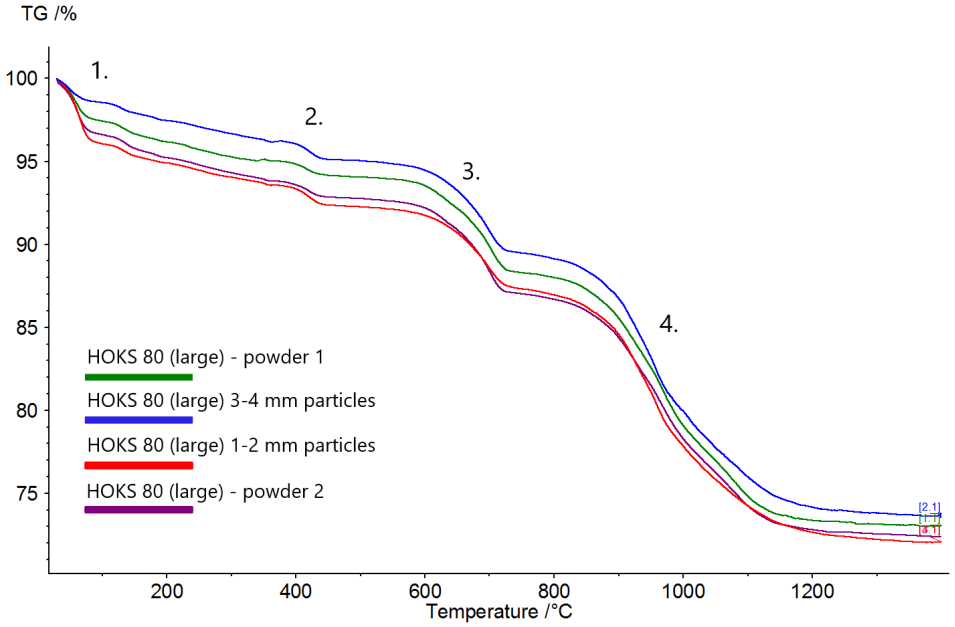

Figure 5.11: TGA results of different HOKS 80 (large) samples

Weightloss due to	Microgranulate	Weight loss (%)
Water (≤100°C)	Pure HOKS HOKS 80 (small) HOKS 76	Negligible
	Pure BOF BOF 85 BOF 76	~1.5
	Pure BOF (old) HOKS 80 (large)	~3
Portlandite	BOF containing microgranulates	Negligible
	HOKS containing microgranulates	~1
Calcite	BOF 76	3.9
	BOF 85	4.3
	The rest	5.5-6.5
Magnetite, wustite and calcium ferrites	Pure HOKS Pure BOF Pure BOF (old)	Negligible
	HOKS 80 (large)	6.2 + 7.9*
	HOKS 76	7.1 + 9.2*
	HOKS 80 (small)	7.1 + 10.2*
	BOF 85	19.0
	BOF 76	26.1
Total mass loss	Pure HOKS	11.0
	Pure BOF	11.3
	Pure BOF (old)	12.1
	HOKS 76	26.2
	HOKS 80 (large)	27.6
	HOKS 80 (small)	28.5
	BOF 85	28.5
	BOF 76	35.3

Table 5.3: Weight loss caused by different compounds derived from the TGA experiments.
* The total weight loss counts up those two numbers but they are separated because of their change in slope.

5.3. Isothermal self-reduction in the horizontal furnace

A small amount of microgranulates as received is used for experiments in the horizontal furnace. The horizontal furnace was used to determine the kinetics of the reactions as well as the final reaction products of the different microgranulates. After heating, the samples were analysed with different characterisation techniques. The microgranulates were heated in the horizontal furnace at 1000°C in an inert atmosphere (N_2). Some microgranulates clearly changed visually during each time step as can be seen in figure 5.12. As received, the microgranulates did not fall apart easily but after 5 minutes, it seemed like part of it had broken down and the particle size was clearly smaller.

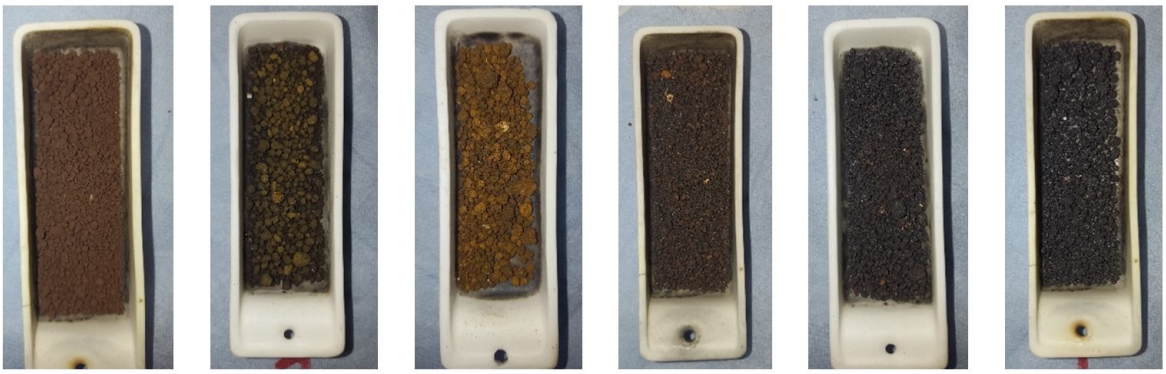

Figure 5.12: Different samples of pure HOKS microgranulates after ascending time spans inside the furnace. From left to right after 0,1,2,5,10 and 30 minutes

5.3.1. Changes in composition over time

The reduction in mass can be seen in figures 5.13. The pure microgranulates did not lose much mass due to the little amount of carbon present which was similar to what was seen after the TGA experiments. Those pure microgranulates did not contain any carbon any more after 5 minutes with the result that they stopped losing mass as well. The carbon and zinc concentrations can be found in figures 5.14.

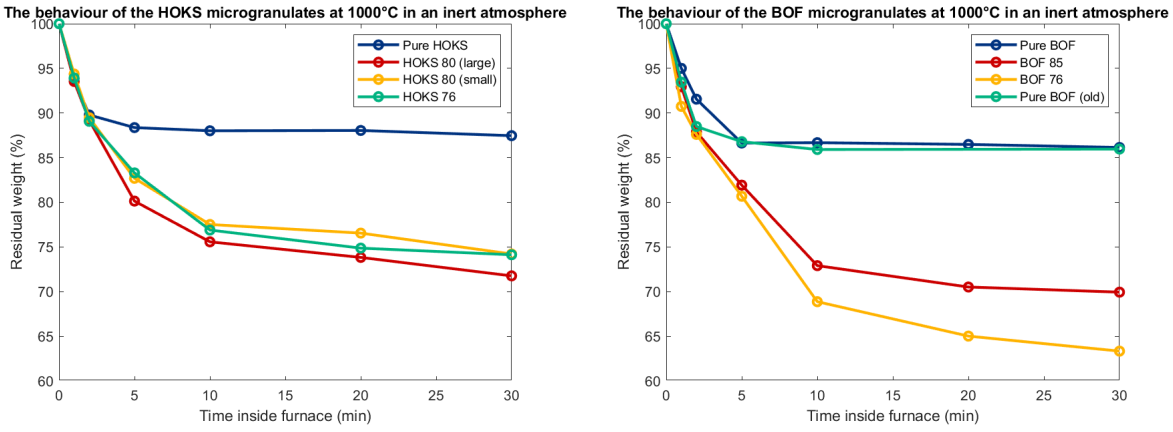

(a) (b)

Figure 5.13: The total weight loss measured over time in the horizontal furnace at 1000°C in a N_2 atmosphere

The three pure microgranulates lost between 33 and 42% of their zinc while 90% of their carbon is gone after 30 minutes. This means that most carbon is used for other reactions. Indeed, the pure BOF microgranulates show that all magnetite, hematite and metallic iron are gone showing only wüstite as final iron compound together with a small amount of calcium ferrites. BOF (old) - which was less oxidised from the beginning - also contained elemental iron and pure HOKS ended up with only calcium

ferrites after 30 minutes, see figures 5.15 and 5.16. Besides that, more mass is lost than can be explained by the oxidation of carbon with the remaining caused by dehydration and the decomposition of portlandite (for HOKS) and calcite.

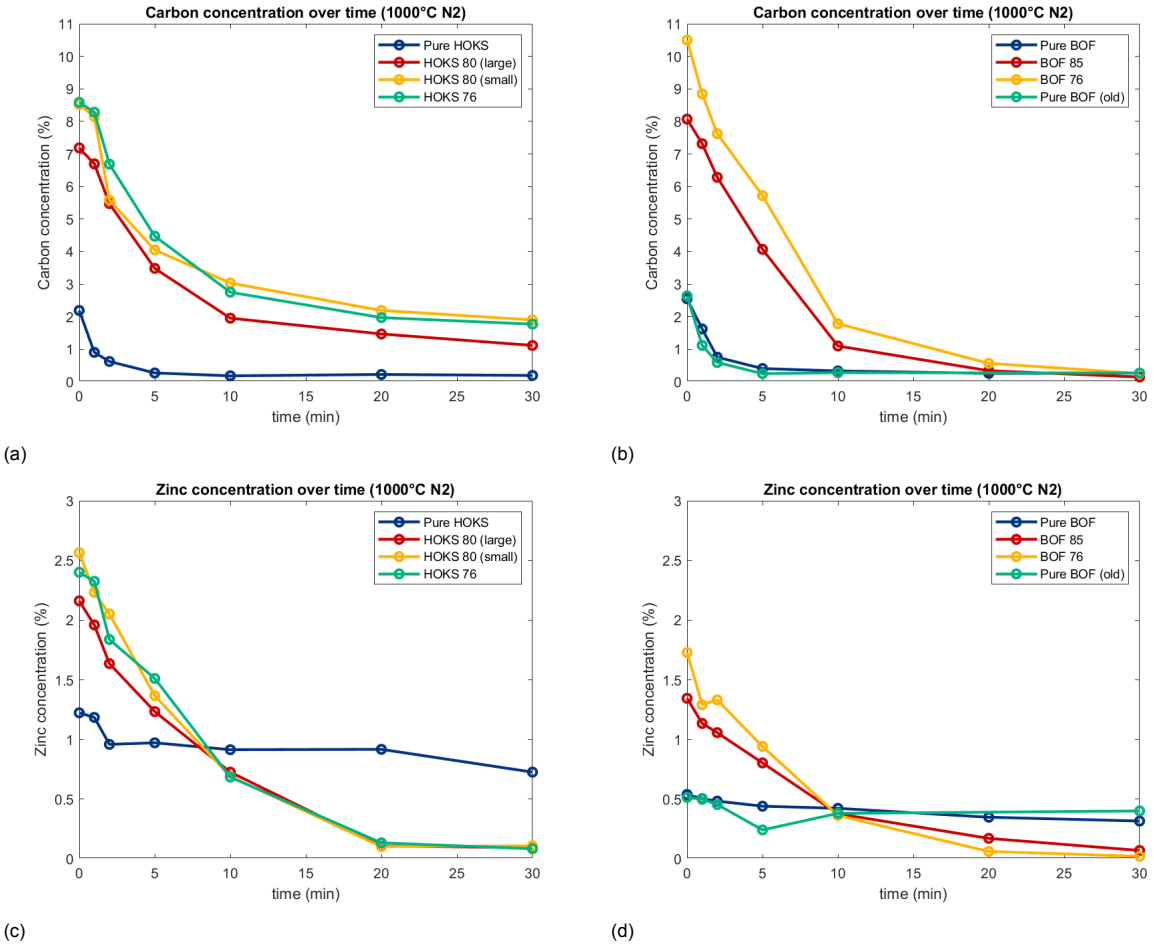

Figure 5.14: The carbon and zinc concentrations measured over time in the horizontal furnace at 1000°C in a N_2 atmosphere. The zinc and carbon percentages are based on the initial amount of material and therefore corrected with the weight loss.

The microgranulates mixed with BF dust show a much larger weight loss. Those losses are similar for the three HOKS microgranulates while the two BOF microgranulates differ quite a bit in final weight loss. All mixed microgranulates lost nearly all zinc after 20 minutes in the furnace. At the end of 30 minutes self reduction in the furnace at 1000°C, 94-96% of all zinc was gone independent of the type of microgranulate mixed with BF dust. Also, BOF 76 contained only metallic iron together with some larnite (Ca_2SiO_4) and lime (CaO) while nearly all carbon was gone, see figure 5.17. This means that enough carbon was present to reduce all oxides as predicted by Peters [60]. For similar reasons, BOF 85 did not contain enough carbon as wüstite is still present next to metallic iron and calcium silicate. The amount of carbon was enough to evaporate all zinc in both cases although it took a little longer for BOF 85 to reach the minimum value.

Remarkable for the HOKS microgranulates is that they still lose some mass between 20 and 30 minutes. This could indicate that the reactions are not done yet. However, no reducible phases could be analysed with XRD (see figure 5.18 for the phases after 30 minutes for HOKS 80 (small)) so it is assumed that these are very small amounts. This is confirmed with a HOKS 80 (small) sample heated for 60 minutes under the same circumstances which has a very similar weight loss as the 30 minute sample (-25.1%). HOKS 80 (large) seems to show the worst reducing properties as this is the only one that still contains some calcium ferrites after 30 minutes. Because it still loses weight between 20 and 30 minutes and

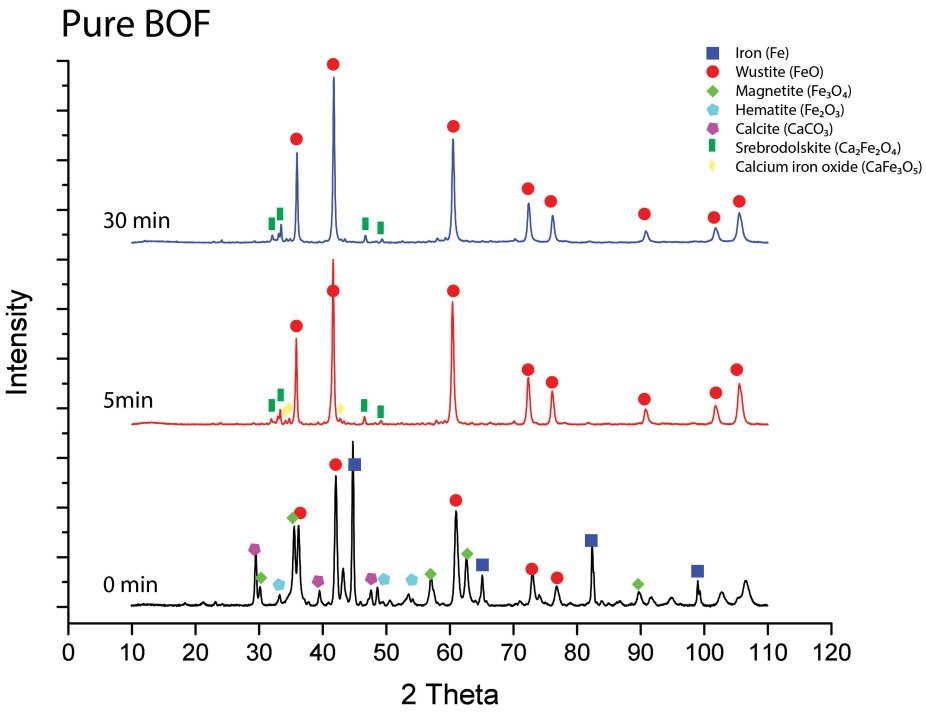

Figure 5.15: The XRD diffractograms from Pure BOF after 0, 5 and 30 minutes in the horizontal furnace at 1000°C in N_2

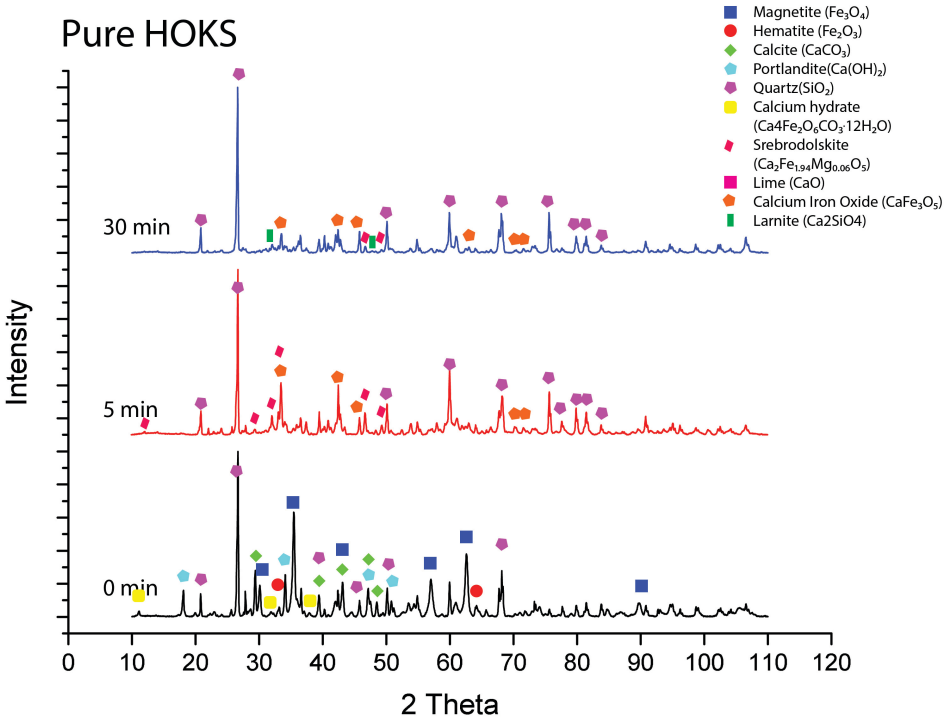

Figure 5.16: The XRD diffractograms from Pure HOKS after 0, 5 and 30 minutes in the horizontal furnace at 1000°C in N_2

because there is still carbon left, it could mean that everything will be reduced with a little more time. This different behaviour could be due to the larger particle size but a lower amount of carbon could also be one of the reasons. However, all BF-HOKS samples contained more carbon than needed for reduction reactions. They only lost 73-79% of all carbon while the remaining carbon was present in the form of graphite as seen in the XRD diffractograms. Those pure carbon particles were detected with EDS as well.

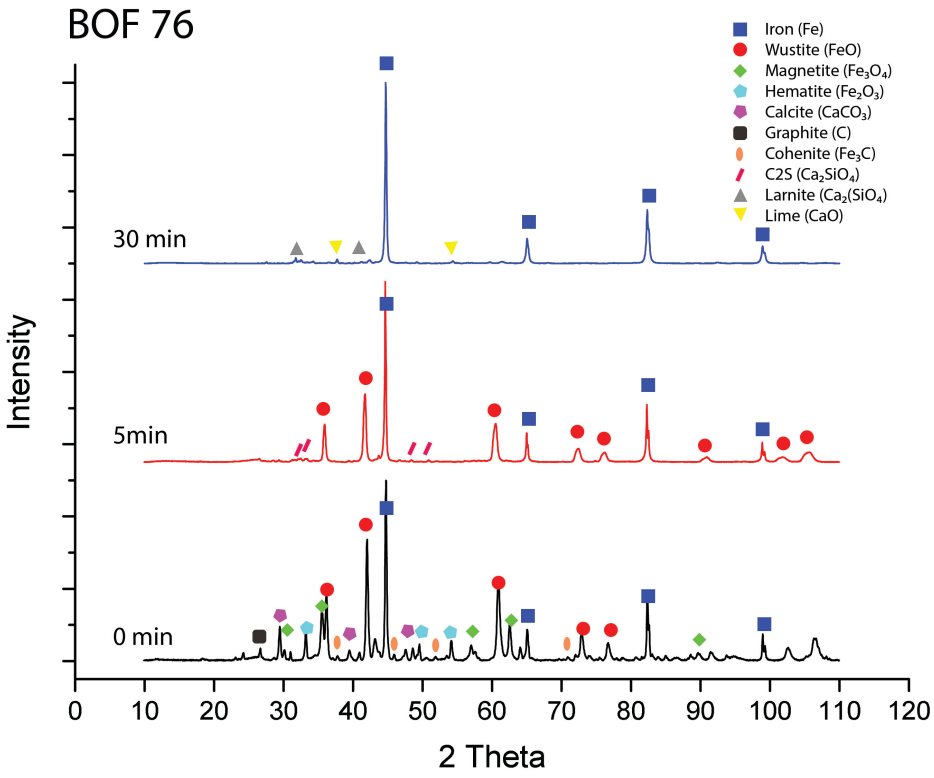

Figure 5.17: The XRD diffractograms from BOF 76 after 0, 5 and 30 minutes in the horizontal furnace at 1000°C in N_2

After heating, calcium was present in the form of calcium oxide, calcium ferrite and/or calcium alumino silicate. Next to these compounds, srebrodolskite ($Ca_2Fe_2O_5$ (with magnesium or sodium)) and $CaFe_3O_5$ were detected in some samples as well. In the case of HOKS, calcium ferrite could be formed by the decalcination of the calcium carbonate hydrate (reaction 5.5) but it is most likely that the majority is formed by a reaction with calcium oxide and hematite or magnetite (reactions 5.6-5.8). The last two equations could be found in HSC chemistry 6.0 which showed that this is indeed a reaction that can occur at the tested temperature because of their negative change in Gibbs free energy above room temperature. With the presence of enough carbon, both are likely to be reduced to metallic iron at temperatures above 800°C, see reactions 5.9 and 5.10. In the presence of silica, the reduction of calcium ferrites is even more in favour while forming $CaSiO_3$ (reaction 5.11).

$$Ca_4Fe_2O_6CO_3 \cdot 12\,H_2O \longrightarrow Ca_2Fe_2O_5 + CaO + CaCO_3 + 12\,H_2O \tag{5.5}$$

$$CaO + Fe_3O_4 \longrightarrow CaFe_3O_5 \tag{5.6}$$

$$CaO + Fe_2O_3 \longrightarrow CaFe_2O_4 \qquad \Delta G^{1000} = -36.96\,\text{kJ} \tag{5.7}$$

$$2\,CaO + Fe_2O_3 \longrightarrow Ca_2Fe_2O_5 \qquad \Delta G^{1000} = -70.73\,\text{kJ} \tag{5.8}$$

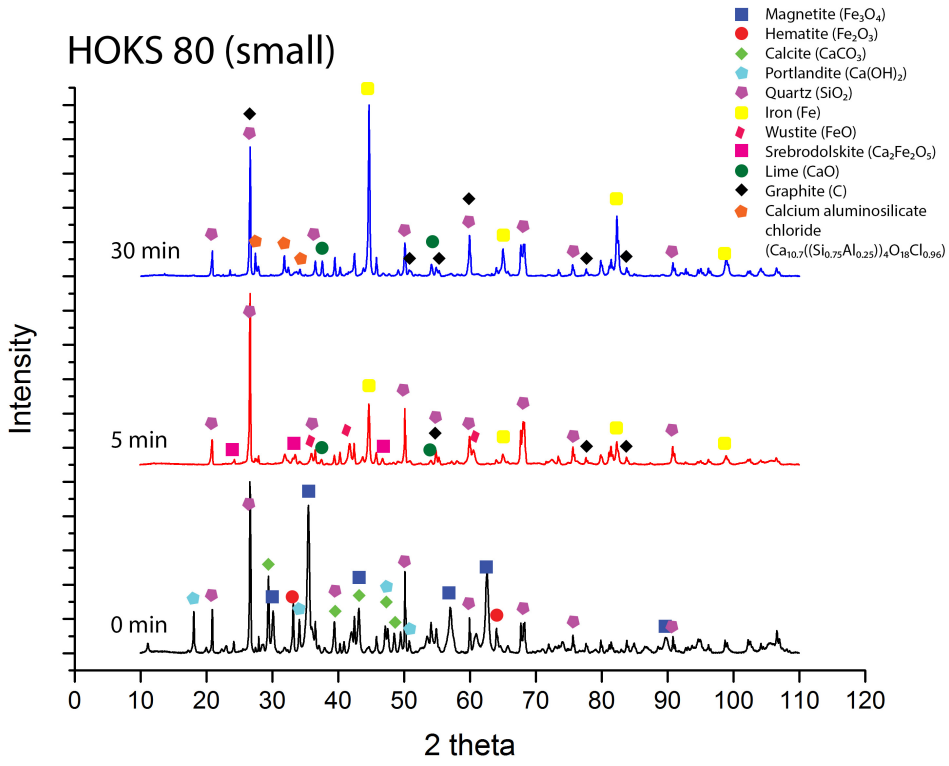

Figure 5.18: The XRD diffractograms from HOKS 80 (small) after 0, 5 and 30 minutes in the horizontal furnace at 1000°C in N_2

$$CaFe_2O_4 + 3\,C \longrightarrow CaO + 2\,Fe + 3\,CO\,(g) \qquad \Delta G^{1000} = -144.30\,kJ \tag{5.9}$$

$$Ca_2Fe_2O_5 + 3\,C \longrightarrow 2\,CaO + 2\,Fe + 3\,CO\,(g) \qquad \Delta G^{1000} = -110.53\,kJ \tag{5.10}$$

$$3\,Ca_2Fe_2O_5 + 6\,SiO_2 + CO\,(g) \longrightarrow 6\,CaSiO_3 + 2\,Fe_3O_4 + CO_2(g) \qquad \Delta G^{1000} = -446.41\,kJ \tag{5.11}$$

As HSC did not have complete data about all calcium ferrite compounds, some papers were consulted. Jeon [74] showed that $Ca_2Fe_2O_5$ is the more stable phase with intermediate calcium ferrite phases formed depending on the starting material; $CaFe_2O_4$ and $CaFe_3O_5$ were formed by a reaction with Fe_2O_3 and Fe_3O_4 respectively. In pure BOF, it seems like srebrodolskite is indeed the most stable phase as only srebrodolskite is left after 30 minutes. The other BOF samples have enough carbon present to either or both minimise the formation of calcium ferrite and reduce the calcium ferrite to lime and an iron oxide. The pure HOKS sample shows the opposite effect as a longer time in the furnace slightly decreases the amount of $Ca_2Fe_2O_5$ and increases $CaFe_3O_5$. More research needs to be done to explain why this could be the case.

5.3.2. Morphology determination

This section is dedicated to the visualisation of the microgranulates. To make this possible, they have been mounted in a cold resin and ground with sandpaper to make the cross section visible for analysation with SEM and EDS. As the particles were not purely conductive, a carbon coating was necessary. SEM analysis showed that the raw microgranulates did not have many clear phases except for some

large silica particles in the HOKS samples, see figure 5.19. This is a big difference to the baked micro-granulates as they show an increasing amount of separate phases which can be seen in figure 5.20. In this particle of HOKS 80 (small), the different phases detected with XRD can be seen.

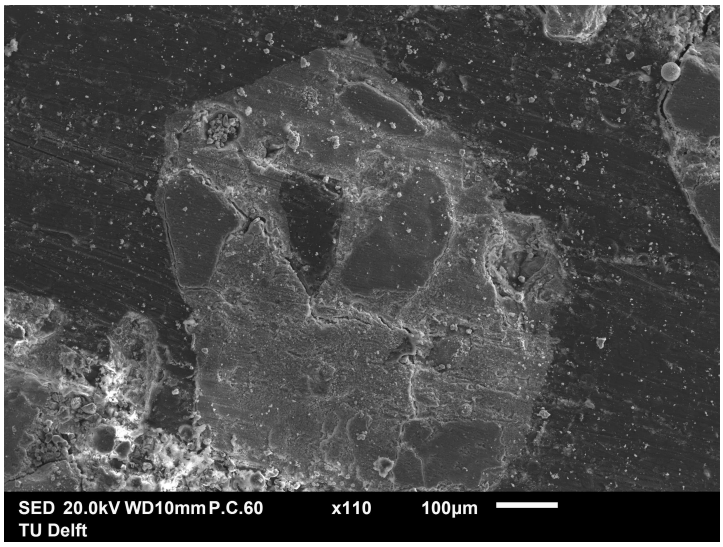

Figure 5.19: The cross section of a pure HOKS particle as received

The dark black particle, surrounded by a red square, is a pure carbon particle. The blue and purple squares are silica particles. It is interesting to mention that the sides (the lighter gray colour at the edges) contain impurities as iron, calcium, potassium and some zinc. The particles surrounded by a green, yellow or pink square contain many iron and calcium oxides. The composition of the green one is at one point close to srebrodolskite with magnesium (table 5.4). However, other points show different calcium ferrite compositions.

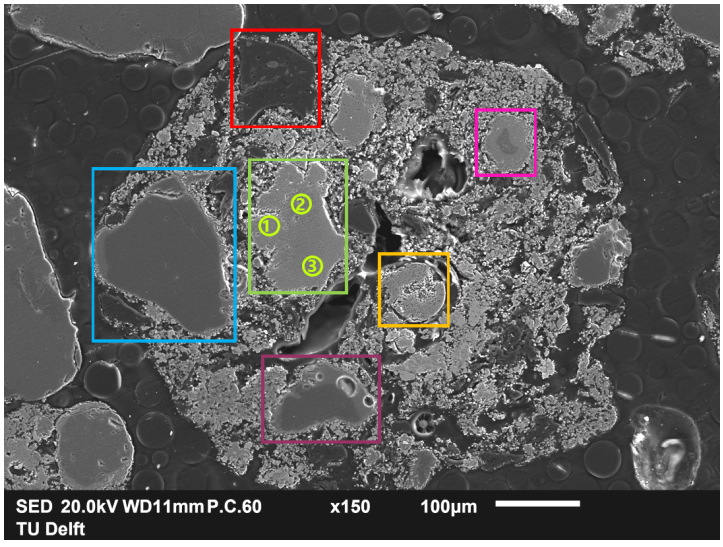

Figure 5.20: Phases in HOKS 80 (small) after 5 min
Red: carbon, blue+purple: SiO_2, yellow+green: calcium ferrites

Pure $CaFe_3O_5$ phases have been detected in a pure HOKS particle. A line analysis has been made to check whether the whole particle has the same phase. Indeed, this seemed to be the case although the amount of iron was slightly increasing towards the middle (the dark color in the middle is a hole filled with resin), see figure 5.21. $CaFe_3O_5$ was the only calcium ferrite phase present in the pure HOKS microgranulate as shown with XRD.

Formula	Fe	Ca	Mg	Zn	C	O	Si	S	Al
atom% - 1	26.77	5.12	8.24	0.81	16.95	42.14		0.18	
atom% - 2	12.38	21.08	6.32	0.33	13.16	46.19	0.37	0.18	
atom% - 3	20.16	16.93	1.43		14.83	44.84	0.82	0.29	0.70

Table 5.4: An EDS analysis on the green particle in figure 5.20

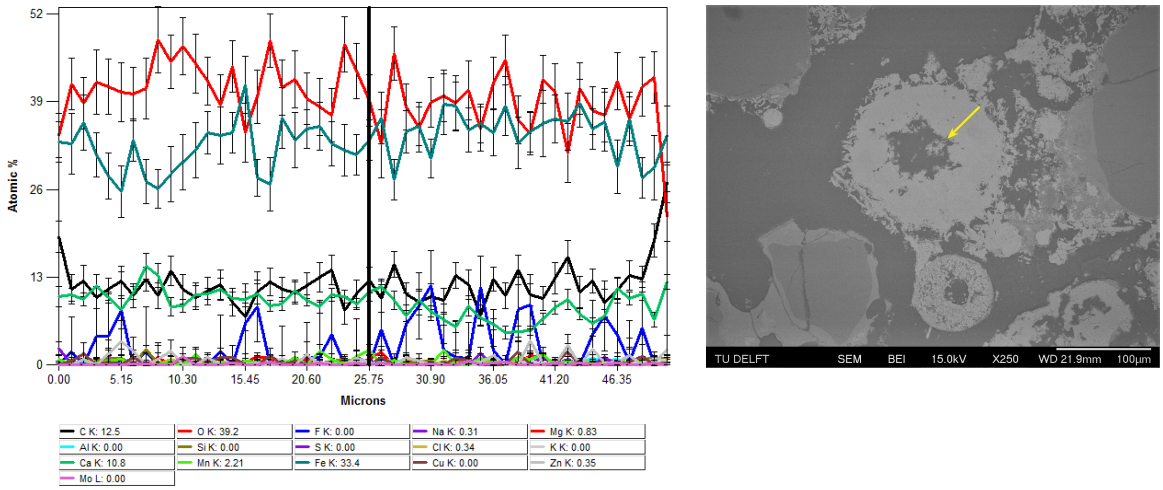

Figure 5.21: A line analysis from a $CaFe_3O_5$ phase in pure HOKS (1000°C, N_2, 30min)

Due to the lower amount of calcium and silicon in the BOF microgranulates, less different phases were distinguished that are present as smaller particles. The raw particles show small distinctive phases as can be seen in figure 5.22. However, after treatment, the material is much more uniform (figure 5.23). This is in agreement with XRD as only three phases were detected: metallic iron with a small amount of larnite and lime.

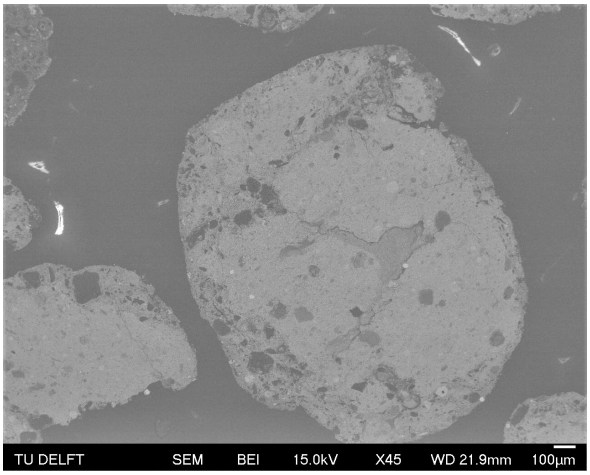

Figure 5.22: An untreated BOF 76 particle

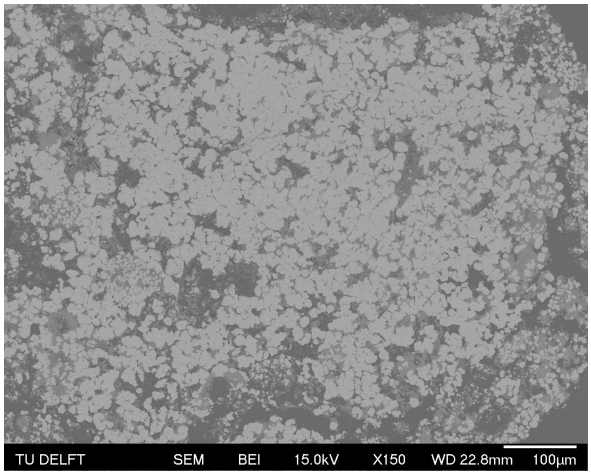

Figure 5.23: BOF 76 particle after treatment at 1000°, N_2, 30 min

5.3.3. Calculated weight loss

The presence of the elements as specific oxides are determined with XRF. However, this is not correct in all cases. For example, XRD has shown that calcium is not present in the form of calcium oxide, but in the form of calcite and not all iron is present in the form of hematite. A guess at the actual compounds is made based on the compounds found with XRD, its intensities on the XRD spectra and the weight loss it caused during the TGA experiments. However, as XRD is not a quantitative analysis method, their intensities can not be quantified and it will stay a guess. For all samples, most weight is lost by the decomposition of hydrates and carbonates, the vaporisation of metals (mainly zinc and lead) and the oxidation of carbon (which leaves the sample as CO or CO_2). BOF 76 contains 10.5% of carbon which on it's own can cause a weight loss between 24.5% and 38.5% depending on whether it leaves as CO or as CO_2.

XRF measures the composition of the material in the form of specific oxides but in reality other compounds are present. This actual composition is calculated with the help of equation equation 5.12. W_{rel} is the assumed composition of the elements relative to each other, XRF_{oxide} are the results of the XRF measurments in w%, M the molar mass of either the oxides or the assumed compounds (comp) and EF the elemental fraction to account for the change in number of cations. After renormalisation to 100% (W_{rel} to W_{norm}), the weight percentage of the leaving components (LC) is calculated based on equation 5.13.

$$W_{rel}(\%) = \frac{XRF_{oxide}(\%)}{M_{oxide}} * M_{Comp} * EF \tag{5.12}$$

$$LC(\%) = \frac{W_{norm}(\%)}{M_{Comp}} * M_{LC} \tag{5.13}$$

Iron in BOF 76, for example, is assumed to be present as 30% metallic iron, 40% wüstite, 10% magnetite, 10% hematite and 10% cohenite which is a guess made on the peak intensities of the XRD spectrum. All oxides reduce towards metallic iron with the help of carbon. The amount of oxides leaving the sample as CO or CO_2 can now easily be calculated assuming all iron oxides reduce to metallic iron. The same is done for $CaCO_3$ of which CO_2 leaves the sample after decomposition. The amount of carbon present in calcite is subtracted from the total amount of carbon. The same is done for cohenite. All sulfide is assumed to be present as ZnS meaning that only a small amount of zinc is present as zinc oxide. This because both ZnS and ZnO are present in BF dust as analysed by Peters [60]. Based on the calculations, a weight loss of 30% would be expected. The reality shows that a weightloss of 35% is possible meaning that the sample is probably a little more oxidised than expected. This is verified with stoichiometric calculations that shows that much more carbon is present than needed for purely the reduction of iron oxides in both BOF 85 and BOF 76, even when all carbon is only partly oxidised to CO. The experiments showed that BOF 76 needed most available carbon while BOF 85 did not have enough carbon for full reduction. This is calculated with equation 5.14 in which $\frac{Oxide}{2}$ is the amount of oxides that need to be oxidised divided by two because each carbon can uptake 2 oxygen atoms. Based on this equation, BOF 76 needed between 4.1 w% and 7.8 w% carbon for full reduction of the iron oxides depending on whether it leaves as CO or as CO_2.

$$C(\%) = \frac{W_{norm}(\%)}{M_{Comp}} * M_{Carbon} * \frac{Oxide}{2} \tag{5.14}$$

The iron oxides in the HOKS samples are more oxidised and are assumed to be present for 50% as magnetite and 50% as hematite. Determining the calcium phases of the HOKS samples is more challenging. Calcite, portlandite, calcium ferrite carbonate hydrate and potassium calcium carbonate where detected with XRD but it is likely that more calcium compounds are present in smaller amounts. The amount of calcite and portlandite is based on the weight loss it had caused in the TGA experiments. This could be an underestimation as the released CO_2 could also have caused some oxidation and

therefore did not directly contribute to the weight loss. The amount of other calcium phases seems too high to not show a clear weight loss in the TGA experiments resulting in an overestimation of the amount of mass lost. HOKS 80 (small) shows to lose about 28% of it's mass while 34% is calculated. Stoichiometric calculations show that between 5.0% and 10.1% carbon is needed for the reduction of the iron oxides. The 8.34% of carbon measured with LECO fits nicely in between but because not all carbon is used for the reaction, this is still an over estimation.

5.4. The reduction behaviour of HOKS/BF (80:20) and BOF/BF (76:24) at different temperatures and in different atmospheres

It was decided that the following tests would only take place using the microgranulates HOKS 80 (small) and BOF 76. Limited difference could be found between the HOKS-BF samples, except HOKS 80 (large) of which not all iron oxides could be totally reduced to metallic iron withing 30 minutes. HOKS 80 (small) was chosen because of its highest zinc content. BOF 76 was chosen as it seemed to have a carbon content that corresponds to the amount needed for self reduction. BOF 76 and HOKS 80 (small) are tested for different time spans inside the horizontal furnace at 1000°C and 1300°C both in an inert atmosphere and with a PCR of 50 (a 50% CO, 50% CO_2 atmosphere). Also, the vertical furnace is used for large scale TGA experiments up to 1500°C in both atmospheres.

5.4.1. The effect of isothermal treatments on the reduction behaviour in varying atmospheres

Figures 5.24a and 5.24b show the weight loss of those samples under the different circumstances. It is clearly visible that the reactions go much faster at the higher temperature of 1300°C independent of the atmosphere used due to the faster kinetics at that temperature. The samples reduced in the CO/CO_2 atmosphere lose their weight slower at 1000°C while the difference is less clear at 1300°C. After 10 minutes in this reducing atmosphere at 1000°C and after 5 minutes at 1300°C, the samples are gaining weight which was due to the reoxidation of the material. This is illustrated for HOKS 80 (small) in figure 5.25. This figure shows the oxidation states of iron after different time intervals in the furnace at 1000°C under an atmosphere with a PCR of 50. After 5 and 10 minutes, some metallic iron is formed, which is totally gone after 20 minutes.

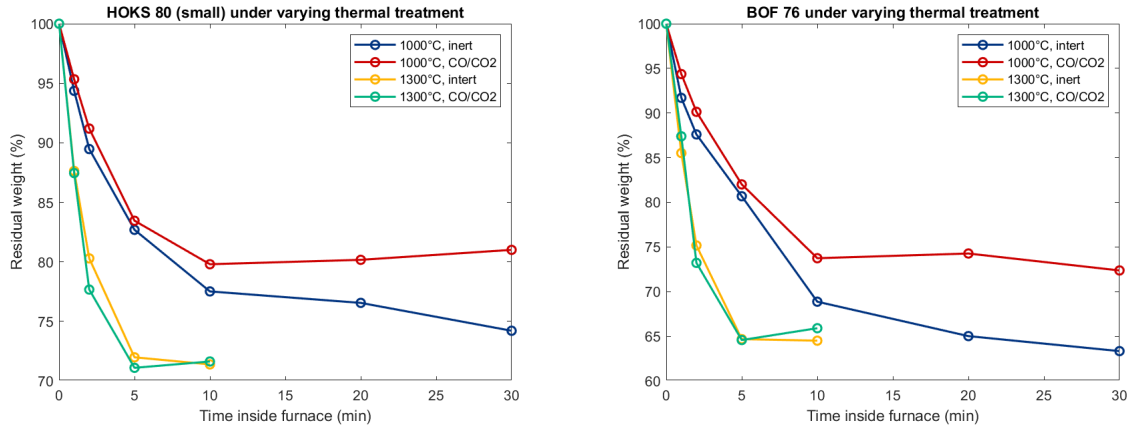

(a) (b)

Figure 5.24: The weightloss of HOKS 80 (small) and BOF 76 under all tested circumstances

In figures 5.26a and 5.26b, the carbon and zinc concentration in the BOF 76 samples can be seen. At 1000°C, it takes 20 minutes for both carbon and zinc to reach almost minimal levels after which the reduction speed significantly decreases. However, the zinc concentration never reaches that low in PCR 50 as in N_2. As the material starts to oxidise after 10 minutes, not all carbon was used for the

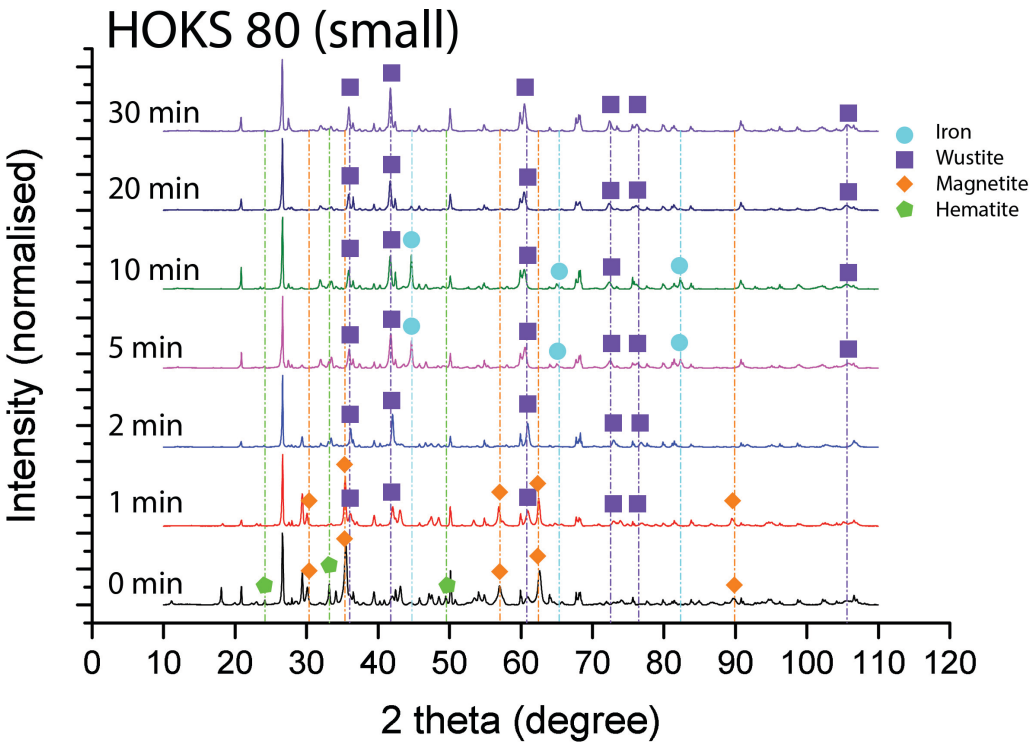

Figure 5.25: The change in iron oxidation state of HOKS 80 (small) in a CO/CO2 atmosphere at 1000°C

reduction of the remaining zinc but it was used for maintaining the low oxidation state of iron. This is confirmed with the theory: when looking at the reactions in table 5.2, the reduction of zinc oxide and zinc sulphide with carbon have a higher ΔG than the reduction of wüstite at 1000°C, meaning that the reduction of wüstite is more favourable, while at 1300°C the ΔG of zinc oxide and zinc sulphide are lower. This difference increases at higher temperatures. At 1300°C, all reactions go much faster with the result that no carbon and zinc are present any more after 5 minutes. As the sample starts to oxidise only after those five minutes, the zinc in the PCR 50 samples was still able to reach that minimum value.

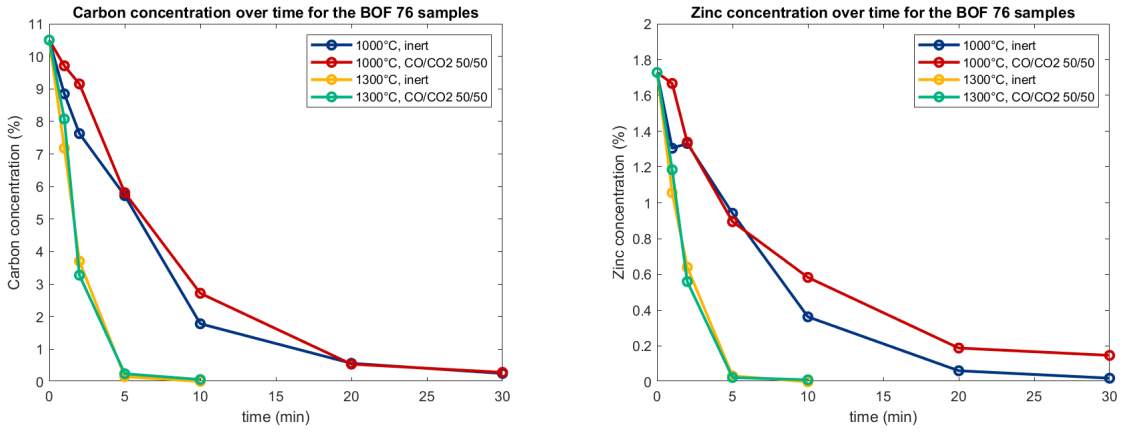

(a) (b)

Figure 5.26: The carbon and zinc concentrations in BOF 76 after isothermal treatment

The off-gas from the 10 minute sample at 1300°C was analysed. These can be seen in figures 5.27a and 5.27b. In a nitrogen environment, the reactions starts with producing CO_2 after which the CO follows shortly. This suggests that the reaction starts with the decomposition of calcite and complete oxidation of carbon. Indeed, after 1 minute, all calcite is gone and the hematite and magnetite are

reduced to wüstite which can be seen in figure 5.28. When the time inside the furnace increaeses, the main differences found in the XRD patters are the increase in metallic iron and decrease of wüstite.

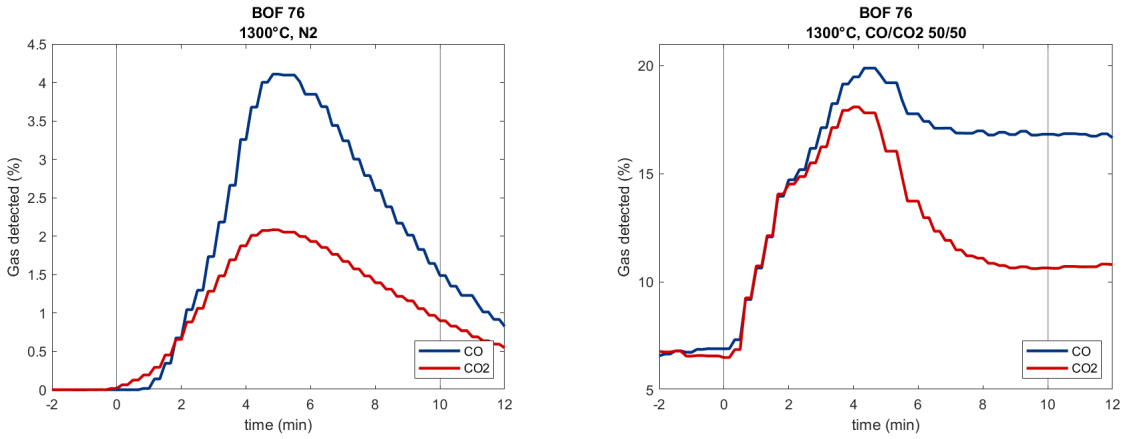

(a) (b)

Figure 5.27: The off-gas analysis of the BOF 76 samples after an isothermal treatment at 1300°C

In a CO/CO_2 atmosphere, the reduction of magnetite is not as fast as in nitrogen because magnetite is still present after 1 minute. The reduction processes have a maximum at 4.5 minutes as can be seen in figure 5.27b. The stable high concentration of CO after that peak shows that the CO_2 is used for oxidising the sample which produces CO.

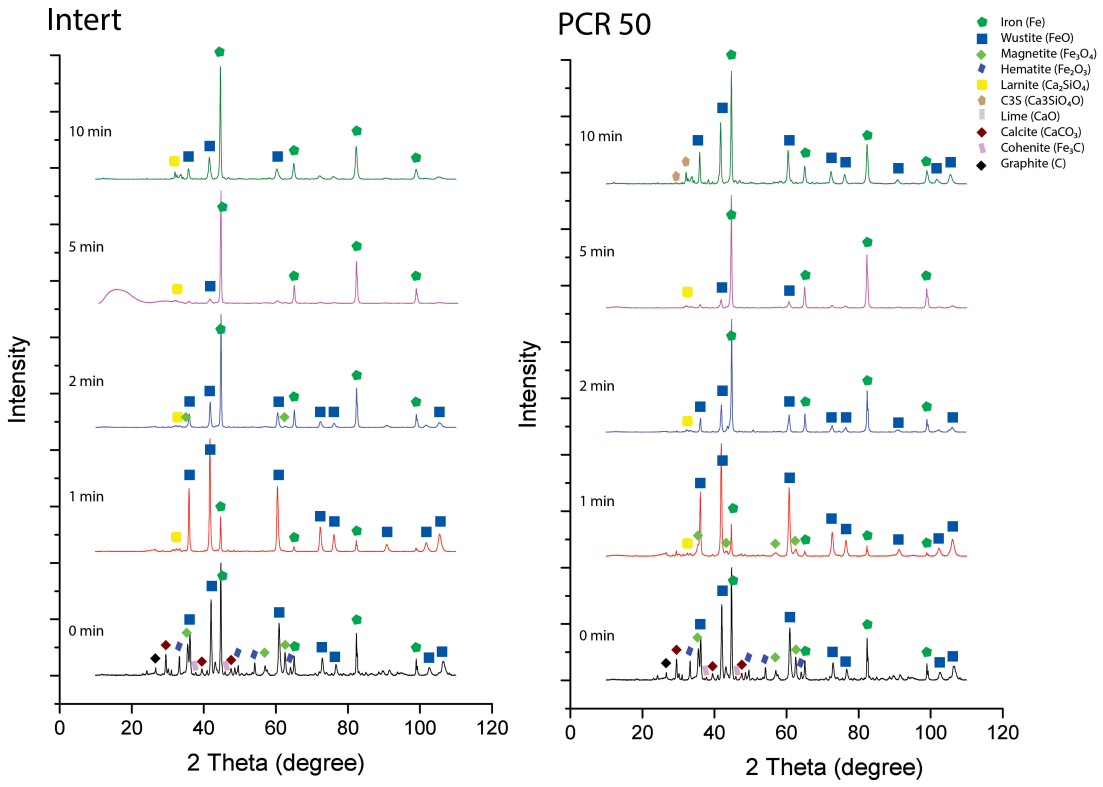

Figure 5.28: XRD diffractograms from BOF 76 after different durations in the horizontal furnace at 1300°C

At last, a calcium silicate is formed in all cases by a reaction between calcium oxide and silica, see reaction 5.15. Multiple calcium silicate phases/ crystal structures are possible but the difference between

them is difficult to distinguish with XRD.

$$2\,CaO + SiO_2 \longrightarrow Ca_2SiO_4 \qquad \Delta G^{1000} = -32.5\,\text{kcal} \tag{5.15}$$

A similar effect can be seen in the HOKS 80 (small) samples regarding to the zinc concentration that is higher at 1000°C in PCR 50 (figure 5.29a and 5.29b). As this sample contains more carbon, this can be used to counteract the oxidation, with the result that the zinc concentration is still reducing until the end of the tested 30 minutes. After 10 minutes, the carbon content suddenly decreases a lot which is around the same time that the oxidation starts to occur. A little more time in the furnace may eliminate the amount of carbon and reduce the amount of zinc to a minimum.

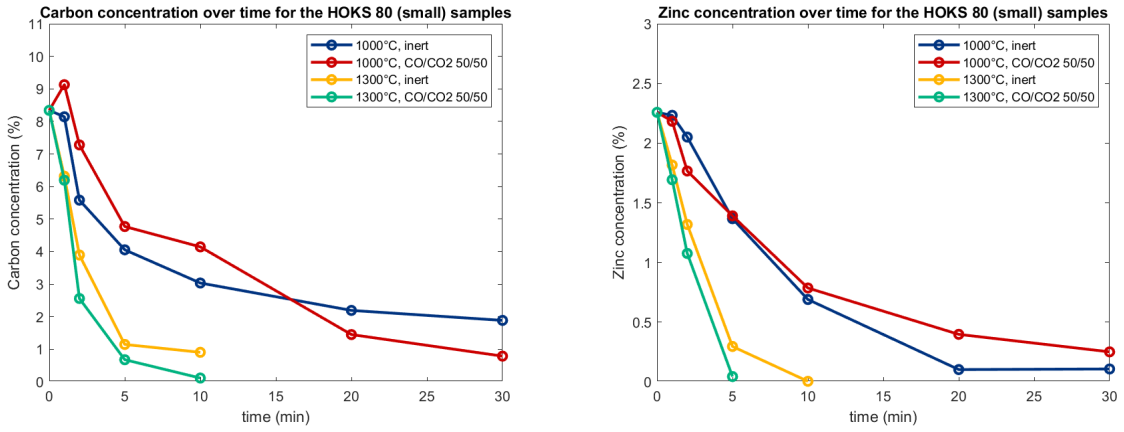

(a) (b)

Figure 5.29: The carbon and zinc concentrations of HOKS 80 (small)

Again, at 1300°C all processes go much faster. Contrary to the results at 1000°C, the zinc level is reduced to a minimum and also the remaining carbon content was halved. In a CO/CO_2 atmosphere, the zinc loss was much faster with the result that all zinc was gone after 5 minutes, before the oxidation had start.

The off-gas composition showed little difference with the BOF 76 samples, see figures 5.30a and 5.30b. Compared to BOF 76, it took longer before the calcite was gone as it was still detected after 1 minute. This could be because more calcite was present. Hematite was directly gone while srebrodolskite was formed from hematite and calcium oxide. The amount of srebrodolskite and magnetite decreased at the 2 minute sample forming wüstite and metallic iron of which the metallic iron increased up to the moment that iron was only present as metallic iron after 10 minutes. At 10 minutes, it was also visible that part of the quartz transformed to christobalite which is known as a silica crystal that forms at high temperatures.

In a CO/CO_2 atmosphere, it is remarkable that a small amount of metallic iron is directly present after 1 minute and all magnetite is gone. This is a contradictory result to the BOF 76 samples. The 5 minute sample only contained metallic iron which was maintained on the 10 minute sample. As almost all carbon was gone after 10 minutes, it is expected that the sample will start oxidising shortly after.

Next to zinc and carbon, the lead, chloride and sodium content seem to decreases as well in HOKS 80 (small) and lead, chloride and potassium content decrease clearly for BOF 76, see figures 5.32a and 5.32b. Especially lead is very rapidly gone as it is not measured any more after 5 minutes at 1300°C and 10 min at 1000°C regardless of the atmosphere. For the other elements, they are not eliminated from the microgranulates but they seem to leave the sample at least a bit which mainly happens in the first 5 minutes. The values stabilise in the longer time spans. Unfortunately, due to the small concentrations, not all tests were very consistent which makes it difficult to give a better understanding of what is happening there.

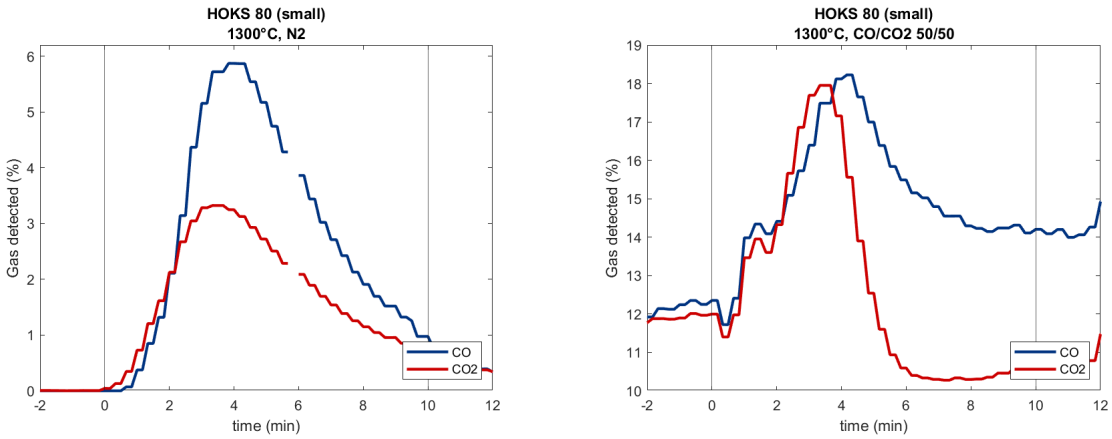

(a) (b)

Figure 5.30: The off-gas analysis of the HOKS 80 (small) samples treated at 1300°C

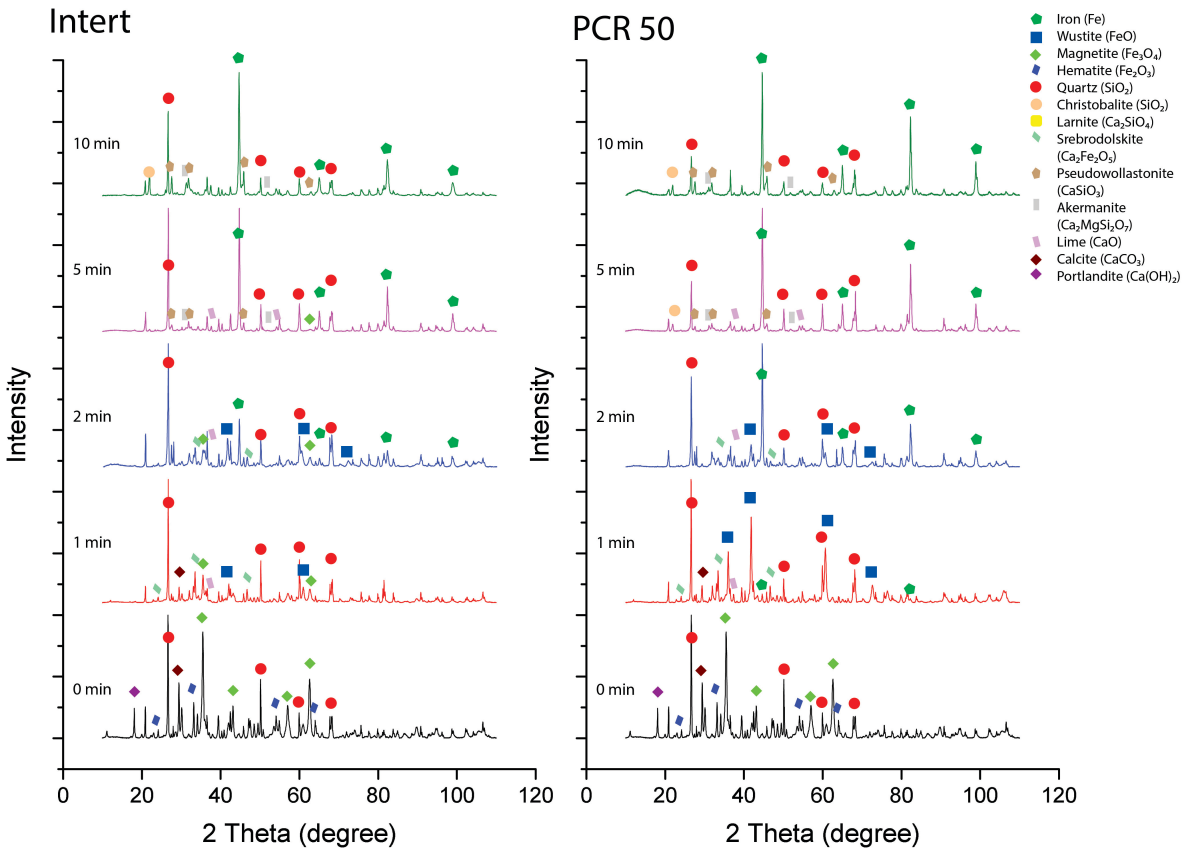

Figure 5.31: XRD diffractograms from HOKS 80 (small) after different durations in the horizontal furnace at 1300°C

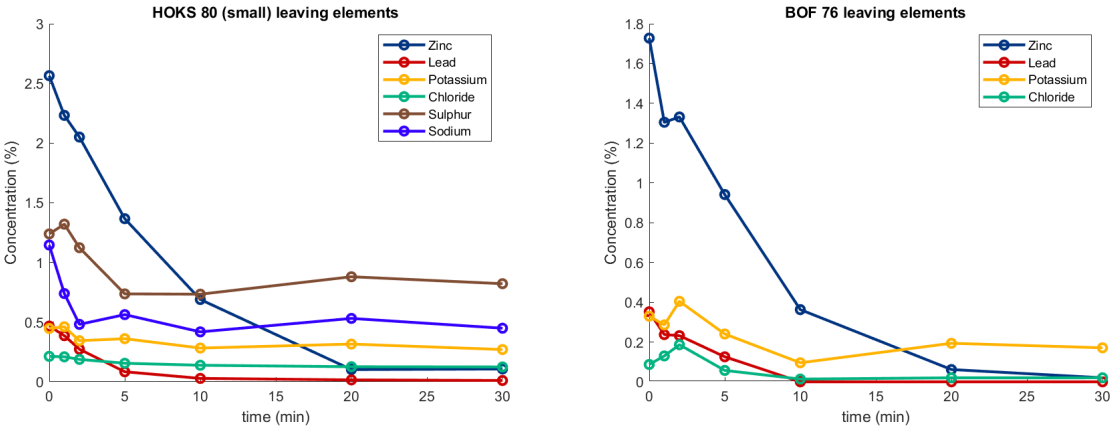

(a) (b)

Figure 5.32: The elements that showed to leave the sample during heating at 1000°C in nitrogen

5.4.2. The effect of other compounds on the reduction of zinc oxide

FactSage 7.0 and FactSage 8.0 were used to determine the equilibrium composition of zinc bearing elements. At first, the effect of different concentrations of C, CO(g) and CO_2 (g) were analysed which can be seen in figure 5.33. All calculations are done under a pressure of 1 atm. The numbers in the figure refer to the following start compositions (in mole):

1. 100 ZnO + 100 C
2. 100 ZnO + 100 C + 100 CO + 100 CO_2
3. 100 ZnO + 100 C + 10000 CO + 10000 CO_2
4. 100 ZnS + 10000 CO + 10000 CO_2

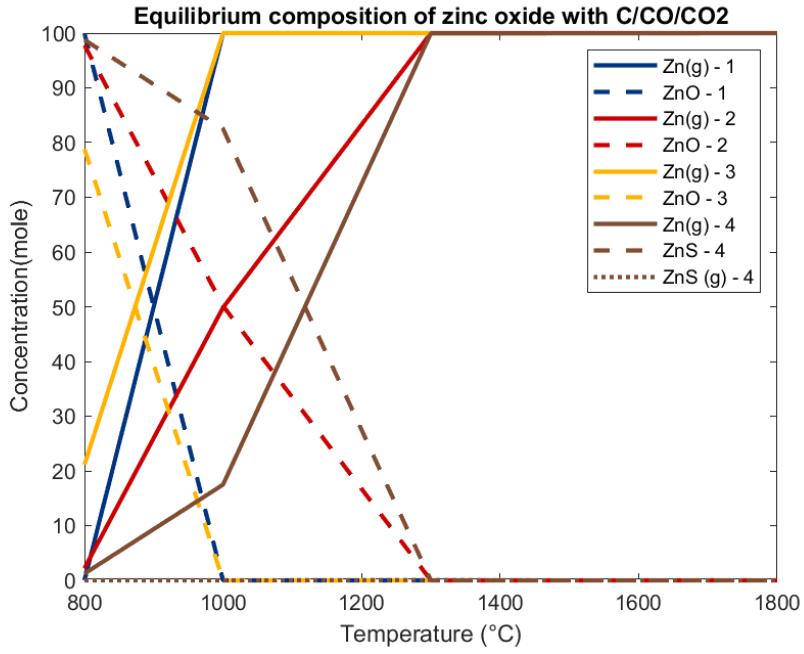

Figure 5.33: The effect of different concentration of C, CO and CO_2 on the reduction of ZnO

Composition number 1. shows the reduction of zinc oxide by only carbon. At the experimental temperatures of 1000°C, 1300°C and 1500°C, it should be possible to reduce all zinc. However, the experiments conducted in a CO/CO_2 require the addition of those gasses. When small similar concentration of CO and CO_2 are added (composition 2.), the reduction will slow down because of the high concentration of CO_2 formed. However, this is not in agreement to the experimental setup because the gas flow makes sure that the reducing gasses are constantly refreshed and it makes sure that formed gasses leave the reaction area. Both formed Zn(g) and CO_2(g) leave the reaction area with the result that the reactions can continue. This is simulated with composition number 3. By using a large amount of CO and CO_2, the reduction potential only changes very little and it can be seen that this CO/CO_2 atmosphere improves the reduction of zinc oxide at lower temperatures. It is known that part of the zinc is present as ZnS. Composition number 4. shows the reduction of ZnS in a CO/CO_2 atmosphere which happens at a higher temperature compared to ZnO under the same circumstances.

Also, the effect of other compounds on the reduction of zinc is analysed. Figure 5.34 shows the effect of the addition of iron, calcium and silicon compounds. The following compositions were used for the calculations:

1. 100 ZnO + 100 C + 10000 FeO
2. 100 ZnO + 100 C + 100 $CaCO_3$ + 100 SiO_2
3. 100 ZnO + 100 C + 10000 FeO + 10000 $CaCO_3$ + 10000 SiO_2
4. 100 ZnO + 100 C + 100 $CaCO_3$ + 100 SiO_2 + 10000 CO + 10000 CO_2
5. 100 ZnO + 100 C + 100 $CaCO_3$ + 100 SiO_2 + 100 FeO + 100 Fe_3O_4
6. 100 ZnS + 100 C + 100 CaO + 100 SiO_2

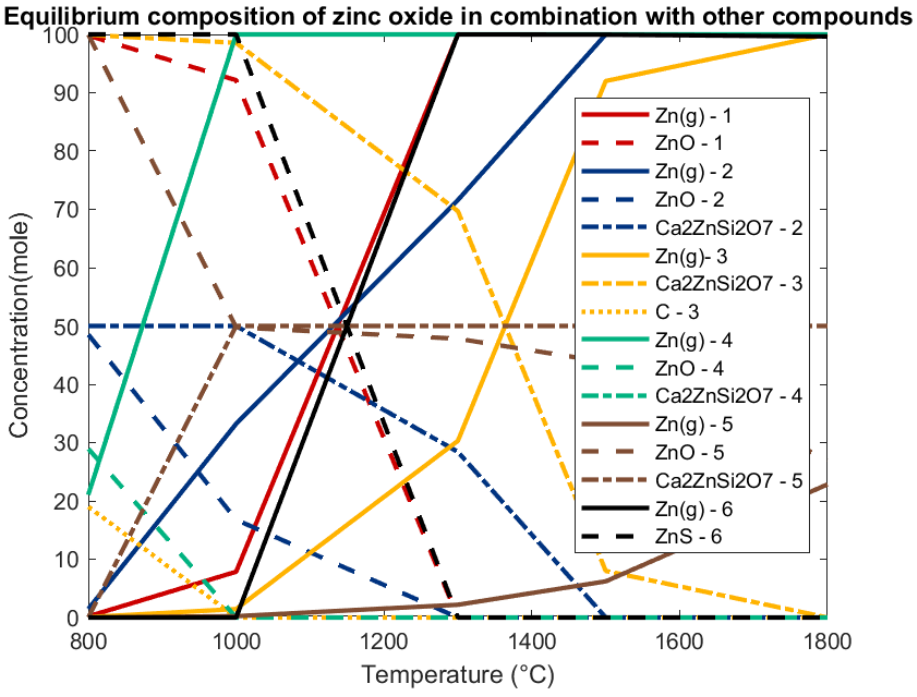

Figure 5.34: The equilibrium composition of zinc oxide in combination with other compounds present in the dusts

Different iron oxides have different effects on the reduction of zinc oxide. In all cases, they seem to decrease the amount of reduced ZnO at lower temperatures because part of the carbon is used for the reduction of the iron oxides. The higher the oxidation state of iron, the more effect it has upon

the oxidation of zinc oxide. The effect of FeO on the reduction of zinc oxide with too little carbon to reduce both can be found in the figure with number 1. However, at temperatures above 1206°C, formed metallic iron also reduces ZnO (see reaction 5.16) with the result that all zinc oxide is reduced at 1300°C and higher.

$$\mathrm{ZnO + Fe \longrightarrow Zn\,(g) + FeO} \qquad \Delta G^{1000} = 28.12\,\mathrm{kJ} \tag{5.16}$$

Under an inert atmosphere, both carbon and the CO_2 released from calcium carbonate will interact and determine a large share of the reduction or oxidation reactions. Composition number 2 shows that a small amount of $CaCO_3$ and SiO_2 causes the formation of $Ca_2ZnSi_2O_7$ which needs a higher temperature than ZnO for full reduction. When the $CaCO_3$ is substituted by the same amount of CaO, it shows complete reduction to Zn(g) at 1300°C. This means that this compound is only formed at lower temperatures and reduction potentials.

With the addition of FeO (number 3.) and FeO and Fe_3O_4 (number 5.), the reduction of zinc oxide to zinc gas needs a much higher reduction potential in order to reduce all zinc at lower temperatures. Again, because a large share of carbon is used for the reduction of iron oxides. The addition of a CO/ CO_2 atmosphere (number 4.) seems to improve the reducibility of zinc oxide as only Zn(g) is present in the equilibrium composition at 1000°C. This is not in agreement with the results from the experiments and it could mean that a longer time inside the furnace at 1000°C would eliminate the amount of zinc oxide as well.

It is not determined in what form zinc is present in the HOKS microgranulates, so they could be present as other compounds than ZnO as well which could make it more difficult to evaporate the zinc. What is known, is that part of the zinc in blast furnace dust is present in the form of ZnS. A possible way to reduce ZnS, is with the help of CaO as shown in reaction 5.17.

$$\mathrm{ZnS + CaO + C \longrightarrow Zn\,(g) + CaS + CO\,(g)} \qquad \Delta G^{1000} = -3.596\,\mathrm{kJ} \tag{5.17}$$

It appears that with the presence of enough SiO_2, the formation of $CaSiO_3$ and Ca_2SiO_4 will be more likely at 1000°C than the formation of CaS (and so Zn(g)). This can result in relatively more ZnS staying left behind in the material at lower temperatures as can be seen in the figure with composition number 6. The reduction of ZnS by $CaSiO_3$ (reaction 5.18) is only favourable at 1300°C and the reduction of ZnS by Ca_2SiO_4 is favourable from 1235°C (reaction 5.19).

$$\mathrm{ZnS + CaSiO_3 + C \longrightarrow Zn\,(g) + CaS + SiO_2 + CO\,(g)} \qquad \Delta G^{1000} = 87.14\,\mathrm{kJ} \tag{5.18}$$

$$\mathrm{2\,ZnS + Ca_2SiO_4 + 2\,C \longrightarrow 2\,Zn\,(g) + 2\,CaS + SiO_2 + 2\,CO\,(g)} \qquad \Delta G^{1000} = 132.43\,\mathrm{kJ} \tag{5.19}$$

Also, the formation of Zn_2SiO_4 could play a role in especially the HOKS samples due to its large silica content, see reaction 5.20. There is a possibility that this is present in the initial sample or formed at places with a shortage of carbon in the first moments of heating. The reduction of this compound by reaction 5.21 starts at 1008°C.

$$\mathrm{2\,ZnO + SiO_2 \longrightarrow Zn_2SiO_4} \qquad \Delta G^{1000} = -34.81\,\mathrm{kJ} \tag{5.20}$$

$$\mathrm{Zn_2SiO_4 + C \longrightarrow 2\,Zn\,(g) + SiO_2 + CO\,(g)} \qquad \Delta G^{1000} = 4.506\,\mathrm{kJ} \tag{5.21}$$

5.4.3. Larger scale TGA experiments in varying atmospheres in the vertical TGA furnace

A larger scale TGA experiment is conducted in the vertical furnace with around 70 grams of the sample added to a crucible. By using such large sample sizes, they can be characterised when cooled down. The maximum temperature reached was 1500°C in which both HOKS samples - in nitrogen and CO/CO_2 - melted, while the BOF microgranulates sintered together, see figures 5.35 and 5.36

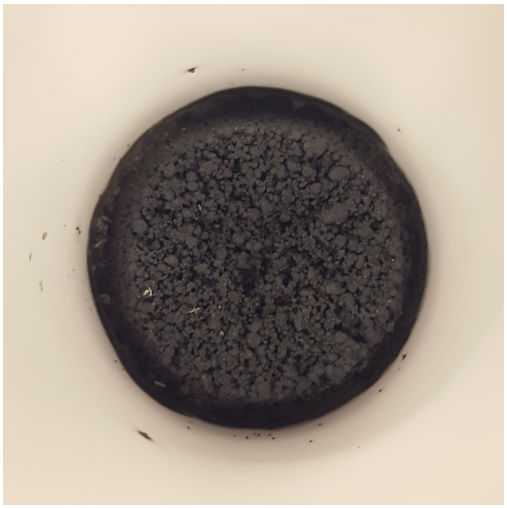

Figure 5.35: BOF 76 after the vertical furnace experiment in CO/CO_2

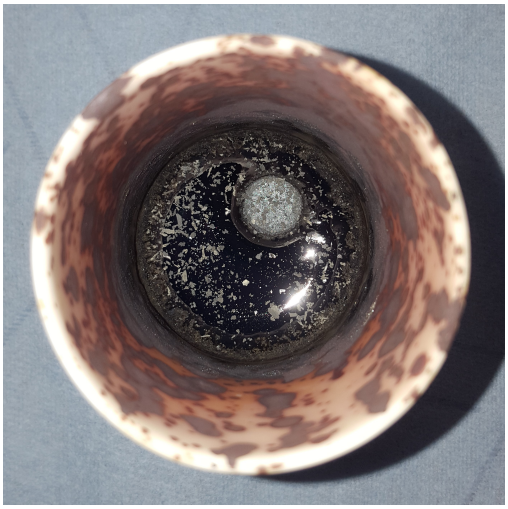

Figure 5.36: HOKS 80 (small) after the vertical furnace experiment in CO/CO_2

Both the mass and the off-gas were analysed during the temperature raise from 0 to 1500°C. Figures 5.37 show the results of the HOKS 80 (small) sample in nitrogen. At the beginning of the experiment, a gradual decrease in mass is visible with two small changes in slope at 390 and 670°C. These should be due to the reduction of portlandite and calcite. Part of the water created by the portlandite reaction is reacted to H_2 and visible in figure 5.37b. The first peak of CO_2 - at 840°C - is created by the calcite reaction which is confirmed because no CO is formed yet. The sharp dip at 900°C and the sharp peak at 1015°C are due to an unfortunate problem in the gas delivery system as no nitrogen was coming through any more. At 1015°C, this problem was solved causing a build-up of gasses to be transported to the gas analyser. The peak formed at 1000°C is created by the reduction of mainly iron oxides which caused the carbon to oxidise partly to CO and partly to CO_2. At 1440°C, an extra peak of CO is visible, this could be the moment that the sample melted, freeing the last carbon particles for reduction.

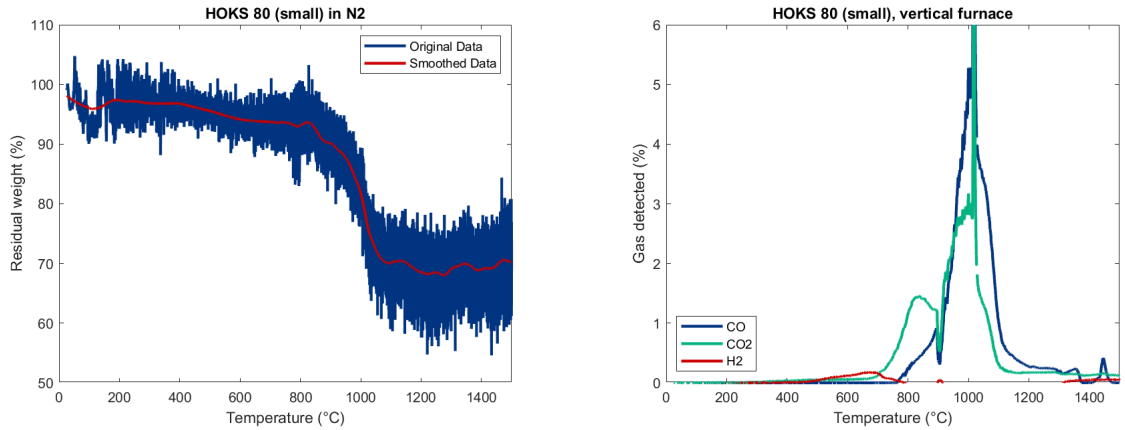

(a) Balance

(b) Off-gas analysis

Figure 5.37: The results from an experiment in the vertical TGA furnace with HOKS 80 (small) under nitrogen

Figures 5.38 show the loss in mass and the off-gas analysis of BOF 76 in nitrogen. A first decrease in mass is seen from 290-500°C which caused the peak of hydrogen and a smaller peak of CO_2 at 600°C. This hydrogen peak cannot easily be explained as no substantial amount of hydrates were previously determined to be present in the raw materials. Most likely, the hydrogen is formed by reaction 5.22. During a drying test in a furnace at 200°C for 3 hours with $\pm$ 30 grams of the samples, BOF 76 lost 2.24% of its weight and HOKS 80 (small) lost 1.97% which is due to the evaporation of water. This does not explain the big difference between the peak height of BOF 76 and HOKS 80 (small). Likely is that part of the water is released through the decomposition of the binder which happens at higher temperatures but again, the amount of binder should be the same for all microgranulates. Next to that, only a very small peak of CO_2 is formed. More research is needed to fully explain this.

$$H_2O + CO \Leftrightarrow H_2 + CO_2 \tag{5.22}$$

Another decrease in weight is starting at 675°C that speeds up at 890°C. The first part is due to calcite decomposition releasing mainly CO_2 after which the reduction of the iron oxides start at 890°C showing an increased peak of CO and CO_2 at the same temperature.

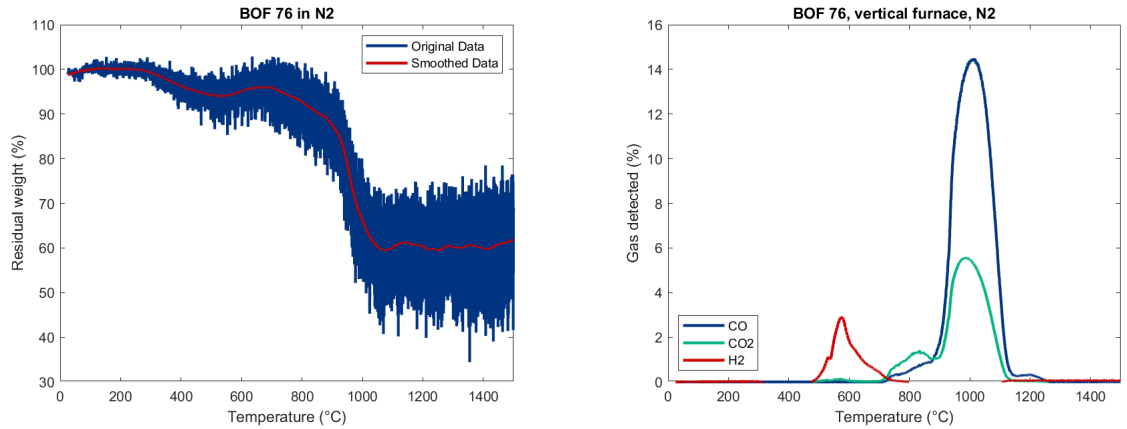

(a) Balance

(b) Off-gas analysis

Figure 5.38: The results from an experiment in the vertical TGA furnace with BOF 76 under nitrogen

The samples conducted in a CO/CO_2 atmosphere are shown in figures 5.39 and 5.40. The balance graph from the HOKS sample shows very similar results compared to the one done in N_2, with a change in slope at 280°C (portlandite), 690°C (calcite) and 790°C (iron oxides). In the off-gas, a first dip in CO is visible at 600°C. This dip is due to the peak of H_2 that is formed by a reaction of H_2O and CO. Subsequently, a peak in CO_2 is visible after which the reduction of the iron oxides starts at 790°C with an increased formation of CO. CO_2 forms slightly later. A second peak of CO is visible at 1240°C which is caused by the reoxidation of the sample. The BOF sample in figures 5.40 shows a very similar pattern to the BOF sample in nitrogen except that no specific peak of calcite reduction is visible in the off-gas analysis.

In all cases, the carbon concentration got to nearly zero and both zinc and lead were not detected at all any more with XRF. The weight loss after the vertical TGA furnace experiment was measured with a separate scale and it showed similar weight losses to the samples heated in the horizontal furnace at 1300°C, see table 5.5. It is remarkable that the highest weight loss was obtained by BOF 76 at 1000°C in an inert atmosphere. This is the case because it was the only sample that fully reduced to metallic iron as shown with XRD. The samples heated at 1000°C in an atmosphere of PCR 50 showed the biggest deviation to the other weight losses because those had the lowest mass loss.

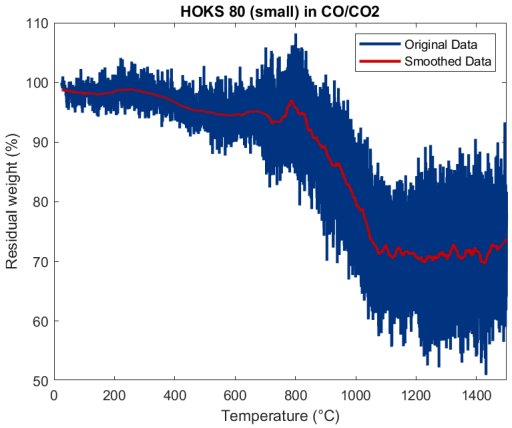

(a) Balance

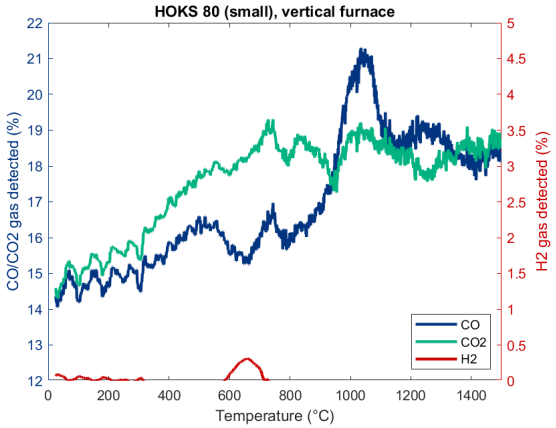

(b) Off-gas analysis

Figure 5.39: The results from an experiment in the vertical TGA furnace with HOKS 80 (small) under PCR 50

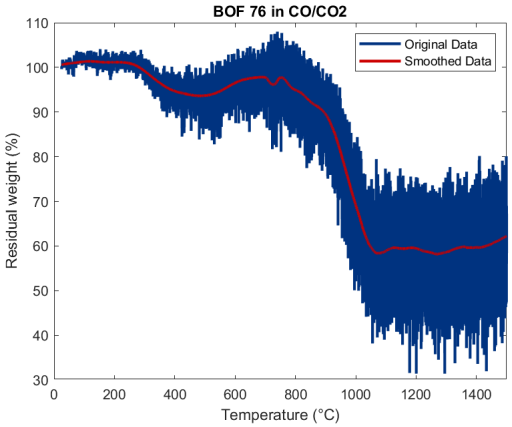

(a) Balance

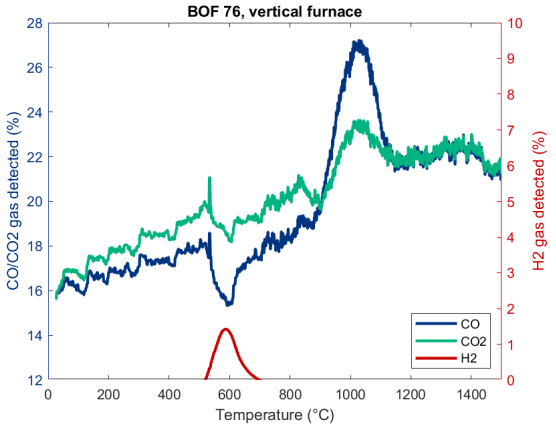

(b) Off-gas analysis

Figure 5.40: The results from an experiment in the vertical TGA furnace with BOF 76 under PCR 50

Atmosphere	Max. T	BOF 76 (%)	HOKS 80 (small) %
Inert	1000°C	63.34	74.21
PCR50	1000°C	72.37	81.01
Inert	1300°C	64.51	71.39
PCR50	1300°C	64.58	71.63
Inert	1500°C	64.34	69.65
PCR50	1500°C	65.30	71.40

Table 5.5: The residual weight of the longest time spans of the experiments conducted under the different circumstances with BOF 76 and HOKS 80 (small)

5.4.4. Composition of the TGA samples

Due to the melting of the HOKS samples between 1300°C and 1500°C, the iron clustered together in an almost pure iron bulb surrounded by a glassy substance as can be seen in figure 5.41 and 5.42.

Figure 5.41: The iron bulb from HOKS 80 (small)

Figure 5.42: Part of the residual material from HOKS 80 (small)

The iron bulb was easily separated and therefore could be analysed on its own. In table 5.6, the weight of the iron bulb is noted with reference to the rest of the material after analysis (total whole sample after) and with reference to the amount of material before analysis (total whole sample before) (equation 5.23). A flat side was created on each bulb after which EDS analysis could be performed. This showed that nearly the whole bulb consisted of pure metallic iron.

$$Massfractionironbulb = \frac{Mass_{\text{Iron bulb}}}{Mass_{\text{Whole sample}}} * 100\% \tag{5.23}$$

HOKS 80 (small)	**Weight relative to (w%)**		**Composition (w%)**			
	total after	total before	Fe	S	C	Si
CO/CO_2	30.14	21.52	98.7	1.3		
N_2	39.14	27.26	97.2		1.5	1.3

Table 5.6: The composition of the iron bulb after a large scale TGA experiment measured with a scale and EDS

The rest of the sample contained a black, glass-like material consisting mainly of calcium silica oxides and a little bit of left over iron in the form of a calcium iron silica compound. This was measured with XRD and can be seen in the top two diffractograms of figure 5.43. The sample from PCR 50 still contained 11.43% of Fe_2O_3- equivalent while the Fe_2O_3- equivalent in the nitrogen sample was almost nothing (0.45%). The higher amount of iron in the CO/CO_2 sample caused that the substance of this sample was brown in stead of black.

The sintered BOF 76 was mounted in a conductive resin and sanded for analysis in the SEM, see figure 5.44. The light gray phases in the figure are detected with EDS as pure iron with ±1.5% carbon. The darker gray and white (lighting up) phases contain impurities as calcium, silicon and magnesium (note, the black in between the particles is the resin used for moulding, this contained carbon as conductor and could have increased the amount of carbon detected with EDS). Indeed, the bottom two diffractograms in figure 5.43 show those same three compounds. Visible is that the samples from both atmospheres contain wüstite. For the sample in nitrogen, it is expected that the wüstite is mainly formed at the top

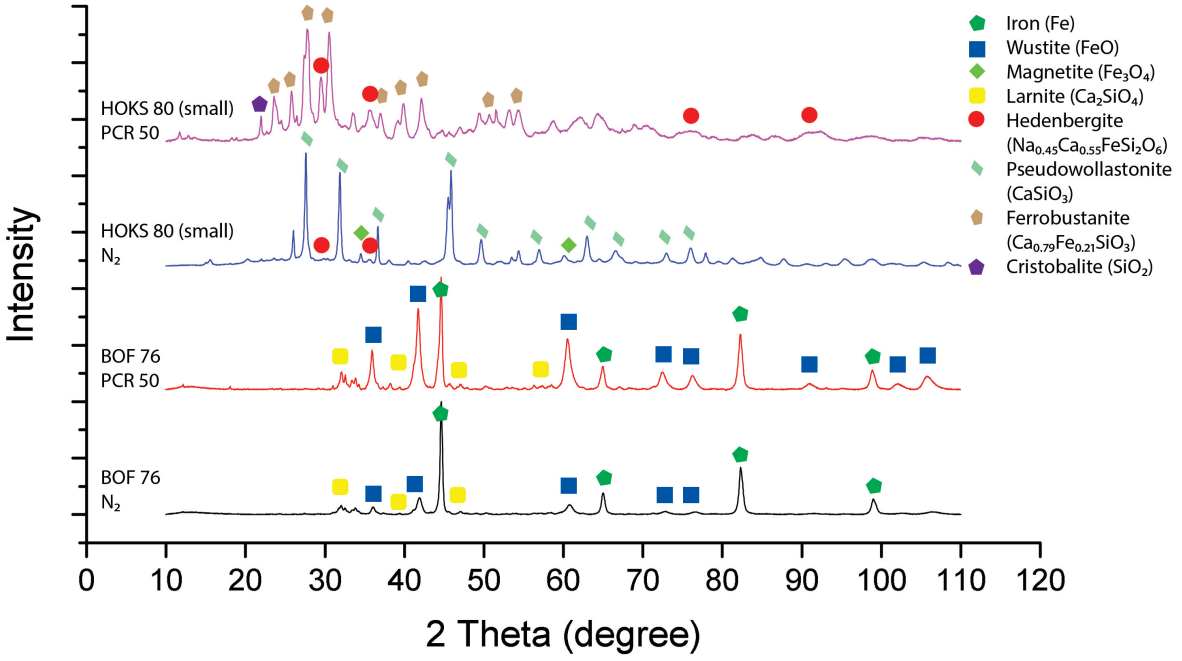

Figure 5.43: XRD diffractograms from the microgranulates treated in the vertical TGA furnace

layer, oxidised by the CO_2 created in the lower layers. For the sample in CO/CO_2, the CO_2 could most probably not reach the bottom layer of the sample therefore oxidising only the top layer. Indeed, relatively more wüstite was found in the top half of the sample compared to the bottom half as analysed with XRD for those different spots on the sample (see figure 5.45). This sample was taken by grinding a big part of the top of the sample separately from the bottom half of the sample after which one gram was analysed with XRD.

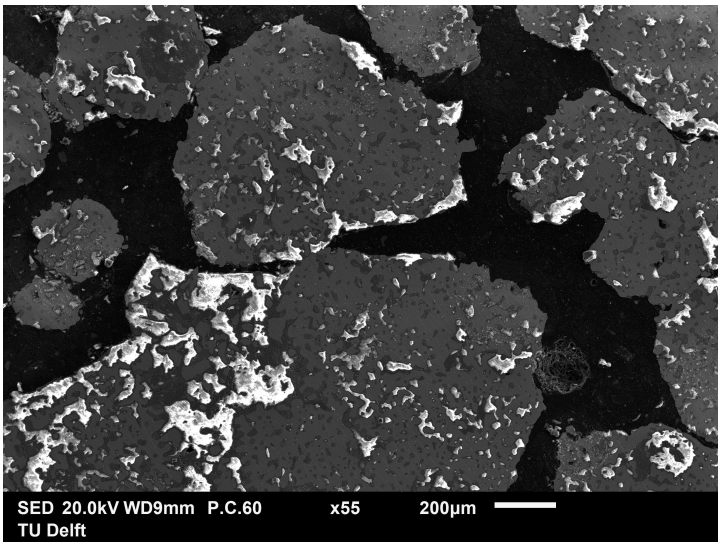

Figure 5.44: Micrograph of sintered BOF 76 after a treatment in the vertical furnace in nitrogen

5.4.5. Composition captured dust

Dust samples from different experiments are recovered in various ways in order to get an expectation of the formed dust in HIsarna. Dust is collected from HOKS 80 (small) in the horizontal furnace in

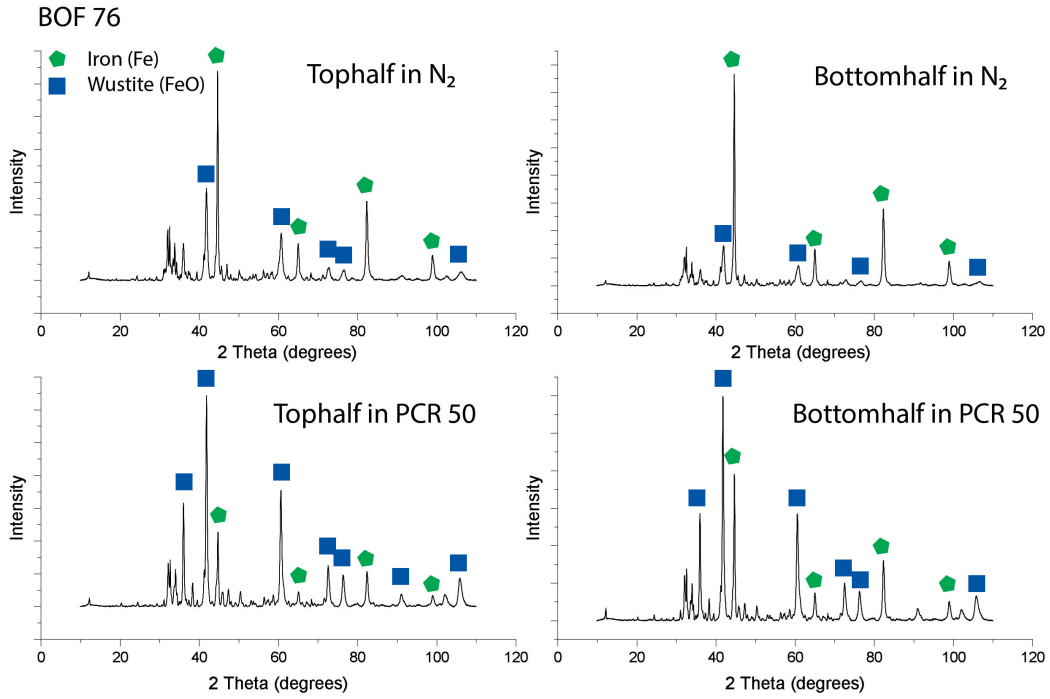

Figure 5.45: XRD diffractograms from BOF 76 samples after heating in the vertical furnace. Top half and bottom half refers to the top side and bottom side of the sample heated in the vertical furnace.

nitrogen. This is done by using a small amount of polycristalline alumina silicate wool at the beginning of the off-gas tube which collected the dusts from all time spans inside the furnace. EDS analysis shows that the elements present in this dust are zinc, lead, potassium, chloride, carbon and sulphur, see table 5.7. These were also the elements shown to leave the sample based on the XRF results from figure **??** except that it was expected to find sodium instead of potassium in HOKS 80 (small) which does not seem to be the case.

Formula	Zn	Pb	S	Cl	K	C	O	Al	Si
Atom %	15.39	3.37	2.39	2.53	0.64	11.72	47.41	13.76	2.80

Table 5.7: EDS analysis on collected dust after heating HOKS 80 (small) at 1000°C in the horizontal furnace

The other dust samples have been taken from the experiments with the vertical furnace. Part of the dust set off at the sides of alumina weighting stick could be recovered from the HOKS 80 (small) sample in nitrogen. The dust was mixed with isopropanol and put in an ultrasonic bath to loosen the particles. A small amount was drop on an aluminium plate after which it could be analysed with the SEM.

Although it was difficult to analyse distinct particles, different compositions could be detected that are shown in figure 5.46 and table 5.8. Based on this data, it is assumed that part of the Zn(g) is oxidised by reacting with CO_2 at lower temperatures. Not enough oxygen is present to have oxidised all zinc (in point 3 and 6) so the remaining should still be present as pure zinc. As most spots have a similar atomic concentration of potassium and chloride, it is expected that KCl has formed which is later confirmed by XRD. Point 2 clearly detected a lead oxide particle although it is likely that part is also present as lead chloride because more chloride is present than can be formed with to KCl. $PbCl_2$ has a boiling point of 950°C and is more energetically stable than the formation of $ZnCl_2$.

For BOF 76, some dust set on the alumina tube could be recovered with a paper tissue. This tissue is subsequently analysed with EDS as can be seen in figure 5.47 and table 5.9. Similar results as with HOKS 80 (small) are visible with elemental zinc, zinc oxide, lead oxide and potassium chloride. In this

secondary BOF sample dust, more potassium is present than chloride which could have entered the off-gas stream due to its low boiling point (T_b K = 759°C).

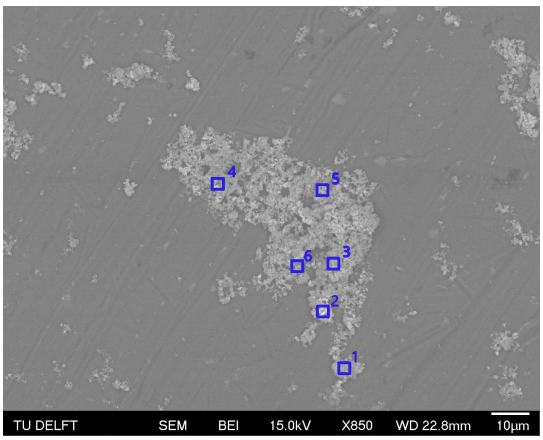

Figure 5.46: SEM image from dust captured from HOKS 80 (small) TGA N_2

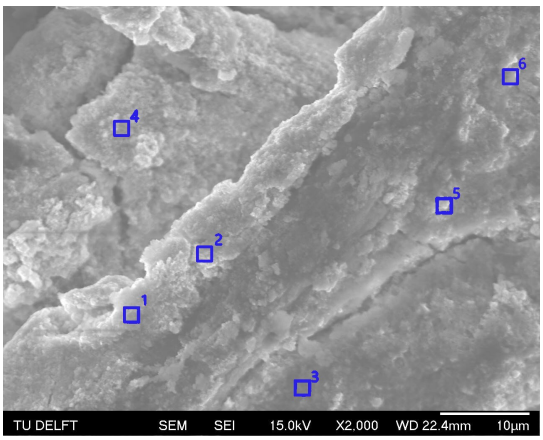

Figure 5.47: SEM image from dust captured from BOF 76 TGA N_2

Analysis number	C	O	Al	S	Cl	K	Zn	Pb
1	6.22	40.45	18.66		5.96	5.53	20.15	3.03
2	11.97	53.54	17.22		3.07	0.46		13.73
3	4.34	32.23	4.85	0.59	3.49	0.91	50.08	3.52
4	8.31	27.23	6.50		20.76	21.83	12.73	2.63
5	6.20	46.93	7.88		4.44	3.36	26.80	4.39
6	4.49	26.18	23.77		2.34	1.77	38.72	2.71

Table 5.8: EDS analysis on dust from HOKS 80 (large) on an aluminium background. Results are shown in atom %

Analysis number	C	O	Al	S	Cl	K	Zn	Pb
1	6.79	29.47				0.94	58.73	4.06
2	17.80	47.76					31.36	3.08
3	21.92	49.95	0.46	5.26	0.49	2.42	19.50	
4	6.25	42.94	1.66			1.49	42.50	5.16
5	9.22	18.35	0.98			2.06	67.10	2.30
6	7.93	23.90			1.61	3.07	60.65	2.84

Table 5.9: EDS analysis on dust from BOF 76 on a paper tissue. Results are shown in atom %

At last, some dust is captured by flowing the gas through a water bottle in which the dust stayed behind. Subsequently, the dust was filtered out and dried for 2.5 hours at 105°C after which a small amount was left behind ($\pm$ 50 mg). This dust as well as the dust collected from the inside of the furnace have been analysed with XRD for BOF 76 in nitrogen and BOF 76 in PCR 50, see figure 5.48. It should be noted that the dust had a black colour after filtration which changed to a gray colour after drying which could

suggest that extra oxidation has occurred. This is proven with the fact that no metallic zinc is found in the XRD pattern while this should be present based on the previous EDS analyses. Again, the main elements found in the off gas are lead and zinc compounds. The collected dust on the stick and in the water bottle show similar results with the main difference that no KCl is detected in the dust collected in the water bottle as this dissolves in water and was filtered out. Also, the dust from the water bottle seems to have a higher lead content. When looking at the dust collected from the furnace, this has a very similar composition in an inert atmosphere and the CO/CO_2 atmosphere except that more sylvite and abellaite were formed in the CO/CO_2 atmosphere.

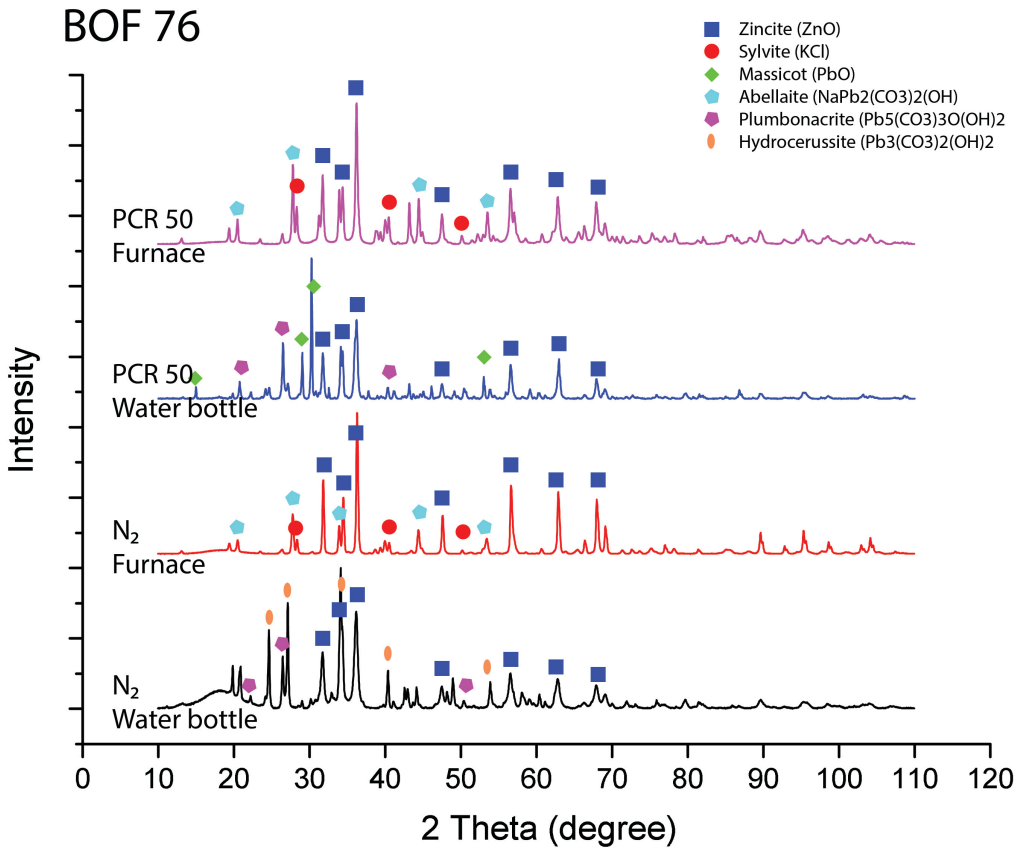

Figure 5.48: XRD diffractograms of the dust collected from the vertical TGA furnace

A very important question is whether the HIsarna dust would be suitable for the zinc smelters. Therefore, the average dust composition detected with EDS is compared with a typical zinc oxide feed to Nyrstar (Source: internal communication). Those compositions can be seen in table 5.10. It shows that the zinc concentration in the dust collected from BOF 76 is high enough for the zinc smelter while this is doubtful for HOKS 80 (small). The biggest issue are the high potassium and chloride contents. These were not found in the dust collected in the water bottle which means that they can be easily washed out. Therefore a washing stage may be required. The high lead content is most probably not a problem as no penalty has been indicated. During trials at the pilot plant of HIsarna, it appeared that there was a lot of feed dust carryover towards the off-gas system. This dust contains a lot of iron with the result that a high amount of zinc ferrite formation was recorded. However, as no iron dust feed was used during the experiments, this effect was not seen. It is something to take in mind about the reliability of these conclusions.

	C	O	S	Cl	K	Zn	Pb
BOF 76	1,42	14,11	0,37	4,61	4,26	60,24	15,00
HOKS 80 (small)	2,23	16,73	0,15	5,36	4,86	50,80	19,88
Max. concentration[1]	2		4	0,2	0,5	75	5
Min. concentration[1]	0		0	0	0	55	0
Penalty ($/t)	?		0	10	?	0	0

Table 5.10: The average composition of the dust collected from the side of the furnace when treated in N_2 measured with EDS in w% as well as their concentrations allowed by zincsmelters

5.5. Future perspective in Tata Steel IJmuiden

At the moment, two blast furnaces and two basic oxygen furnaces are present in IJmuiden. In 2030, one of these blast furnaces should be replaced by an industrially producing HIsarna.

5.5.1. Dust accessibility

In the 2030 scenario, the amount of BF dust will decrease while the amount of BOF dust will remain similar to the current situation. Based on this scenario, Tata Steel has inventoried the amount of dusts created:

- 12 kt/year BF dust
- 84 kt/year BOF dust

If this is the case and all BF dust can be used for the production of BOF/BF dust microgranulates, a ratio of 87.5 BOF dust : 12.5 BF dust can be reached. This means that not enough BF dust is available to reach the ratio of 76 BOF dust : 24 BF dust. The idea is to recycle 50 kt/year of the HOKS. In that case, the 80:20 HOKS:BF dust ratio would consume all BF dust available per year. However, as the 20% BF dust seems to provide an overshoot on carbon, a lower ratio could be used. Next to those dusts, there are also plans to recycle among others EAF dust and goethite. They may also need some carbon as reducing agent which would be ideally supplied by BF dust. To solve this problem, either another carbon source need to be found or it could be tested how high the zinc separating efficiency is when using less BF. In BOF 85 for example, only 0.07% Zn was present after half an hour of self reduction at 1000°C in the horizontal furnace. This is only slightly more compared to the 0.02% of BOF 76 with the big difference that not all iron oxides were reduced to metallic iron in a nitrogen atmosphere. As this would not happen in the atmosphere of HIsarna, with wüstite being the equilibrium phase, its behaviour under different reducing circumstances should be further elaborated.

Another option is to look for other carbon supplies. There are many blast furnaces in Europe which produce dusts with high carbon contents. However, the composition could be very different. A main difference is caused by the way of recycling the steelmaking dusts in the furnaces themselves. Tatasteel recycles them through sintering causing a high zinc concentration in the BF dust. Other plants recycle their dusts in the BOF furnace which results in a high zinc concentration in the BOF dust. Most ideal would be to recycle the higher zinc bearing dusts together (high zinc bearing BF dust with high zinc bearing BOF dust) and optimise them for zinc recovery while the lower zinc bearing dusts do not need the high carbon supply and may be fed to the cyclone together with the iron ore fines.

[1] The minimum and maximum allowed contents in table 5.10 show values for normal operation. It may be possible to have a higher amount of impurities but a penalty has to be paid for that. No penalty is required for lead.

5.5.2. Comparison with the circumstances in HIsarna

The results of the experiments that are performed for this thesis do only simulate a small part of what is happening in HIsarna. Isothermal experiments at 1000°C and 1300°C were executed. These are low temperatures compared to the temperature in the cyclone of HIsarna but are chosen to be better able to analyse the reactions taking place in the microgranulates. This is easier because of the slower reaction rates. At first, the self reduction behaviour of the microgranulates was analysed by performing the reactions in an inert, nitrogen atmosphere. This is totally not similar to the atmosphere in HIsarna but as the gasses do not directly reach the core of the microgranulates, this is still important to know.

Later, the reduction behaviour in an inert atmosphere was compared to the reduction behaviour in a 50% CO and 50% CO_2 atmosphere. This is not the atmosphere at the feed inlet of the cyclone but more or less the last atmosphere the microgranulate will experience before entering the SRV. The effect of different atmospheres on the reduction behaviour of zinc oxide was analysed with FactSage. These can be seen in figure 5.49. The numbers in the legend belong to the following compositions:

1. 100 ZnO + 100 C + 10000 CO + 10000 CO_2
2. 100 ZnO + 10000 CO + 40000 CO_2
3. 100 ZnO + 100 C + 50000 CO_2
4. 100 ZnO + 10000 CO + 10000 CO_2
5. 100 ZnO + 10000 CO + 40000 CO_2 + 5000 O_2
6. 100 ZnO + 50000 CO2

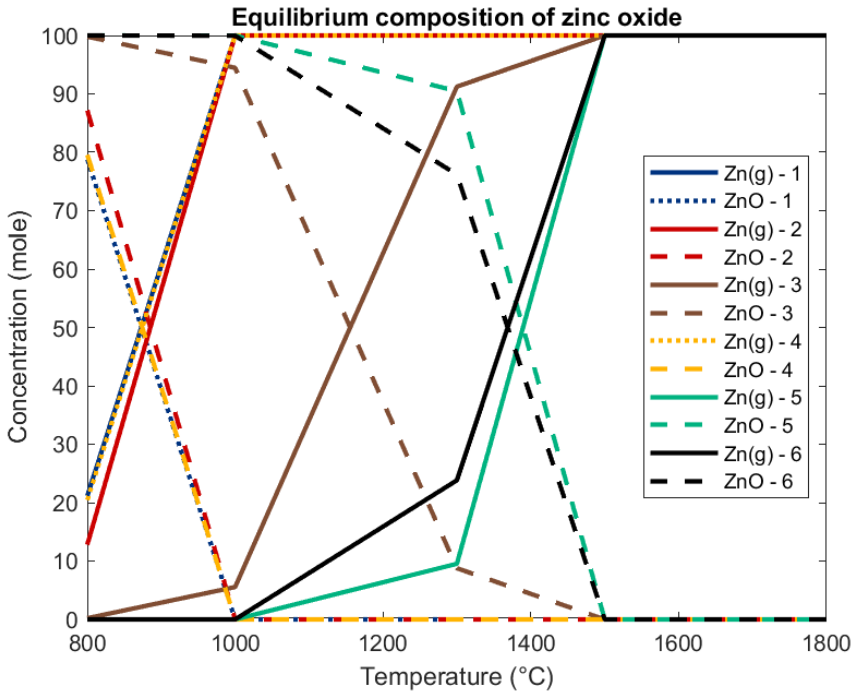

Figure 5.49: The equilibrium composition of zinc oxide under different reducing atmospheres

The less reducing atmospheres of composition number 1, 2 and 4 show complete reduction of zinc oxide below 1000°C but not much is happening at that temperature in the more oxidising atmospheres. On the other hand, zinc oxide does not seem to need a high amount of CO(g) to be reduced at higher

temperatures. It can be seen that all zinc oxide is reduced to zinc(g) at 1500°C in all calculated atmospheres. This looks promising for the zinc reduction at the more oxidising atmosphere at the feed inlet of HIsarna which is closest to composition number 5. Earlier calculations have shown that other compounds affect the reduction behaviour of zinc oxide so it is recommended to do more experiments at higher temperatures and in more oxidising atmospheres.

6

Conclusions and recommendations

The production of steel requires an enormous process with the result that a lot of waste is generated. Part of it can be re-utilised within new applications but dusts remain difficult to process in an economical manner. A literature review has described the many processes that have been in action or under development trying to deal with those dusts. Lower zinc containing dusts like BOF dust and BF dusts are sometimes recycled with specialised furnaces. However, the advantage of HIsarna is that it will focus on the production of crude iron whilst also being able to recycle both zinc and iron bearing materials in separate streams with the result that they both can be recycled into high quality new materials.

6.1. Conclusions

Microgranulates made from HOKS + BF dust and BOF dust + BF dust were heated at different temperatures and under different atmospheres to determine its ability to separate the zinc and prereduce the iron oxides. In HIsarna, this zinc should be carried away together with the off-gas after which it will be recycled by the zinc industry. The research questions shown in chapter 3 will be answered in this chapter.

1. *What is the exact composition of the microgranulates and how could that affect the reduction behaviour?*

The BOF microgranulates contained mainly elemental iron and wüstite as iron bearing phase (81.7%). Next to that, calcite was present in noteworthy amounts as well (9.6%). The iron in HOKS was more oxidised and mostly present as magnetite and hematite (55%). The amount of calcium was double the amount (26%) present in BOF dust and XRD showed the presence of calcite, portlandite and calcium iron oxide carbonate hydrate. HOKS also contains a lot of quartz (9%). The addition of BF dust, which is mainly a carbon source (40%), is important because the carbon can be used to reduce the oxides. Next to that, a significant amount of iron is present mostly as hematite (35%) and about 6% of zinc oxide/zinc sulphide.

2. *What processes take place at which temperature?*

During non-isothermal experiments in an inert atmosphere, the reaction temperature of different reactions that caused a reduction in mass was analysed. Around 400°C, the HOKS samples lost H_2O through the decomposition of portlandite. Both BOF and HOKS samples lost CO_2 through the decomposition of calcite around 600°C.

The samples mixed with blast furnace dust as carbon source show a large weight loss caused by the reduction process starting at 870°C. This is mostly caused by the reduction of iron oxides (magnetite and wüstite) and calcium iron oxides. The latter ones are mainly formed in the HOKS samples due to the presence of large amount of calcium but show to be reduced by carbon. The reduction of zinc oxide happens in the same temperature range with the result that it is not visible separately.

3. *What mechanisms take place during isothermal self reduction processes and what is its timescale?*

To determine the mechanisms that take place during the reduction processes, the self reduction behaviour of the microgranulates at 1000°C were analysed at first. The results showed that most microgranulates mixed with BF dust could be fully reduced in 30 minutes at 1000°C except for BOF 85 of which the iron oxides only reduced to wüstite. The HOKS + BF microgranulates contained too much carbon for self reduction meaning that a smaller percentage of BF could be used. At the beginning, calcium ferrites were formed in the HOKS samples due to the large amount of calcium. In smaller amounts, this happened as well in the BOF samples. At the end of reduction, all calcium ferrites were reduced to metallic iron although it seemed to decrease the reduction speed slightly. The calcium oxide and silica subsequently formed calcium silicates.

Two microgranulates were chosen to be used for experiments in other atmospheres and at higher temperatures. The pure HOKS and pure BOF microgranulates were not studied as they did not contain enough carbon for optimal reduction. Little difference could be found between the HOKS samples so HOKS 80 (small) was chosen because of its highest zinc content. As BOF 76 was the only BOF dust containing sample that fully reduced all iron in an inert atmosphere, this sample was also chosen to continue with.

The biggest difference between the experiments at 1000°C and 1300°C is that the final equilibrium composition was reached in a shorter time span. Also, the iron in the finished BOF 76 sample was slightly more oxidised which suggest that the carbon was better used for other reactions. Indeed, the 5 or 10 minute samples at 1300°C did not contain any significant amount of zinc and lead any more. Besides that, different compositions of calcium silicon oxide compounds were detected in the HOKS samples when comparing the different temperatures.

4. *Can the reduction behaviour be optimised by using different atmospheres?*

The same two microgranulates are used for experiments in a 50% CO and 50% CO_2 atmosphere which is a similar atmosphere to the bottom part of the cyclone. The microgranulates were mostly reduced in similar ways as in nitrogen but after some time the CO_2 caused that the iron oxidised again towards wüstite which is the equilibrium phase of iron in this atmosphere. At 1000°C, this atmosphere slowed down the reduction of zinc oxide with the result that a higher amount of zinc oxide was still present after 30 minutes compared to self reduction. At 1300°C, the reduction of zinc was completed before the samples starting oxidising again which seems promising as HIsarna operates at even higher temperatures.

5. *What is the composition of the HIsarna dust and is it suitable for the zinc industry?*

Although the furnaces used do not simulate the off-gas system of HIsarna perfectly, an idea was obtained about what elements would enter this off-gas system. This appeared to be mainly zinc, lead, potassium, sodium and chloride. Potassium, sodium and chloride are undesirable for the zinc industry. However, this can be easily separated by dissolving the dust in water which was already shown during the experiments. The amount of lead appeared to be too high as well. This is not necessarily a problem but should be properly consulted with the zinc smelters.

How does the self reduction behaviour of zinc present in the microgranulates compare with this behaviour in an atmosphere of 50% CO and 50% CO_2?

This was the main question of this thesis. During the self reduction behavior of the BOF + BF dust containing microgranulates at 1000°C, the zinc was reduced to a level below 0.1% in 20-30 minutes. In a 50% CO, 50% CO_2 atmosphere, this reduction was slower which resulted in a higher concentration of zinc in the BOF 76 sample after 30 minutes at 1000°C. On the other hand, because HOKS contained an overshoot of carbon, the same low zinc concentration as in a nitrogen atmosphere was reached after 30 minutes but this took more time than in nitrogen. At 1300°C, the opposite effect is seen with zinc being removed before the sample started to oxidise again. Especially in the HOKS samples, the zinc loss is faster in CO/CO_2 than in nitrogen. In CO/CO_2, all zinc was gone in both samples after 5 minutes in the furnace.

The separation of zinc and iron in HIsarna show to be promising based on the experimental work done for this thesis. The microgranulates are robust and are expected to be a good solution as feed material for HIsarna. However, additional research is needed to simulate the circumstances in HIsarna even better.

6.2. Recommendations

Supplementary research should be undertaken in a couple of aspects. Firstly, the composition of the HOKS + BF microgranulates appear to contain more carbon than necessary for complete self reduction. The effect on its reduction behaviour with less BF dust should be analysed. It is recommended to analyse a microgranulate with 86% HOKS and 14% BOF dust based on the amount of carbon that is left after self-reduction at 1300°C. It was also shown that not enough BF dust is available at Tatasteel to provide enough carbon for the microgranulates produced with the current ratios. It is recommended to analyse the effect on the separation of zinc with a lower BF dust content in both HOKS and BOF microgranulates and to find a supply for an alternative carbon source.

Much effort has been put in operating the vertical furnace but it is believed that it should be possible to optimise the results. Among others, the effect of the temperature on the balance readings should be eliminated. Besides, due to the crucible, the gasses do not optimally reach all microgranulates which could be improved by using a smaller crucible or one through which the gasses can penetrate.

This thesis dealt with an inert atmosphere and a CO/CO_2 atmosphere with a PCR of 50%. However, at the inlet of the feed which is at the top of the cyclone, the atmosphere is much more oxidising and it should be tested whether it is possible to reduce and evaporate all zinc before all carbon is gone in that atmosphere. Next to that, the comparison between the vertical furnace and HIsarna can be optimised by doing an isothermal experiment whilst measuring the change in weight during the reaction. When the furnace has reached a stable temperature, the crucible with sample could be inserted and the weight changes and off-gasses can be recorded. These experiments can also be done at different temperatures and in different (changing) atmospheres.

At last, the dust created by the experiments was analysed and showed a lot of zinc oxide and lead oxide together with some potassium and chloride. However, the circumstances in which this off-gas dust is created, is not similar to the dust capture in HIsarna. The dust created during these experiments is close to the best case scenario. It is recommended to simulate this better to obtain good knowledge about the exact composition of the HIsarna dust.

Bibliography

[1] Dan Sandoval. SDI to build EAF mill in Southwest US - Recycling Today, 2018.

[2] Nnamdi Anyadike and IZA. Zinc recycling. *Lead and Zinc*, 2010:132–139, 2011.

[3] Statista. Global production of zinc metal from 2004 to 2019, 2020.

[4] NSC. An introduction to steelmaking, 2017.

[5] Jiayun Zhang, Hiroyuki Matsuura, and Fumitaka Tsukihashi. *Processes for Recycling*, volume 3. Elsevier Ltd., 2014.

[6] H. Y. Sohn and M. Olivas-Martinez. *Lead and Zinc Production*, volume 3. Elsevier Ltd., 2014.

[7] I. E. Doronin and A. G. Svyazhin. Commercial methods of recycling dust from steelmaking. *Metallurgist*, 54(9-10):673–681, 2011.

[8] B. Garcia-egocheaga and N. Goicoechea. Recovery of zinc oxide from secondary raw materials: new developments of the waelz process. *Fourth International Symposium on Recycling of Metals and Engineered Materials*, pages 333–344, 2000.

[9] H Tsutsumi, S Yoshida, and M. Tetsumoto. Features of fastmet process. 2010.

[10] R. Frieden, T. Hansmann, J.L. Roth, M. Solvi, and R. Engel. Primus, a new process for the recycling of steelmaking by-products and the prereduction of iron ore.

[11] TATA Steel. HIsarna smelting reduction technology. (April), 2017.

[12] Koen Meijer, Christiaan Zeilstra, Cornelis Teerhuis, Maarten Ouwehand, and Jan Van Der Stel. Developments in alternative ironmaking. *Transactions of the Indian Institute of Metals*, 66(5-6):475–481, 2013.

[13] Orestis Almpanis-Lekkas, Bernd Weiss, and Walter Wukovits. Modelling of an ironmaking melter gasifier unit operation with multicomponent/multiphase equilibrium calculations. *Journal of Cleaner Production*, 111:161–171, 2016.

[14] G. Ruiz-Martinez, D. Rivillas-Ospina, I. Marino-Tapia, and G. Posada-Vanegas. SANDY: a Matlab tool to estimate the sediment size distribution from sieve analysis. *Computers & Geoscience*, pages 104–116, 96.

[15] James M McClelland and Gary E Metius. Recycling Ferrous and Nonferrous Waste Streams with FASTMET. *Jom*, 55(8):30–34, 2003.

[16] United nations. Sustainable development goal 12, 2020.

[17] World steel assosiation. Steelfacts. 2018.

[18] Félix A López and Aurora López-Delgado. Enhancement of Electric Arc Furnace Dust by Recycling to Electric Arc Furnace. *Journal of Environmental Engineering*, 128(12):1169–1174, 12 2002.

[19] World zinc Association. About cycles, recycling and circular economy.

[20] IZA-europe, IZA, Eurofer, and Egga. ZINC COATED STEEL, 2006.

[21] Gavin M. Mudd, Simon M. Jowitt, and Timothy T. Werner. The world's lead-zinc mineral resources: Scarcity, data, issues and opportunities. *Ore Geology Reviews*, 80:1160–1190, 2017.

[22] M. Shamsudding. *PHYSICAL CHEMISTRY OF METALLURGICAL PROCESSES*. John Wiley & Sons, 2016.

[23] World steel assosiation. Energy use in the steel industry. *Worldsteel Association Fact Sheet*, (Lci):1–3, 2013.

[24] Horizon. Technical analysis – Iron and Steel sector. (693845), 2020.

[25] Britannica. Basic oxygen steelmaking.

[26] Luiten. Chapter 6 Smelting reduction technology. pages 167–204, 2001.

[27] Jorge Madias. Electric Furnace Steelmaking. In *Treatise on Process Metallurgy*, volume 3, pages 271–300. Elsevier Ltd., 2014.

[28] M. H. Morcali, O. Yucel, A. Aydin, and B. Derin. Carbothermic reduction of electric arc furnace dust and calcination of waelz oxide by semi-pilot scale rotary furnace. *Journal of Mining and Metallurgy, Section B: Metallurgy*, 48(2):173–184, 2012.

[29] Cahn Robert W Flemings Merton C Ilschner Bernhard Kramer Edward J Mahajan Subhash Buschow K.H. Jürgen. Iron Resources and Direct Iron Production, 2001.

[30] European Union. NON-CRITICAL RAW MATERIALS PROFILES. 2014.

[31] NYRSTAR. Introduction to Zinc and Lead Smelting Business. (November), 2009.

[32] Zinc india. zinc production: from ore to metal.

[33] Jeroen Kuenen, Jan Berdowski, Pieter Van Der Most, Chris Veldt, Jan Pieter Bloos, Jozef M Pacyna, Dagmar Oertel, Ute Karl, Tinus Pulles, and Wilfred Appelman. 2.C.6 Zinc production. *EMEP/EEA emission inventory guidebook*, pages 1–26, 2013.

[34] Erkan Guler, Abdullah Seyrankaya, and Ebru Tufan. Removal of Impurity Ions from Zinc Sulfate Solution by Cementation. (December 2018), 2014.

[35] A. W. Richards. Zinc processing, 2019.

[36] Hannu Tapani Makkonen, Jyrki Heino, Leena Laitila, Aimo Hiltunen, Esko Pöyliö, and Jouko Härkki. Optimisation of steel plant recycling in Finland: Dusts, scales and sludge. *Resources, Conservation and Recycling*, 35(1-2):77–84, 2002.

[37] Christof Lanzerstorfer, Birgit Bamberger-Strassmayr, and Klaus Pilz. Recycling of blast furnace dust in the iron ore sintering process: Investigation of coke breeze substitution and the influence on offgas emissions. *ISIJ International*, 55(4):758–764, 2015.

[38] Janusz Stecko, Ryszard Stachura, Marian Niesler, Mikolaj Bernasowski, and Arkadiusz Klimczyk. Utilisation of metallurgical sludge by multi-layer sintering. *Ironmaking and Steelmaking*, 45(9):779–786, 2018.

[39] Christof Lanzerstorfer. Zinc Enrichment in In-Plant Electrostatic Precipitator Dust Recycling by Air Classification in Converter Steelmaking. *Steel Research International*, 90(2):1–7, 2019.

[40] Gerhard Endemann, Hans Bodo Lüngen, and Carl Dieter Wuppermann. Dust, scale and sludge generation and utilisation in German steelworks, 2006.

[41] Kenichi Nakajima, Kazuyo Matsubae-Yokoyama, Shinichiro Nakamura, Satoshi Itoh, and Tetsuya Nagasaka. Substance flow analysis of zinc associated with iron and steel cycle in Japan, and environmental assessment of EAF dust recycling process. *ISIJ International*, 48(10):1478–1483, 2008.

[42] J. Ruetten, C. Frias, G. Diaz, D. Martin, and F. Sanchez. Processing EAF Dust through Waelz kiln and ZINCEX solvent extraction: the optimum solution. 2011.

[43] Jürgen Antrekowitsch, Gernot Rösler, and Stephan Steinacker. State of the Art in Steel Mill Dust Recycling. *Chemie-Ingenieur-Technik*, 87(11):1498–1503, 2015.

[44] G Harp, S Möhring, C Hillman, and W Bsirske. *Alternative Processing Sinter Plant Recycling Materials*. 2007.

[45] Karl Josef Sassen and Carsten Hillmann. The DK process - For the recovery of iron and zinc from BOF dusts and sludges, 2011.

[46] Carsten Hillmann, Christopher M. Moore, and Karl Josef Sassen. Solutions for dusts and sludges from the BOF process, 2007.

[47] H. Ishikawa, J. Kopfle, and J. Ppke. rotary hearth furnace technologies for iron ore and recycling applications. 2008.

[48] N. Masson and P. Briol. A brief summary of zinc oxide processing methods available for the Bongara deposit. *Zinc One*, page 11.

[49] Shuzo Kikuchi, Shoichi; Ito. ITmk3 process. *Kobelco technology review*, 29, 2010.

[50] G E Totten and R Colas. *Encyclopedia of Iron, Steel, and Their Alloys (Online Version)*. Metals and Alloys Encyclopedia Collection. CRC Press, 2016.

[51] B. Anameric and S. Komar Kawatra. Direct irin smeling reduction processes. *Mineral Processing and Extractive Metallurgy Review*, 30(1):1–51, 2009.

[52] Hiroshi Oda, Tetsuharu Ibaraki, and Youichi Abe. Dust recycling system by the rotary hearth furnace. *Nippon Steel Technical Report*, (94):147–152, 2006.

[53] Hiroshi Ichikawa and Hiroaki Morishige. Effective use of steelmaking dust and sludge by use of rotary hearth furnace, 2002.

[54] M. Holtzer, A. Kmita, and A. Roczniak. The Recycling of Materials Containing Iron and Zinc in the OxyCup Process. *Archives of Foundry Engineering*, 15(1):126–130, 2015.

[55] Paul wurth. PRIMUS ® Recycling of Residues and Wastes from Ironmaking , steelmaking and non-ferrous metallurgy. 2015.

[56] B.M. Tieman. *Terugwinning van zink bij de recycling van verzinkt staal (schroot)*. 2008.

[57] C Cao, Y Meng, and F Yan. Analysis on energy efficiency and optimization of HIsmelt process. In *Energy Technology 2019: Carbon Dioxide Management and Other Technologies*, pages 3–11. 2019.

[58] K Meijer, C Guenther, and R J Dry. HIsarna Pilot Plant Project. *InSteelCon*, (July):1–5, 2011.

[59] Jan Van Der Stel, Koen Meijer, Stanley Santos, Tim Peeters, Pieter Broersen, and Tata Steel. Hisarna , an Opportunity for Reducing CO 2 Emissions from Steel Industry. *CATO Meets the Projects Utrecht*, (November), 2017.

[60] A.G.A Peters. *Zinc vapourisation from sludge wastes under thermal shock*. PhD thesis, 2019.

[61] T. C. Eisele and S. K. Kawatra. A review of binders in iron ore pelletization. *Mineral Processing and Extractive Metallurgy Review*, 24(1), 2003.

[62] N. A. El-Hussiny and M. E.H. Shalabi. A self-reduced intermediate product from iron and steel plants waste materials using a briquetting process. *Powder Technology*, 205(1-3):217–223, 2011.

[63] Gedeputeerde Staten and Provinciale Staten Van Noord-holland. Provincie. (34362354), 2019.

[64] Yongxiang Yang, Yanping Xiao, and Tim Peeters. Recycling of ironmaking and steelmaking dust : challenges and opportunities – European perspective. 2019.

[65] Yingxia Qu. *Experimental Study of the Melting and Reduction Behaviour of Ore Used in the HIsarna Process PhD thesis Yingxia Qu*. 2013.

[66] Fui Tong Lee. The mechanisms and kinetics of reduction of zinc oxide solid solutions. *Mineral Processing and Extractive Metallurgy Review*, 23(1):11–50, 2010.

[67] A.L. Beyzavi and C. Mattich. Operational practice with the waelz kiln and leaching plant of TSU in Taiwan. *Fourth International Symposium on Recycling of Metals and Engineered Materials*, pages 345–360, 2000.

[68] N. Antuñano, J. F. Cambra, and P. L. Arias. Hydrometallurgical processes for Waelz oxide valorisation – An overview. *Process Safety and Environmental Protection*, 129(December):308–320, 2019.

[69] G.A. Kolta, S.Z. El-Tawil, A.A. Ibrahim, and N.S. Felix. KINETICS AND MECHANISM OF ZINC FERRITE FORMATION. *Thermochimica Acta*, 36:359–366, 1980.

[70] Klára Drobíková, Daniela Plachá, Oldřich Motyka, Roman Gabor, Kateřina Mamulová Kutláková, Silvie Vallová, and Jana Seidlerová. Recycling of blast furnace sludge by briquetting with starch binder: Waste gas from thermal treatment utilizable as a fuel. *Waste Management*, 48:471–477, 2016.

[71] B. Asadi Zeydabadi, D. Mowla, M. H. Shariat, and J. Fathi Kalajahi. Zinc recovery from blast furnace flue dust. *Hydrometallurgy*, 47(1):113–125, 1997.

[72] Marcos Vinícius Cantarino, Celso De Carvalho Filho, and Marcelo Borges Mansur. Selective removal of zinc from basic oxygen furnace sludges. *Hydrometallurgy*, 111-112(1):124–128, 2012.

[73] Hesham Mohamed Ahmed, Amanda Persson, Lena Sundqvist Ökvist, and Bo Björkman. Reduction behaviour of self-reducing blends of in-plant fines in inert atmosphere. *ISIJ International*, 55(10):2082–2089, 2015.

[74] Ji Won Jeon, Sung Mo Jung, and Yasushi Sasaki. Formation of calcium ferrites under controlled oxygen potentials at 1 273 K. *ISIJ International*, 50(8):1064–1070, 2010.

A

XRF data

This appendix shows the concentrations of the different elements in the form of oxides from the samples used in the experiment.

Size fractions

	<500µm	500-1000µm	1-2mm	>2mm
Fe2O3	44,13	54,95	56,19	60,11
SiO2	24,17	10,04	8,87	7,37
CaO	23,11	26,25	26,42	24,89
ZnO	0,88	1,11	1,25	1,28
Al2O3	1,66	1,06	1,00	0,71
MgO	1,37	1,49	1,47	0,93
C	1,80	2,34	2,18	2,20
SO3	0,21	0,28	0,26	0,24
MnO	0,74	0,92	0,89	0,97
PbO	0,18	0,20	0,24	0,24

Table A.1: XRF data pure HOKS size fractions

	<500µm	500-1000µm	1-2mm	>2mm
Fe2O3	52,08	51,63	53,47	54,45
SiO2	10,88	9,86	8,43	8,14
CaO	20,89	21,92	21,36	20,76
ZnO	2,14	2,01	2,05	2,19
Al2O3	1,83	1,80	1,75	1,67
MgO	1,49	1,55	1,54	1,51
C	6,57	7,11	7,14	7,21
SO3	1,19	1,17	1,19	1,14
MnO	0,66	0,72	0,73	0,79
PbO	0,45	0,42	0,40	0,45

Table A.2: XRF data HOKS 80 (large) size fractions

	<200µm	200-500µm	0.5-1mm	>1mm
Fe2O3	50,28	51,19	53,06	56,18
SiO2	17,65	10,43	7,58	7,49
CaO	16,63	18,39	19,52	20,09
ZnO	2,10	2,80	2,57	2,18
Al2O3	2,14	1,83	1,81	1,81
MgO	1,35	1,37	1,49	1,27
C	5,56	8,29	9,55	6,85
SO3	1,28	1,26	1,33	0,96
MnO	0,64	0,70	0,76	0,83
PbO	0,35	0,53	0,45	0,40

Table A.3: XRF data HOKS 80 (small) size fractions

	<200µm	200-500µm	0.5-1mm	>1mm
Fe2O3	50,64	51,97	55,39	56,94
SiO2	14,86	9,41	6,31	7,70
CaO	17,72	18,85	19,86	21,48
ZnO	2,70	2,58	2,31	1,66
Al2O3	2,04	1,95	1,64	1,60
MgO	1,40	1,49	1,45	1,30
C	5,98	9,28	8,83	5,28
SO3	1,34	1,40	1,16	0,66
MnO	0,67	0,65	0,85	1,11
PbO	0,59	0,50	0,46	0,34

Table A.4: XRF data HOKS 76 size fractions

	<1mm	1-2mm	>2mm
Fe2O3	82,12	82,70	83,31
SiO2	1,38	1,25	1,27
CaO	9,48	9,18	8,78
ZnO	0,51	0,50	0,51
Al2O3	0,15	0,13	0,15
MgO	2,12	2,19	2,08
C	2,66	2,45	2,30
SO3	0,11	0,10	0,11
MnO	0,90	0,96	0,93

Table A.5: XRF data Pure BOF size fractions

	<1mm	1-2mm	>2mm
Fe2O3	75,72	76,02	76,61
SiO2	2,17	2,23	2,10
CaO	7,57	7,83	8,11
ZnO	1,32	1,24	1,16
Al2O3	0,76	0,76	0,67
MgO	1,84	2,04	2,14
C	8,16	7,36	6,87
SO3	0,60	0,60	0,54
MnO	0,82	0,82	0,84

Table A.6: XRF data BOF 85 size fractions

	<1mm	1-2mm	>2mm
Fe2O3	69,67	72,83	73,17
SiO2	3,15	2,65	2,56
CaO	6,99	7,04	7,06
ZnO	1,79	1,62	1,63
Al2O3	1,34	1,08	1,01
MgO	2,18	2,07	2,11
C	11,53	9,78	9,58
SO3	0,98	0,83	0,80
MnO	0,71	0,75	0,79

Table A.7: XRF data BOF 76 size fractions

After treatment at 1000°C in the horizontal furnace in nitrogen

Pure HOKS	1min	2min	5min	10min	20min	30min
Fe2O3	54,418	55,316	53,593	53,004	58,083	50,881
SiO2	9,619	10,03	13,879	17,031	14,254	21,571
CaO	26,463	27,577	26,642	24,438	22,176	22,114
ZnO	1,263	1,068	1,1	1,039	1,042	0,825
Al2O3	1,003	1,201	1,146	1,2	1,175	1,405
MgO	1,4	1,341	1,006	0,917	0,898	0,744
C	0,965	0,696	0,308	0,209	0,256	0,222
SO3	0,284	0,289	0,217	0,225	0,159	0,227
MnO	0,93	0,93	0,821	0,827	0,91	0,743

Table A.8: XRF data Pure HOKS 1000°C horizontal furnace in nitrogen

HOKS 80 (large)	1min	2min	5min	10min	20min	30min
Fe2O3	55,403	55,983	54,715	56,728	57,845	53,479
SiO2	7,746	6,746	11,694	13,422	13,475	18,419
CaO	21,071	22,61	21,794	19,911	20,148	19,801
ZnO	2,095	1,834	1,54	0,961	0,144	0,122
Al2O3	1,729	1,823	1,9	2,096	2,139	2,18
MgO	1,511	1,397	0,762	1,028	1,301	1,36
C	7,16	6,14	4,35	2,588	1,991	1,46
SO3	1,132	1,076	0,906	1,114	0,913	0,882
MnO	0,739	0,712	0,664	0,725	0,678	0,73

Table A.9: XRF dataHOKS 80 (large) 1000°C horizontal furnace in nitrogen

HOKS 80 (small)	1min	2min	5min	10min	20min	30min
Fe2O3	47,563	51,977	52,461	50,975	50,362	50,558
SiO2	14,237	11,456	16,904	17,057	20,625	19,963
CaO	19,174	20,48	17,425	20,381	18,104	19,034
ZnO	2,366	2,292	1,653	0,89	0,134	0,145
Al2O3	2,162	2,266	2,328	2,392	2,829	2,759
MgO	1,463	1,408	0,934	1,142	1,469	1,511
C	8,63	6,24	4,9	3,916	2,866	2,54
SO3	1,4	1,256	0,891	0,947	1,15	1,109
MnO	0,638	0,663	0,626	0,634	0,624	0,662

Table A.10: XRF data HOKS 80 (small) 1000°C horizontal furnace in nitrogen

HOKS 76	1min	2min	5min	10min	20min	30min
Fe2O3	51,917	51,873	56,555	52,071	55,703	47,937
SiO2	9,805	10,677	12,265	17,634	14,371	21,98
CaO	19,044	20,417	17,61	18,948	19,909	19,46
ZnO	2,476	2,063	1,814	0,89	0,179	0,114
Al2O3	2,097	2,146	2,032	2,483	2,377	2,907
MgO	1,478	1,429	0,916	1,2	1,481	1,585
C	8,82	7,51	5,37	3,58	2,635	2,4
SO3	1,321	1,212	0,942	0,947	1,095	1,136
MnO	0,679	0,641	0,696	0,65	0,677	0,65

Table A.11: XRF data HOKS 76 1000°C horizontal furnace in nitrogen

Pure BOF	1min	2min	5min	10min	20min	30min
Fe2O3	81,985	82,759	83,459	85,471	86,233	84,001
SiO2	1,674	1,835	2,054	1,632	1,519	2,214
CaO	9,763	9,967	9,859	8,73	8,454	9,672
ZnO	0,53	0,528	0,509	0,488	0,403	0,366
Al2O3	0,171	0,185	0,251	0,258	0,239	0,309
MgO	2,338	2,153	1,779	0,917	1,464	1,635
C	1,71	0,826	0,47	0,385	0,301	0,309
SO3	0,179	0,188	0,189	0,13	0,111	0,201
MnO	0,964	0,944	0,948	0,917	0,909	0,948

Table A.12: XRF data Pure BOF 1000°C horizontal furnace in nitrogen

BOF 85	1min	2min	5min	10min	20min	30min
Fe2O3	74,327	74,678	76,781	75,353	81,464	77,661
SiO2	2,617	3,221	3,474	5,367	3,896	5,501
CaO	8,24	7,656	8,551	9,245	8,741	10,19
ZnO	1,221	1,203	0,981	0,518	0,243	0,099
Al2O3	0,776	1,056	1,012	2,095	1,239	1,253
MgO	1,891	1,974	1,499	2,732	1,705	2,095
C	7,87	7,15	4,97	1,51	0,484	0,211
SO3	0,964	0,795	0,949	1,099	0,621	1,185
MnO	0,814	0,818	0,829	0,868	0,852	0,921

Table A.13: XRF data BOF 85 1000°C horizontal furnace in nitrogen

BOF 76	1min	2min	5min	10min	20min	30min
Fe2O3	71,397	73,771	72,653	78,213	75,534	63,912
SiO2	3,13	3,187	4,501	3,922	5,741	8,168
CaO	7,569	6,394	8,124	9,058	9,414	12,974
ZnO	1,423	1,52	1,167	0,527	0,095	0,032
Al2O3	1,048	1,534	1,535	1,367	2,339	2,728
MgO	2,09	1,791	1,585	1,893	2,94	6,579
C	9,75	8,705	7,09	2,59	0,875	0,406
SO3	1,274	0,706	1,309	0,718	0,968	2,487
MnO	0,784	0,71	0,794	0,868	0,82	1,15

Table A.14: XRF data BOF 76 1000°C horizontal furnace in nitrogen

BOF (old)	1min	2min	5min	10min	30min
Fe2O3	83,771	84,201	83,588	87,147	83,806
SiO2	1,334	1,378	2,211	1,203	2,234
CaO	9,172	9,127	9,956	8,268	9,604
ZnO	0,534	0,514	0,279	0,443	0,401
Al2O3	0,129	0,151	0,286	0,155	0,295
MgO	2,217	2,332	1,602	1,065	1,742
C	1,2	0,67	0,29	0,326	0,27
SO3	0,103	0,102	0,198	0,107	0,19
MnO	0,914	0,901	0,957	0,915	0,975

Table A.15: XRF data BOF (old) 1000°C horizontal furnace in nitrogen

After treatment of HOKS 80 (small)

HOKS 80 (small)	1min	2min	5min	10min	20min	30min
Fe2O3	48,524	46,284	51,573	52,22	51,417	49,214
SiO2	13,717	17,983	15,792	17,109	23,753	27,212
CaO	18,423	18,434	18,759	18,084	16,001	15,599
ZnO	2,29	1,937	1,666	0,985	0,496	0,31
Al2O3	2,045	2,215	2,261	2,335	2,458	2,718
MgO	1,408	1,335	0,938	0,892	0,685	0,66
C	9,576	7,981	5,718	5,196	1,811	0,975
SO3	1,197	1,124	0,942	0,971	0,796	0,75
MnO	0,683	0,616	0,631	0,676	0,651	0,595

Table A.16: XRF data HOKS 80 (small) 1000°C horizontal furnace with PCR 50

HOKS 80 (small)	1min	2min	5min	10min
Fe2O3	45,508	44,21	44,026	27,424
SiO2	18,767	24,762	29,885	46,769
CaO	19,075	17,593	16,444	16,838
ZnO	1,995	1,562	0,399	0,006
Al2O3	2,431	2,613	2,572	3,112
MgO	1,437	1,059	1,404	1,43
C	6,75	4,52	1,6	0,91
SO3	1,248	1,002	1,078	0,904
MnO	0,598	0,584	0,622	0,641

Table A.17: XRF data HOKS 80 (small) 1300°C horizontal furnace in nitrogen

HOKS 80 (small)	1min	2min	5min
Fe2O3	50,14	52,78	45,972
SiO2	14,582	16,106	29,154
CaO	19,1	19,206	16,991
ZnO	1,936	1,385	0,062
Al2O3	2,24	2,393	2,342
MgO	1,237	1,107	1,064
C	7,083	3,296	0,956
SO3	1,042	0,909	0,967
MnO	0,668	0,854	0,657

Table A.18: XRF data HOKS 80 (small) 1300°C horizontal furnace with PCR 50

After treatment of BOF 76

BOF 76	1min	2min	5min	10min	20min	30min
Fe2O3	71,668	71,867	74,02	75,391	80,318	82,004
SiO2	2,917	3,156	3,971	4,771	4,358	3,826
CaO	6,597	6,554	7,541	8,543	8,447	8,17
ZnO	1,766	1,485	1,091	0,791	0,254	0,204
Al2O3	1,369	1,531	1,822	2,231	1,899	1,612
MgO	2,188	2,121	1,545	1,583	1,229	1,093
C	10,09	10,15	7,08	3,69	0,731	0,4
SO3	1,039	0,764	0,866	0,936	0,92	0,845
MnO	0,741	0,678	0,704	0,745	0,803	0,87

Table A.19: XRF data BOF 76, 1000°C horizontal furnace with PCR 50

BOF 76	1min	2min	5min	10min
Fe2O3	72,795	75,604	76,579	71,105
SiO2	3,699	4,255	5,284	7,216
CaO	7,138	7,682	9,514	12,835
ZnO	1,235	0,852	0,051	0
Al2O3	1,754	2,053	1,948	2,22
MgO	1,939	1,742	2,775	2,843
C	8,39	4,93	0,24	0,01
SO3	0,779	0,854	1,107	1,53
MnO	0,715	0,748	0,966	1,118

Table A.20: XRF data BOF 76, 1300°C horizontal furnace with PCR 50

BOF 76	1min	2min	5min	10min
Fe2O3	72,241	76,568	78,856	72,584
SiO2	3,534	4,192	5,023	6,946
CaO	6,68	7,579	9,164	12,177
ZnO	1,356	0,765	0,037	0,017
Al2O3	1,62	2,01	1,772	2,106
MgO	1,757	1,538	1,911	2,288
C	9,241	4,473	0,385	0,07
SO3	0,691	0,72	0,767	1,471
MnO	0,706	0,711	0,869	1,114

Table A.21: XRF data BOF 76, 1300°C horizontal furnace with PCR 50

B

Weightloss calculations

Table B.1: Weight loss calculations BOF 76

Compound name	XRF oxide wt%	Fraction	Compound name	M	Relative weight	normalised weight (%)	LC name	LC wt%
Fe2O3	71,0	0,3	Fe	55,9	14,9	16,0		
		0,4	FeO	71,8	25,5	27,5	O	6,1
		0,1	Fe3O4	231,5	6,9	7,4	4O	2,0
		0,1	Fe2O3	159,7	7,1	7,6	3O	2,3
		0,1	Fe3C	179,5	5,3	5,7		
CaO	7,1		CaO	56,1				
			CaCO3	100,1	12,6	13,6	CO2	6,0
C	10,5		C	12,0	8,5	9,2	C	9,2
ZnO	1,7		ZnO	81,4				
SO3	1,2		ZnO	81,4	0,5	0,5	Zn + O	0,5
			SO3	80,1				
			ZnS	97,5	1,5	1,6	Zn	1,1
SiO2	3,3		SiO2	60,1				
			SiO2	60,1	3,3	3,5		
MgO	1,8		MgO	40,3				
			MgO	40,3	1,8	2,0		
MnO	0,8		MnO	70,9				
			MnO	70,9	0,8	0,8	O	0,2
Al2O3	1,0		Al2O3	102,0				
			Al2O3	102,0	0,5	0,6		
PbO	0,4		PbO	223,2				
			PbO	223,2	0,4	0,4	Pb + O	0,4
H2O	2,2		H2O	18,0	2,2	2,4	H2O	2,4
Sum	98,8				91,8	98,8		**30,2**

Table B.2: Weight loss calculations HOKS 80 (small)

Compound Name	XRF oxide wt%	Fraction	Compound Name	M	relative weight	normalised weight (%)	LC name	LC wt%
Fe2O3	52,87	0,00	Fe	55,85	0,00	0,00		
		0,00	FeO	71,84	0,00	0,00	O	0,00
		0,50	Fe3O4	231,53	25,55	23,18	4O	6,41
		0,50	Fe2O3	159,69	25,79	23,40	3O	7,03
CaO	19,14		CaO	56,08				
		0,50	CaCO3	100,09	17,08	15,50	CO2	6,81
		0,20	Ca(OH)2	74,09	5,06	4,59	H2O	1,12
		0,10	Ca4Fe2O6CO3*12H2O	644,20	5,50	4,99	CO2 + 4O	0,84
							12 H2O	1,67
		0,05	K2Ca(CO3)2	238,29	4,07	3,69	2 CO2	1,36
		0,15	CaO	56,08	2,87	2,60		
C	8,34		C	12,01	6,29	5,71	C	5,71
ZnO	2,57		ZnO	81,38				
SO3	1,24		ZnO	81,38	1,31	1,18	Zn + O	1,18
			SO3	80,06				
			ZnS	97,47	1,51	1,37	Zn	0,92
SiO2	8,87		SiO2	60,08				
			SiO2	60,08	8,87	8,05		
MgO	1,41		MgO	40,30				
			MgO	40,30	1,41	1,28		
MnO	0,75		MnO	70,94				
			MnO	70,94	0,75	0,68	O	0,15
Al2O3	1,83		Al2O3	101,96				
			Al2O3	101,96	0,91	0,83		
PbO	0,47		PbO	223,20				
			PbO	223,20	0,47	0,42	Pb + O	0,42
Sum	97,47				107,42	97,47		**33,63**